Hutton Symposium V, Field Guidebook
Geological Survey of Japan, Interim-Report no.28, p. 3－21, 2003

Trip A1

Quaternary and Pliocene granites in the Northern Japan Alps

Satoru HARAYAMA[1], Hajime WADA[2] and Yoshiaki YAMAGUCHI[3]

Abstract: The Kurobegawa Granitic Pluton is a young batholith (*ca.* 2 Ma) exposing 700 to 2900 m elevations, in the northern Northern Japan Alps of central Japan. Field relations and petrographical features indicate that the pluton represents a well exposed typical cross-section of a magma chamber beneath island-arc volcanoes. The pluton is vertically zoned by fractional crystallization from the lower granite (70-74 wt% SiO_2) to the upper granite (72-77 wt% SiO_2). Hydrous mafic microgranular enclaves (MME, 0.1-2 m in major axis) of basaltic to dacitic composition (54-68 wt% SiO_2) containing biotite and hornblende occur throughout most of the pluton. The MME generally have sharp fine chilled margins and show no in situ mixing between the MME and the host granite. Field relations reveal that mafic magma intruded into the chamber from the bottom, and ascended as a restricted feeder dyke in the lower crystal mush. The mafic magma underwent vapor exsolution by second boiling on cooling during ascending, reducing the bulk density relative to that of the host felsic magma. The mafic magma eventually fragmented to form MME and the MME rose upward, resulting in their dense distribution throughout the pluton.

The Quaternary Hotaka-Takidani volcano-plutonic complex, exposed in the eastward tilting block of the Northern Japan Alps, consists of the Hotaka Cauldron and an immediately subjacent granitoid pluton (Takidani Granodiorite). The Takidani Granodiorite is a pluton (13×4km) situated along major axis of the Japan Alps and intruded into Early Pleistocene (1.76 Ma) volcanic rocks. U-Pb, K-Ar, and fission track dates on coexisting minerals from the pluton are 1.4 - 0.9 Ma. Tephrochronological constraints for air-fall tephras supplied from the cauldron and mineral dates for the Takidani Granodiorite indicate that the emplacement and cooling of the pluton occurred in the Early Pleistocene time. Postemplacement tilting of the Northern Japan Alps caused rapid denudation of the Takidani Granodiorite as well as the Hotaka Cauldron.

Keywords: Hutton Symposium, field excursion, granite, hydrous mafic magma, mafic microgranular enclave, fractional crystallization, magma mingling, mylonitization, cooling history, K-Ar dating, uplifting, thermochronology, Japan Alps, Quaternary, Pliocene.

1. Mafic microgranular enclaves floating through a vertically fractionating felsic magma chamber: The Kurobegawa Granitic Pluton, Northern Japan Alps, central Japan (Hajime WADA, Satoru HARAYAMA, and Yoshiaki YAMAGUCHI)

1.1 Introduction

The young Kurobegawa Granitic Pluton (*ca.* 2 Ma) and its roof volcanics, exposed in the Northern Japan Alps, form a volcanic-plutonic complex in the back-arc region of central Japan. The pluton is expected to provide us a typical cross-section of a magma chamber beneath island-arc volcanoes. The pluton is exposed in the north part of the Northern Japan Alps (Fig. 1: *e.g.* Harayama *et al.*, 1991; Harayama *et al.*, 2000). Rapid uplift and subsequent erosion during the Pleistocene in the Northern Japan Alps, exposing the youngest granitic pluton (Harayama, 1992), provides us an excellent vertical exposure of the pluton. Densely crowded MME extensively occupy the upper part of the pluton; in contrast MME occur sparsely in the lowermost part of the pluton. We describe here the geologic and petrologic features of the Kurobegawa Granitic Pluton, and will demonstrate that rapidly cooled mafic magmas which injected into the vertically fractionated felsic magma chamber ascended through the pluton as MME without mixing. We present here their field relations and petrographical and geochemical features of this pluton to discuss the mechanism of MME floatation through vertically fractionated felsic chamber.

1.2 Geology and the cross-section of the pluton

The Kurobegawa Granitic Pluton is, with batholithic dimension in an area of approximately 100 km^2, elongated from north to south parallel to the Kurobegawa Gorge and along the Northern Japan Alps (Fig. 2). The pluton extends to the main ridgeline of the Northern Japan Alps in the east and is deeply eroded in the west with its vertical exposure ranging from 700 and 2900 m elevations. Although only the cooling

[1] Department of Geology, Faculty of Science, Shinshu University, Asahi 3-1-1, Matsumoto, Nagano 390-8621, Japan, e-mail: shara@gipac.shinshu-u.ac.jp
[2] Environmental System Science, Graduate School of Science and Technology, Shinshu University, Asahi 3-1-1, Matsumoto, Nagano 390-8621, Japan, e-mail: th98409@ gipac.shinshu-u.ac.jp
[3] Department of Geology, Faculty of Science, Shinshu University, Asahi 3-1-1, Matsumoto, Nagano 390-8621, Japan, e-mail: yyamagu@gipac.shinshu-u.ac.jp

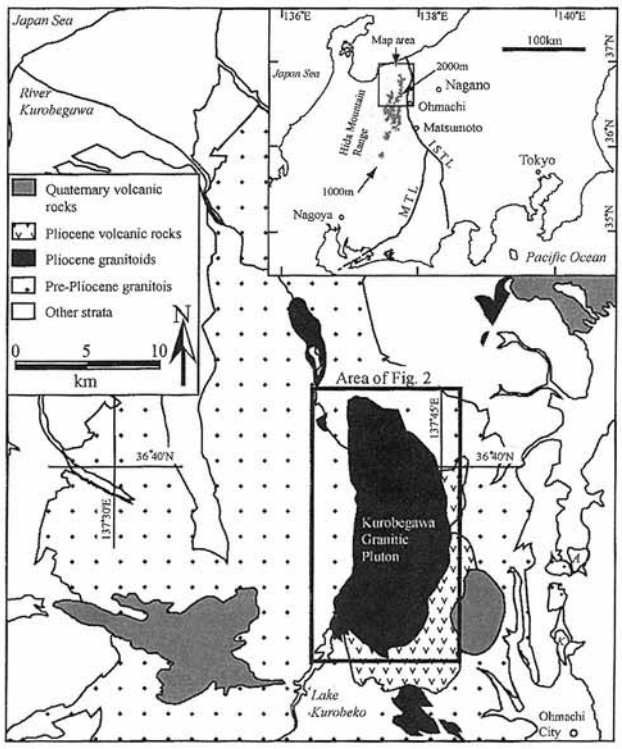

Fig. 1. Simplified location map of study area in the north part of the Northern Japan Alps. [modified from the 1:200,000 geological map of the Toyama (Harayama *et al.*, 1995) and the Takayama (Yamada *et al.* 1988) districts]. Abbreviations; MTL: Median Tectonic Line; ISTL: Itoigawa-Shizuoka Tectonic Line; A: Lake Aokiko; K: Lake Kizakiko.

ages (*e.g.* 1.20 ± 0.29 Ma K-Ar biotite age, Uchiumi *et al.*, 1995; 1.90 ± 0.45 Ma FT zircon age, Yamada and Harayama, 1999) were determined, the pluton is thought to be a Late Pliocene pluton based on the intrusive relations (Harayama *et al.*, 2000). The pluton is cut by the Takasegawa fault in the southwest part and by the Kurobegawa shear zone in the northwestern margin.

Postemplacement uplift has tilted the pluton and the roof volcanics (Jiigatake Volcanic Rocks) eastward steeply (Harayama *et al.*, 2003). From the succession and structure of the Jiigatake Volcanic Rocks, the roof volcanics are 3.5 to 5 km in total thickness (Harayama *et al.*, 2003), and the pluton exposes the vertical cross section of 6 km thick. The Kurobegawa Granitic Pluton intrudes a block of Permian metamorphic rocks at the north part of the pluton (Harayama *et al.*, 1995) at the contact that has a northwest strike and a vertical dip. At the western margin, the pluton intrudes Jurassic to Miocene granites (Harayama *et al.*, 2000). The western boundary is interpreted to dip steeply eastward on the basis of the shape of the boundary trace and topography (Fig. 2). At the eastern margin, the pluton intrudes a Cretaceous to Paleogene granite (Kato *et al.*, 1989). The pluton intrudes the Pliocene Jiigatake Volcanic Rocks at the south and east margin and contact metamorphism effects are observable (Ishizawa, 1982). Harayama *et al.* (2000) suggested that the Kurobegawa Granitic Pluton and the Jiigatake Volcanic Rocks form a volcanic-plutonic complex. The boundary between the volcanic rocks and the pluton dips moderately southward at the southern margin of the pluton. The eastern boundary is interpreted to dip moderately to steeply eastward (Fig. 2). At the contacts, the pluton becomes leucocratic and includes no mafic microgranular enclaves.

Four peripheral diorites (the Meiken, the Keyakidaira, the Daikoku and the Jujikyo Diorite) are exposed around the Kurobegawa Granite as satellites. The Jujikyo Diorite is intruded by the Kurobegawa Granitic Pluton but hardly shows a contact aureole. The Daikoku Diorite is a Pliocene stock aged 4.45 Ma (K-Ar biotite age, Uchiumi *et al.*, 1995). Harayama *et al.* (2000) suggested that these diorites and the Kurobegawa Granitic Pluton belonged to a successive magmatism in the Pliocene in the north part of the Northern Japan Alps. Felsite dykes (approximately 1.0 Ma K-Ar whole-rock ages, Nishimura and Mogi, 1986; 1.0 ± 0.2 Ma FT zircon age, Yamada and Harayama, 1999) ranging in width from several meters to 100 meters cut the Kurobegawa Granitic Pluton. The felsites strike north to south along the Kurobegawa Gorge and northeast to southwest on the mountain ridge.

1.3 Petrography

1.3.1 Vertical zoning of the Kurobegawa Granitic Pluton

The pluton is vertically zoned with no foliated structures. The granitic pluton is textually and compositionally divided into two rock types, that is, the lower and the upper granite. The pluton consists of the lower, the middle and the upper units. The lower and the upper units are comprised of the lower granite and the upper granite, respectively. In the middle unit, the two granites irregularly contact each other, as described below. Miarolitic cavities (< several centimeters across) occur throughout the pluton. The lower granite, a medium-grained and equigranular to porphyritic amphibole-bearing biotite granodiorite to granite (Figs. 3, 4A and 4B), is exposed along the Kurobegawa Gorge and in the tunnel just under the mountain ridge at lower elevations, whereas the upper granite, a fine-grained porphyritic biotite granite (Figs. 3 and 4C), occupies the mountain ridge at higher elevations (Fig. 2).

In the middle unit, the contacts between the lower and the upper granites are sharp and truncated. There is no thermal recrystallization in both the granites. This zone is exposed ranging from 2 to 3.5 km in width in a direction from east to west (Fig. 2). Mafic microgranular enclaves (MME) sometimes are in sharp contact with the lower and the upper granite. MME are sometimes fringed with the lower granite.

Modal compositions of minerals for representative rocks are shown in Fig. 3. The two granites range in modal composition from granodiorite to granite in the IUGS nomenclature (Streckeisen, 1976). MME generally with elliptic shape ranging from 10 cm to 2 m in major axis occur densely in the upper granite and the uppermost part of the lower granite (Figs. 2B, 2C and 5). Although this dense occurrence of MME (the MME dense zone) strikingly

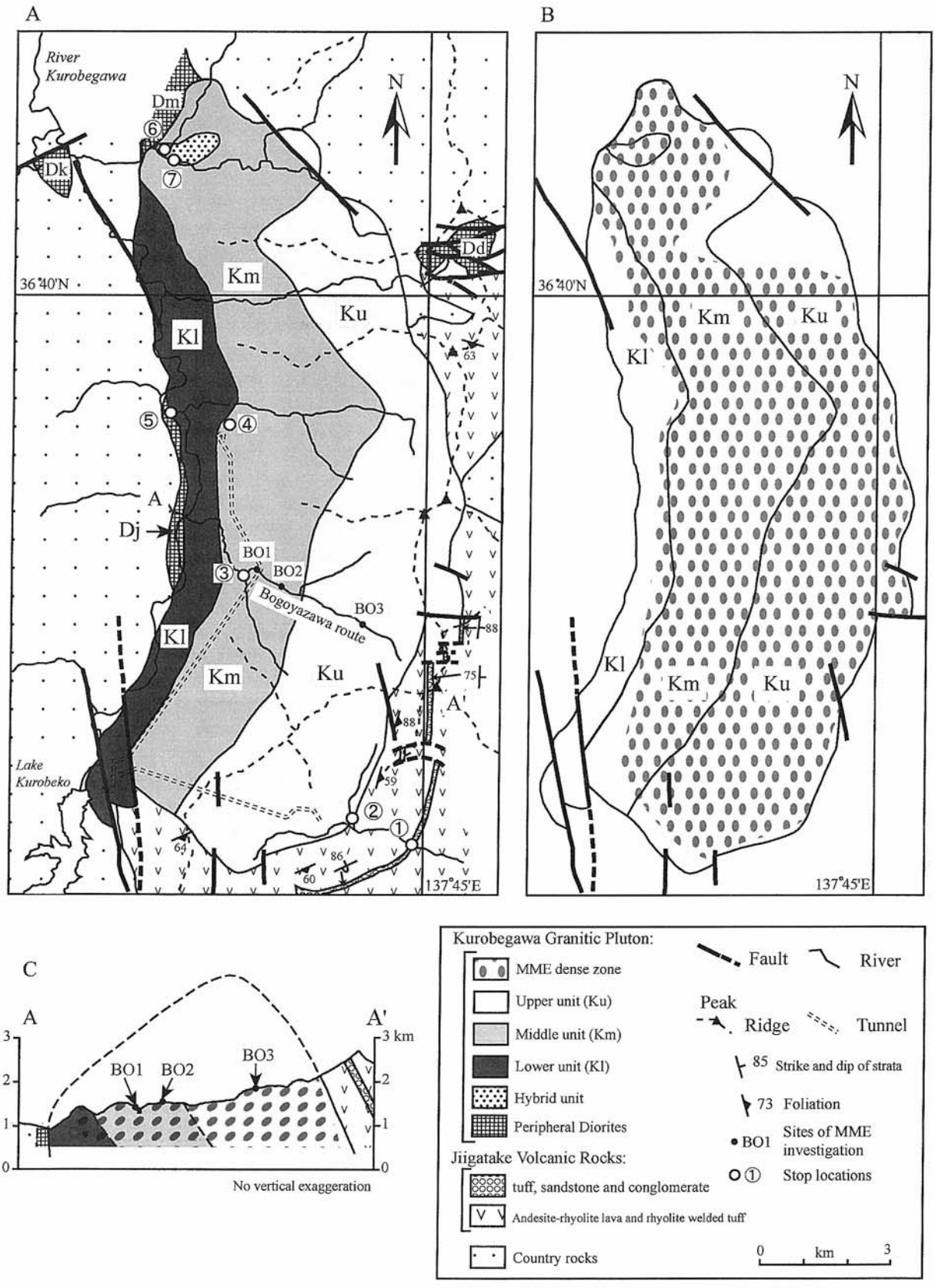

Fig. 2. (A) Geologic map of the Kurobegawa Granitic Pluton, showing the distribution of the main petrographic rock types. The data for the Daikoku diorite are from Nakano *et al.* (2002). Abbreviations; Dm: Meiken diorite; Dk: Keyakidaira diorite; Dd: Daikoku diorite; Dj: Jujikyo diorite. (B) The MME dense zone of the Kurobegawa Granitic Pluton. The MME dense zone occurs in nearly 80% of the exposed area of the pluton. (C) A cross section shows that the pluton is vertically divided and tilts eastward. The MME dense zone occupies extensively the pluton except the lowermost and the uppermost part of the pluton.

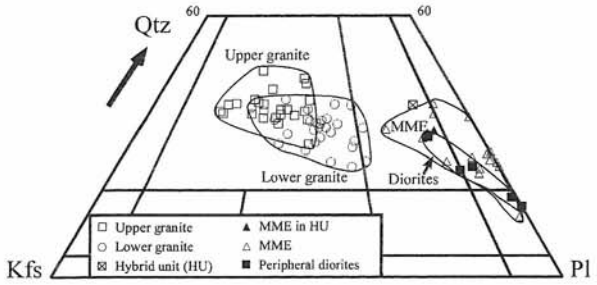

Fig. 3. Modal composition of minerals for the Kurobegawa Granitic Pluton and the associated rocks. Abbreviations; Qtz: quartz; Kfs: K-feldspar; Pl: plagioclase.

characterizes the pluton, MME are hardly mixed with the host granite. Mixing occasionally occurs restrictedly around MME on a small scale. The minor hybrid rocks occur only in the north part of the pluton as described below, showing textures of mixing and mingling of the host crystal-rich felsic magma with the mafic magma.

1.3.2 Granite petrography

The lower granite: The lower granite grades in texture from medium-grained equigranular to medium-grained porphyritic (Figs. 4A and 4B). This granite sparsely contains only small enclaves (2 to 5 cm in major axis) in contrast to the uppermost part of the lower granite. Plagioclase and quartz phenocrysts are up to 8 mm. Biotite is a common mafic phase. Amphibole occurs only in the relatively mafic part of this granite. Patchy-zoning is present in some plagioclase phenocrysts. Perthitic K-feldspar and quartz are interstitial. The most abundant accessory phase is magnetite that occasionally has ilmenite lamellae. Magnetite is commonly overgrown with anhedral titanite. Apatite and zircon are euhedral and frequently included in biotite. Subhedral allanite attaches to biotite and occasionally encloses small biotite, apatite and magnetite.

The upper granite: The upper granite is light gray in color and shows a fine-grained porphyritic texture (Fig. 4C). In the southern part of this granite near the upper contact with the Jiigatake Volcanic Rocks, the granite becomes leucocratic and contains no enclaves. Elliptic MME with major axis of 10 cm to 2 m are particularly common in this granite except near the intrusive margin and the roof contacts. Quartz phenocrysts up to 6 mm and plagioclase phenocrysts as large as 2 mm occur in a fine-grained matrix consisting of plagioclase, quartz and K-feldspar. Graphic texture is present. Plagioclase commonly shows oscillatory zoning and often has compositional patches. In the MME dense zone of this granite, sieve-textured zones are common in plagioclase phenocrysts. Euhedral to subhedral biotite is the only mafic silicate phase in this granite. The accessory phases are magnetite, ilmenite, apatite, zircon and allanite. Some magnetites are fringed with titanites. The titanite-magnetite-quartz assemblage indicates a relatively high oxygen fugacity condition of the magma (Wones, 1989).

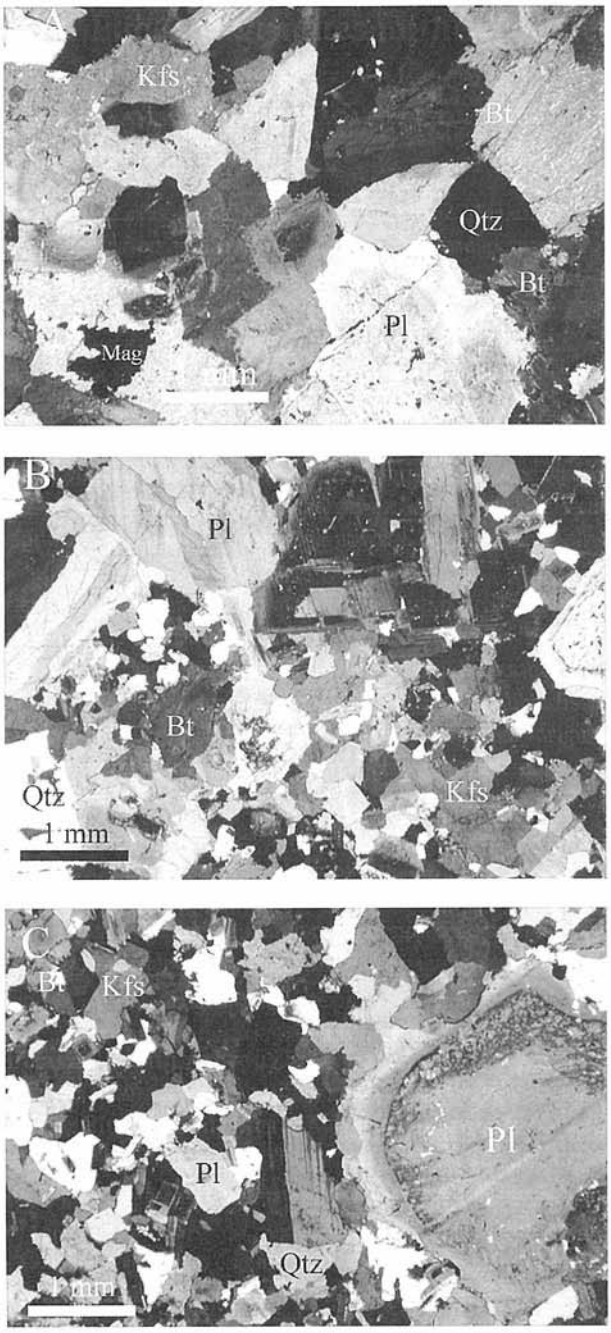

Fig. 4. Photomicrographs of (A and B) the lower granite and (C) the upper granite of the Kurobegawa Granitic Pluton, showing that the granite becomes finer and more porphyritic toward the upper part of the pluton. Abbreviations; Bt: biotite; Pl: plagioclase; Kfs: K-feldspar; Qtz: quartz. (A) The lower part of the lower granite. This granite shows equigranular textures. (B) The porphyritic upper part of the lower granite. This granite contains plagioclase and quartz phenocrysts. (C) The upper granite. This granite becomes finer and contains less phenocrysts than the lower granite.

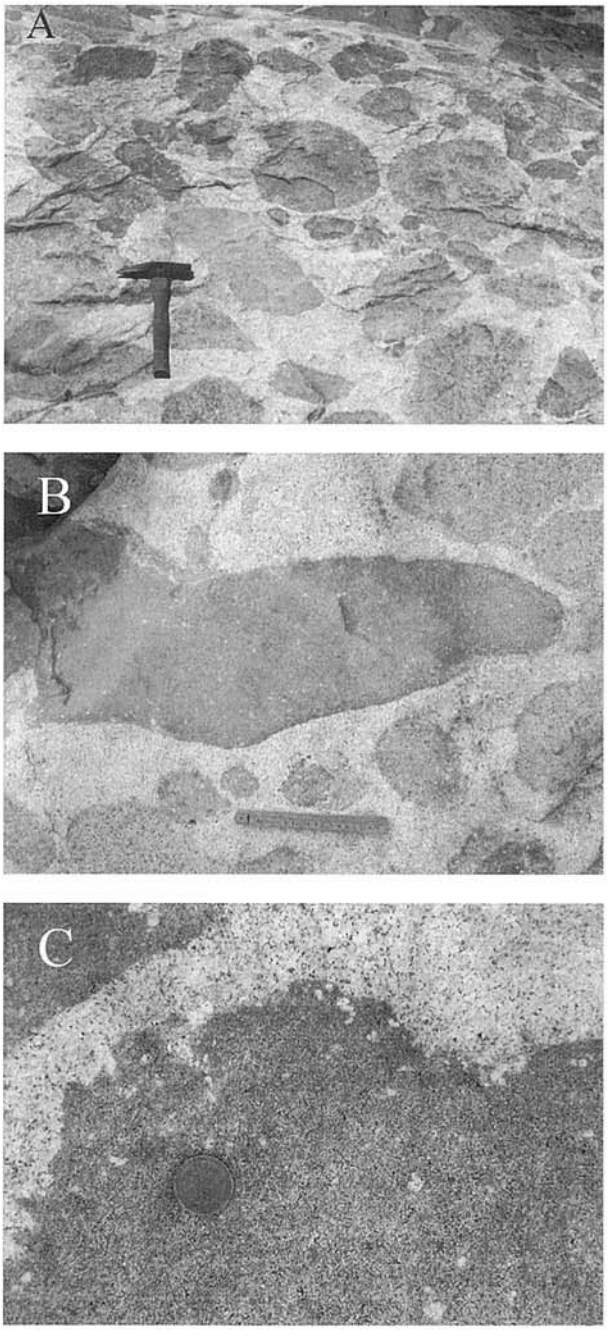

Fig. 5. Field photographs of the Kurobegawa Granitic Pluton. (A) View of the MME dense zone in the upper granite. The pluton densely contains elliptic MME in the upper part of the pluton. MME are discrete and not tightly packed. (B) Chilled margin in an MME. Most MME have sharp fine chilled margins with the host granite. (C) Mingled crystals in MME. Plagioclase and quartz phenocrysts and granitic inclusions are locally engulfed by a mafic microgranular enclave along its contact. A few plagioclase and quartz phenocrysts are trapped into MME.

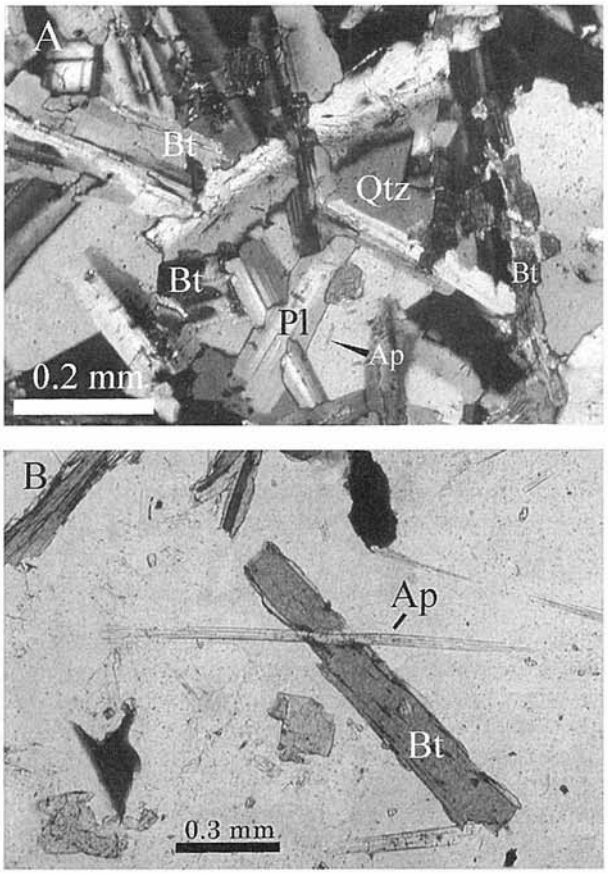

Fig. 6. Photomicrographs of chilled and dissolved textures in MME. (A) Bladed biotite (Bt) in MME. MME mainly consist of networks of acicular amphibole, bladed biotite and lath-like plagioclase (Pl) with interstitial quartz (Qtz). (B) A needle-shaped apatite (Ap) in MME. An apatite needle with a hollow resembles to that produced experimentally by rapid crystallization from a melt (Wyllie *et al.*, 1962).

1.3.3 MME Petrography

Occurrence: The MME range in average diameter from 10 cm to 2 m (up to 5m), and occurs densely in most parts of the upper unit and in the uppermost part of the lower unit (Figs. 2 and 5). At lower elevations in the western (lower) part of the lower unit (the MME sparse zone), only small MME ranging from 2 to 5 cm occur sparsely, while swarms of MME with similar size to those of the dense zone are present sporadically in the MME sparse zone in this lower unit.

MME show fine to medium-grained texture and range from quartz dioritic through tonalitic to granodioritic composition (Fig. 3). MME are generally "matrix-supported" and discrete and have sharp fine chilled margins (Fig. 5B). Although crenulate margins sometimes develop around MME, depositional features such as load-cast and pipe structure have not been seen in MME. We have not found the well-packed chilled mafic pillows and the mafic enclaves with way-up indicators, described by Wiebe and Collins (1998) and Wiebe et al. (2001).

Texture: MME consist of plagioclase and quartz phenocrysts and randomly intergrown networks of

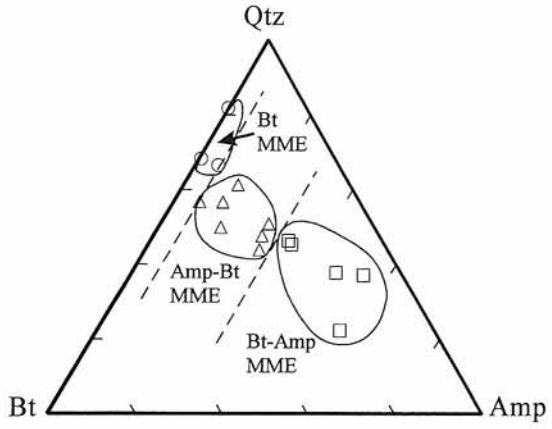

Fig. 7. Modal composition of quartz-biotite-amphibole for MME in the Kurobegawa Granitic Pluton. Abbreviations; Qtz: quartz; Bt: biotite; Amp: amphibole.

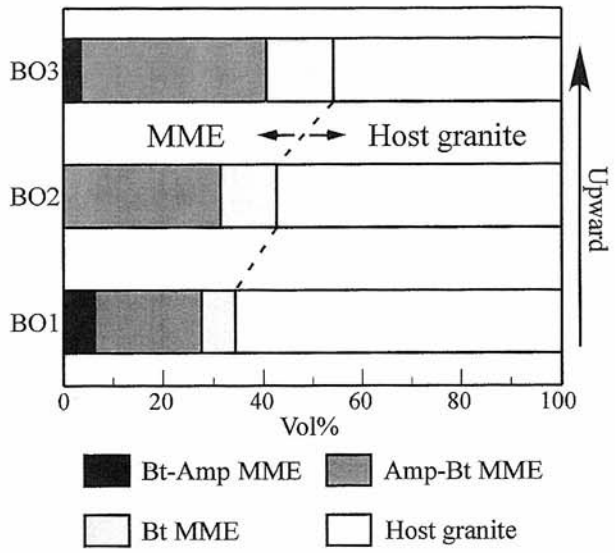

Fig. 8. Volumetric proportion of each type of MME and a total of three MME types at the three sites.

microphenocryts of acicular amphibole, bladed biotite and lath-like plagioclase in a fine-grained matrix consisting of interstitial quartz ± K-feldspar (Fig. 6A). MME lack pyroxene. MME commonly show quenched textures such as acicular amphibole and acicular apatite, characteristic of rapid crystallization (Fig. 6B) (Wyllie *et al.*, 1962). Amounts of acicular amphibole and bladed biotite vary. Plagioclase in the matrix generally shows rectangular shape with normal zoning and a high aspect ratio. On the other hand, plagioclase phenocrysts usually show cores of dissolved texture such as a sieve-like texture. Quartz phenocrysts generally show ovoidal dissolved shape and some of them are surrounded by fine-grained amphiboles and biotites (quartz-amphibole/biotite ocellus texture, Sato, 1975; Hibbard, 1991). Some MME engulf quartz and plagioclase phenocrysts of the host granite at their margins (Figs. 5B and 5C), implying that these phenocrysts in MME are derived from the host granite. Rounded pyrrhotites occur as inclusions in biotite and oxide minerals. Ilmenite commonly composites with magnetite. The assemblage of titanite-magnetite-quartz develops around primary magnetite.

MME types and vertical distribution in the pluton: MME are classified into three types based on their biotite-amphibole modal composition; (1) biotite-amphibole MME, (2) amphibole-biotite MME, and (3) biotite MME (Fig. 7). In biotite-amphibole MME, a bladed biotite-rich rim is occasionally present. Vertical distribution of the three types of MME was examined at three sites along the west-east profile (the Bogoyazawa route, in Figs. 2A and 2C) of the pluton. We selected three sites available for investigation of sufficiently wide areas (>10m^2). Total volumes of MME are shown to increase toward the roof (Fig. 8). The volume proportions of the amphibole-biotite MME and the biotite MME show the same systematic roofward increasing. Such a systematic order is, however, unclear for the biotite-amphibole MME in our investigation. In our field observation, relatively larger MME seem to be more abundant in the shallower level of the pluton.

1.3.4 The hybrid unit

A fine- to medium-grained, heterogeneous unit of granodiorite to granite occurs in the northern part of the pluton (Fig. 2A). The modal proportion of plagioclase and quartz phenocrysts varies in places, representing a characteristically heterogeneous feature of the hybrid rock. This unit is characterized by two contrasting types of biotite occurrence in addition to ovoidal quartz and plagioclase phenocrysts. Juxtaposition of bladed and blocky biotites suggests two different stages of growth. Typical quartz-amphibole/biotite ocelli, similar to those characteristic of mechanical mixing of quartz-rich crystal mush with mafic magma (Sato, 1975; Hibbard, 1991), are often developed in the fine-grained matrix. Blade-shaped biotite is scattered in the matrix consisting of fine plagioclase, K-feldspar and quartz (similar to the texture G in Fig. 1, p. 434-435, Hibbard, 1991).

In this unit, MME (10cm to 2m) vary greatly in shape, ranging from rounded to irregular. Generally, chilled crust develops in various degrees in the outermost part of MME. No plagioclase and quartz phenocrysts are found in the area within strongly chilled margins, whereas they are often present in the interior of MME bounded by a very weakly developed chilled margin. Quartz-amphibole/biotite ocelli are also well developed.

1.3.5 The peripheral intrusives

The diorites have a medium-grained equigranular texture and range in composition from quartz dioritic through tonalitic to granodioritic similar to those of MME. Mafic phases in the diorites are mainly amphibole and biotite. Some amphiboles are partially replaced by a cluster of subhedral biotite crystals. Clinopyroxene is found only in the Daikoku Diorite as a relict incompletely altered into amphibole. Plagioclase in the Daikoku, the Keyakidaira and the Jujikyo Diorite usually has calcic patches while most plagioclase in

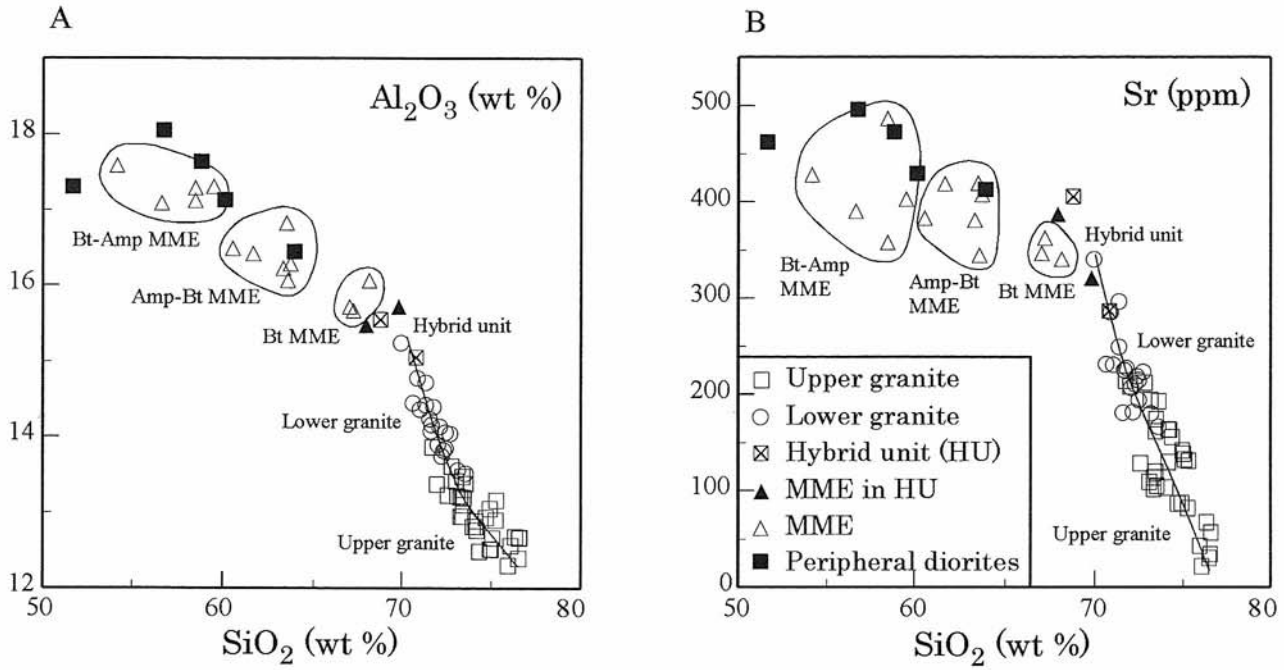

Fig. 9. Geochemical variations of major and trace elements plotted against SiO_2 for the Kurobegawa Granitic Pluton and the associated rocks. There are clear bends between the compositions for the host granites and the mafic rocks (MME and the diorites).

the Meikenzawa Diorite show clear normal zoning. Fe-Ti oxide minerals, apatite and allanite are accessory minerals in the four diorites. The Jujikyo Diorite locally contains Permian metamorphic rocks as xenoliths.

1.4 Mineralogy

Plagioclase phenocrysts commonly show oscillatory zoning (An_{24} - An_{18}) and often has compositional patches throughout the granites. Some crystals of the granites in the MME dense zone have thin sieve-like textured dissolution surfaces (An_{39}) similar to the texture L in figure 1, page 434-435, Hibbard (1991), surrounding a clear core (An_{17}). Plagioclase phenocrysts in MME show various degrees of dissolution. Many of the phenocrysts have sieve-like textured cores that extend out to the rim, similar to the left texture of EHS in the texture L in figure 1, page 434-435, Hibbard (1991), and some of them also have sieve-like textured dissolution surfaces (An_{53} - An_{41}) surrounding a clear core (An_{54} - An_{30}), similar to the right texture of EHS in the texture L in Figure 1, page 434-435, Hibbard (1991). These crystals are always mantled by a sodic, clear, normally zoned margin (An_{22}). Microcrystalline plagioclase in the matrix shows strong, clear normal zoning (An_{58} - An_{30}) similar in composition to the *An*-rich sieve-textured zones.

In MME, amphibole always occurs as euhedral, elongated crystal, and shows strong patchy zoning. The original amphibole composition remains in the patchy core. The compositions yield an amphibole crystallization condition (0.3 - 0.4 GPa, about 860°C; in preparation), estimated by the amphibole thermobarometer (Ernst and Liu, 1998). Biotite is often euhedral. Quartz is always interstitial to amphibole and biotite, similar to the feature of a very H_2O-rich mafic magma characteristic of those in Quaternary back-arc volcanism (Sakuyama, 1979).

Magnetite occurs throughout the host granite and MME. Titanite is generally developed extensively on magnetite. The titanite-magnetite-quartz assemblage typical for a high oxygen fugacity condition (Wones, 1989) develops in the granite and MME. In MME, rounded sulfide occurs as grains surrounded by biotite and Fe-Ti oxide phases. Ilmenite composites with magnetite, associated with the titanite-magnetite-quartz assemblage. Apatite in MME is divided into two different types in chlorine content, relatively high Cl apatite (0.5 - 0.9 wt%) and low Cl apatite ($\leq$ 0.2 wt%). Allanite usually occurs as a composite grain with biotite throughout the granites. The lower granite contains more allanite than the upper granite.

1.5 Petrochemistry

The SiO_2 contents of the host granites of the Kurobegawa Pluton range from 70 to 74 wt% for the lower granite and from 72 to 77 wt% for the upper granite. MME range widely in silica composition between 54 and 68 wt%. The MME compositions correspond well to their modal variations from Biotite-Amphibole MME (54 - 59 wt% SiO_2) through Amphibole-Biotite MME (61 - 64 wt% SiO_2) to Biotite MME (67 - 68 wt% SiO_2). The peripheral diorites have silica compositions between 52 and 64 wt%, similar to those of MME. In the hybrid unit, the host has 69 and 71 wt% SiO_2 and MME have 68 and 70 wt% SiO_2.

Major element variations are displayed in the Harker diagrams (Fig. 9). The lower granite chemically grades into the upper granite in spite of sharp boundaries between the two rock types in the field relations. The trends of Al_2O_3 are

convex-downward from the lower granite to the upper granite. MME and the diorites show the other trend different from that of the granites with a change in slope at about 69wt% SiO_2. Compositions of the hybrid rock lie near both the extension of trends of the host granite and MME.

1.6 Discussion

1.6.1 Vertical view of the pluton

The Kurobegawa Granitic Pluton has been eroded deeply to form the Kurobegawa Gorge and is exposed at elevations ranging from 700 to 2900 m elevations. Harayama *et al.* (2000) suggested that the pluton and the Jiigatake Volcanic Rocks form a volcanic-plutonic complex. Both of them have been tilted eastward by postemplacement uplift. On the basis of the depositional structure of the Jiigatake Volcanic Rocks, the pluton has been steeply tilted eastward (Harayama *et al.*, 2003). It therefore gives a vertical view over 5000 m of this frozen granitic magma chamber. This provides us an excellent opportunity to examine the vertical distribution of MME and to discuss their origin and behavior throughout the pluton.

1.6.2 Evolution of the felsic magma chamber

The Kurobegawa Granitic Pluton is vertically zoned and texturally divided into two main rock types, the lower and the upper granite. Field relations of the pluton, their textural relations, modal composition, chemical trends of major and trace elements indicate that fractional crystallization played a principal role in the evolution of the felsic magma chamber. The convex-upward and -downward trends of major element strongly suggest that magma mixing is not the principal process for the vertical compositional variation of this pluton.

Two differentiation processes of a magma chamber were discussed by Marsh (1996): (1) Gravitational settling of crystals throughout a chamber; and (2) solidification fronts developed at the margins of the body by cooling and crystallization. In the Kurobegawa Granitic Pluton, field relations show no evidence of solidification fronts at the contacts. Therefore, it is suggested that gravitational settling of crystals may be a principal process to differentiate the felsic magma chamber (Fig. 10A), although it is possible that solidification fronts were removed by convective erosion or intrachamber stoping (Bergantz, 1999). Bachl et al. (2001) suggested that the velocity of crystal settling ranges from 0.1 m yr^{-1} to 10 m yr^{-1} in the granitic magma chamber at 750 to 800°C with 2 to 3 wt% H_2O. Similarly, gravitational settling of crystals is also probably possible for the hydrous felsic magma of the Kurobegawa chamber.

In the binary variation diagrams, there are no linear mixing relations between the host granite and MME (Fig. 9), indicating that magma mixing was not the principal process affecting compositional variation in the Kurobegawa Granitic Pluton. Hybridization of these two magmas was restricted to the northern part of this pluton, where the rocks show mechanical mixing textures. Further mixing is, however, not expected to occur because complete mixing requires a large mass fraction of the mafic end member and small

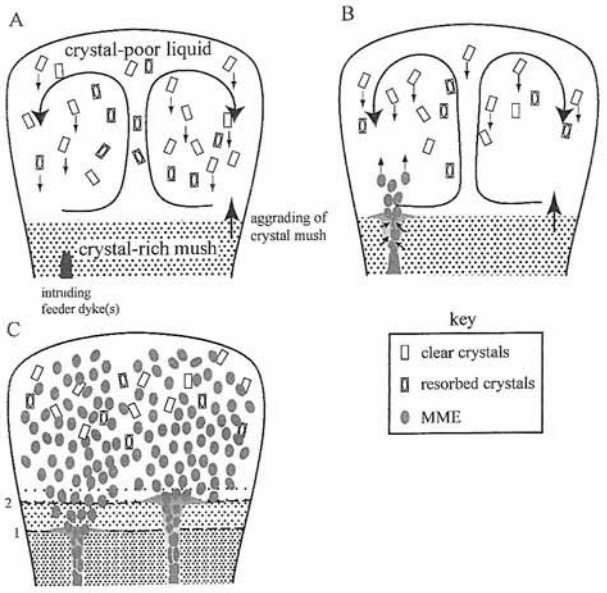

Fig. 10. Schematic illustrations of fractional crystallization of the chamber, and MME flotation through the lower mush in the Kurobegawa Granitic Pluton. (A) Formation of vertical zonation of the Kurobegawa chamber by fractional crystallization. (B and C) MME floatation throughout the chamber after feeder dykes reach the surface of the crystal mush. Numerals; 1 and 2: former boundaries between crystal mush and crystal-poor liquid.

compositional differences between two magmas (*e.g.* Sparks and Marshall, 1986). Although plagioclase phenocrysts in the granite of the MME dense zone commonly show dissolved textures similar to the dusty zoning in volcanic rocks of magma mixing origin (Tsuchiyama, 1985), these dissolved textures can be explained by such different mechanisms from magma mixing as self-mixing (Couch *et al.*, 2001) or crystal recycling (Tepley *et al.*, 1999; Troll and Schmincke, 2002) in fractional crystallization systems.

1.6.3 Origin of MME

The Field relation and petrographical evidence, described above, indicate that MME principally existed in a liquid state in the felsic magma chamber. Nakada and Motomura (1997) explained on the basis of the side-wall crystallization model of Huppert and Sparks (1989) that mafic enclaves in dacite lavas of the 1991-1995 eruption at Unzen Volcano originated at the side-wall of the magma chamber. This side-wall crystallization model hardly explains our field and petrological evidence that MME are fringed with chilled margins and do not occur near the side-wall of the pluton where the pluton becomes leucocratic and pegmatitic, and most MME compositions are much too mafic for sidewall crystallization from granitic magma. Magma mingling of mafic melt with felsic crystal mush is a reasonable process, considering that MME generally have sharp, crenulate and fine chilled margins (Figs. 5B and 5C) with the host granite and contain quenched products such as amphibole laths and apatite needles.

Field relations reveal that MME are densely distributed in

the upper part of the pluton. Possible mechanisms for the fragmentation of mafic magma to form MME include: (1) mafic magma foams were initially formed and floated as plumes from the bottom of the chamber (Eichelberger, 1980; Thomas *et al.*, 1993; Bindeman and Bailey, 1994); and (2) mafic magma ascended through the restricted feeder dykes in the lower crystal mush, and fragmented to form MME during ascent (Wiebe, 1974; Wiebe and Collins, 1998; Collins *et al.*, 2000). If MME floated through the crystal-rich bottom of the chamber, they would have been sheared (Williams and Tobisch, 1994; Blake and Fink, 2000). Most of the Kurobegawa MME, however, show an elliptical shape with a low aspect ratio and retain chilled margins (Fig. 5). Although there is no dense occurrence of MME in the lowermost part of the pluton, dyke-like swarms of MME locally occur. Therefore, it is suggested that MME were formed by fragmentation of mafic magma in feeder dykes during its ascent through the lower crystal mush and dispersed in the upper, crystal-poor part of the chamber.

Collins *et al.* (2000) have proposed a model of two-stage hybridization: stage 1 hybridization of two compositionally different magmas occurs below a magma chamber in composite 'back-bone' dykes; and stage 2 hybridization occurs within a chamber by mixing between stage 1 hybrids and megacryst-rich (crystal mush) granitic magma. Chemically, MME show clear linear compositional trends in the Harker diagrams, as seen on the plot of Al_2O_3 and Sr against SiO_2 (Fig. 9). And, they do not mingle with crystal mush. These features could be explained by mafic and felsic melts mixing which occurs in dykes below the Kurobegawa chamber before dykes intruded into the chamber bottom (stage 1 hybridization of Collins *et al.*, 2000). Locally, mixing and crystal-mush mingling took place to form the hybrid unit in the northern part of the pluton. The hybrid rock might have been formed by a similar mechanism to the stage 2 hybridization suggested by them.

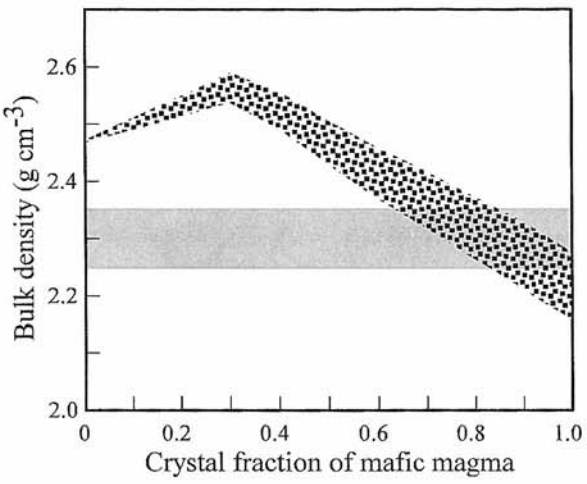

Fig. 11. Calculated bulk density of vesicluated andesitic magma plotted against crystal fraction on the basis of the calculation of Eichelberger (1980). The curve is for andesite with 5 wt% H_2O at 0.3 GPa. To calculate bulk density as a function of crystal fraction, density of the crystal fraction was assumed to be ranging from 2.72 to 2.91 g cm^{-3}, based on measured values of density of microphenocryst in MME. Melt density of andesitic magma was assumed to be 2.47 g cm^{-3} (Bottinga and Weill, 1970). Vapor fraction of the system was calculated from solubility of water in melt (Burnham and Jahns, 1962) and density of the vapor phase (Burnham *et al.*, 1969). Density of dacitic to rhyoritic magma is hatched (Murase and McBirney, 1973). As crystallization advances, volatile component was concentrated in the interstitial melt, and is expected to have vesiculated H_2O-rich vapor by second boiling, resulting in reducing the bulk densities of MME as low as that of the host felsic magma.

1.6.4 MME flotation through the felsic magma chamber

Depth of the chamber: The higher-level, shallow emplacement of the Kurobegawa Granite is well indicated by the relatively fine porphyritic texture and the extensively developed miarolitic cavities. From the succession and structure of the Jiigatake Volcanic Rocks, the roof volcanics are 3.5 to 5 km in total thickness (Harayama *et al*, 2003), suggesting that the roof of the pluton crystallized at ~ 0.1 GPa. Based upon the 6 km exposed thickness at the pluton, the depth of the base of the Kurobegawa Granite is therefore inferred to be 10 km (about 0.3 GPa). The *P-T* conditions (0.3 - 0.4 GPa, about 860℃), estimated from the patchy core compositions of zoned euhedral amphibole, likely recorded a depth of the beginning of MME crystallization during ascent through the lower part of the chamber (Wada *et al.*, 2003).

Primarily hydrous nature of original magma of MME: We discuss here H_2O content of the primary mafic magma of MME. Sakuyama (1979) discussed lateral variations of H_2O contents in Quaternary magmas on northeastern Japan based on the presence and absence of hornblende or biotite phenocrysts. In the Kurobegawa MME, amphibole and biotite were crystallized prior to quartz on cooling. This crystallization sequence indicates a high H_2O content of the primary mafic magma (H_2O > 3.5 wt%, based on Robertson and Wyllie, 1971 and Wyllie, 1977), corresponding to the most H_2O rich magmas of the back-arc side in the northeastern Japan by Sakuyama (1979). In the peripheral diorites intruding just before the emplacement of the Kurobegawa Granitic Pluton, mafic silicate phases are dominantly hydrous, indicating the original hydrous nature of the mafic magmas. In the phase assemblages of andesitic to dacitic melt, similar in composition to the MME, a magma crystallizing plagioclase ($\sim An_{50}$) contains more than 4.6 wt% H_2O to stabilize amphibole (Rutherford and Devine, 1988). Water-undersaturated basaltic to andesitic melts have liquidus temperatures between 1050 and 1150℃ at crustal pressures (Green, 1972), higher than those of granitic magmas by a few hundred degrees centigrade. On the other hand, the lower granite commonly contains allanite, and therefore, the crystallizing temperature is indicated to be at least lower than 800℃ (Chesner and Ettlinger, 1989).

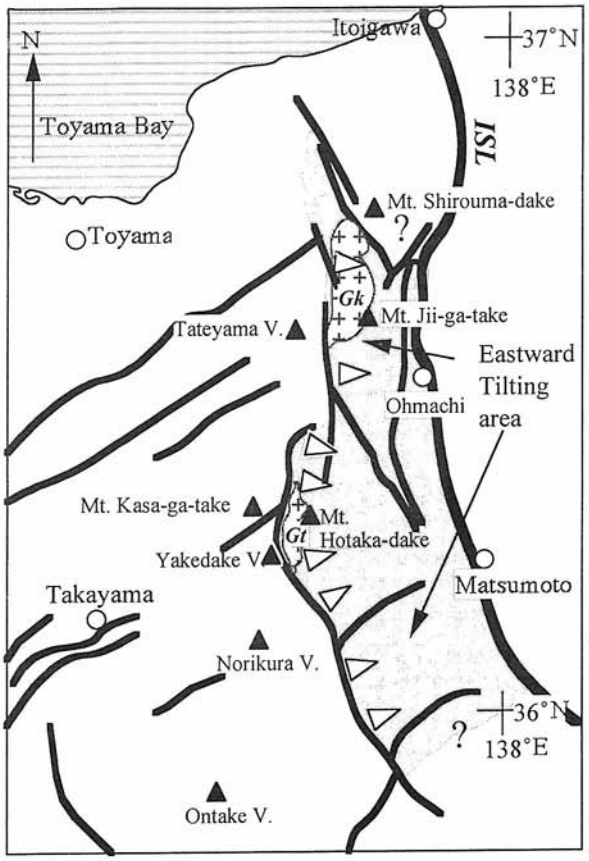

Fig. 12. Pleistocene tilted area in the Northern Japan Alps. Gk: Kurobegawa Granitic Pluton, Gt: Takidani Granodiorite Pluton

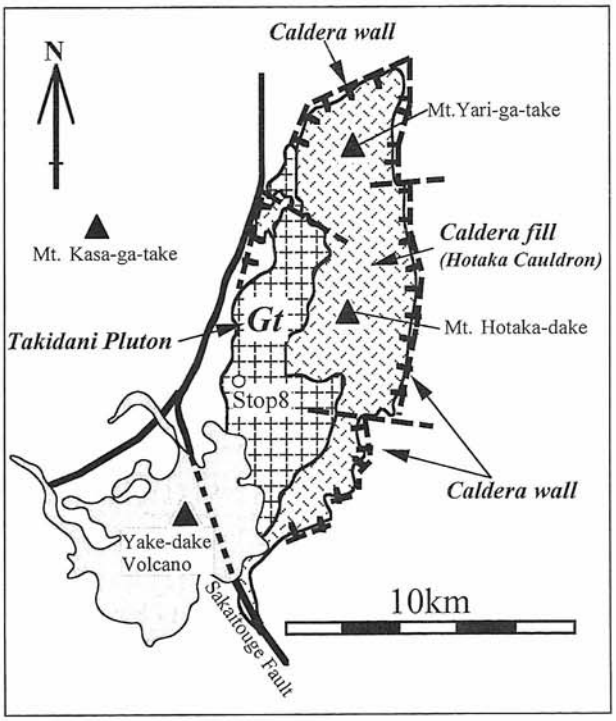

Fig. 13. Generalized geological map of the Hotaka Cauldron and the Takidani Pluton.

Acicular amphibole and plagioclase with a high aspect ratio in MME suggest that mafic magmas crystallized under rapid cooling conditions. The bimodal variation in Cl contents of apatite in MME suggests that mafic magmas lost much of their Cl during crystallization (in prep.). Tsuchiya (1986) explained that such an abrupt decrease in Cl content of apatite indicates H_2O vapor saturation during solidification of magma.

Possibility of MME floating by vapor vesiculation: We here examine the possibility of MME floating through a felsic magma chamber as Figure 11 shows, on the basis of their relative density estimation by Eichelberger (1980). We assumed the H_2O content of the mafic magma to be 5 wt%, according to the estimation by Johnson *et al.* (1994), that basaltic magmas derived from subduction zones have 3 to 6 wt% dissolved H_2O contents.

As crystallization of the acicular crystals proceeded, the crystals likely formed chains and networks, segregating interstitial melt (Philpotts *et al.*, 1998). The volatile component was concentrated in the interstitial melt, and is expected to have vesiculated H_2O-rich vapor by second boiling, resulting in reducing the bulk densities of MME to as low as that of the host felsic magma (Eichelberger, 1980). If felsic magma was also vesiculated, the H_2O bubbles could be removed toward the roof. Instead, bubbles in MME should be trapped in the segregated melt and by the chilled crustal margin of MME. Therefore, this vesiculation causes gravitational instability between MME and felsic magma, resulting in the MME floating through the chamber (Fig. 10C). Additionally, convection of the host magma might disperse MME throughout the chamber if the density difference between MME and the host magma was small. The important role of the H_2O behavior for the MME floating is supported by the field evidence that relatively H_2O-rich MME, indicated by the larger modal content of biotite rather than that of amphibole, are abundant in the shallower level of the Kurobegawa pluton. Eventually, MME might have lost bubbles before they were completely solid, and it is possible that they settled downward into crystal mush. We, however, have no field evidence of MME settling such as load-cast, pipe and tightly packed structures described by Wiebe and Collins (1998) and Wiebe (2001).

2. Takidani Granodiorite and related volcanism: Emplacement, cooling and rapid denudation processes for the Quaternary volcano-pluton (Satoru HARAYAMA)

2.1 Introduction

The Northern Japan Alps (Hida Mountain Range) are typical alpine mountain range with summit levels 3000 m above sea level. Uplifting occurred in two stages, from Late Pliocene to earliest Early Pleistocene, and late Early Pleistocene to Middle Pleistocene (Harayama *et al.*, 2003). Emplacement of felsic magmas (2.3 - 1.5 Ma) into the shallow level crust of island arc caused the first stage uplifting of the Northern Japan Alps, and large volumes of

the magmas erupted as ignimbrites and air-fall tephras from calderas. Shortening tectonics, starting from *ca.* 1.3 Ma in central Japan, made N-S trending reverse faults at the most thinned part of elastic crust above the felsic magmas, and resulted in the eastward tilting (20 - 80°) of the eastern half area of Northern Japan Alps (second stage uplifting) (Fig. 12). The second stage uplifting of the mountain range has tilted the volcano-plutonic complex toward the east (20°) and revealed the volcanic to plutonic cross section (3 km+1.8 km) providing us an excellent opportunity to investigate the temporal and space relation between volcanic and plutonic processes.

2.2 Geology

2.2.1 Hotaka Cauldron

Late Cenozoic volcanic rocks composed of potassic calc-alkaline andesite to rhyolite and subordinate of basalts are exposed in the southern part of the Japan Alps. On the basis of isotopic ages, I divide the volcanic activity into three stages: 2.7 - 1.5 Ma, 0.8 - 0.4 Ma, and 0.27 Ma- present.

The Hotaka Andesite, a volcanic and subvolcanic complex of the first stage activity, was intruded by the Takidani Granodiorite pluton (Fig.13). Previous studies of the geology and petrology of the Hotaka Andesite and Takidani Granodiorite (Harayama,1990; 1992; 1994; Harayama *et al.* 1991) showed that they form a volcano-plutonic complex with close genetic relations. The Hotaka Andesite is composed chiefly of andesitic to dacitic ignimbrites and subordinate lavas, collapse breccias, diorite porphyry sheets, and a granophyre dike. These volcanics accumulated within a volcano-tectonic graben (Hotaka Cauldron) elongated in a north-south direction (Fig.13).

2.2.2 Takidani Granodiorite

The Takidani Granodiorite is to a first approximation a dike-shaped pluton 13 km long and 4 km in maximum width and is situated along the main ridge of the Japan Alps (Fig. 13). The pluton has an area of about 21 km^2 in the highly rugged mountain range, and its vertical exposure ranges from 1450 to 2670 m above sea level. Post emplacement uplift has tilted the pluton and roof rocks toward the east. Thus, the vertical variation in textual and compositions observable from the top to a ~1800 m deeper 1evel below the roof on the western side of the main ridge. The Takidani Granodiorlte intruded Paleozoic greenstones, a Jurassic accretionary complex, and Late Cretaceous to Oligocene granitoids on the western contact and the Early Pleistocene Hotaka Andesite on the east. The plutonic contact has a near vertical dip along the western contact, but the eastern roof contact has a shallow eastward dip (10 - 30°). The andesitic to dacitic ignimbrites have been metamorphosed into hornblende hornfels within ~300 m, and biotite hornfels within ~ 800 m, from the eastern contact.

The Takidani Granodiorite has vertical gradational zoning from equigranular medium-grained biotite-hornblende granodiorite in the deepest part through hornblende-biotite granodiorite to hornblende-bearing porphyritic biotite granite and fine-grained biotite granite at the shallowest level (Fig. 14). SiO_2 contents increase roofward from 65 wt% to 74 wt %, and chemically exhibit typical I-type properties.

2.3 Emplacement and cooling age

Emplacement and solidification of the Takidani Pluton postdated the eruption of the Hotaka Andesite (cauldron), the youngest wall rock and volcanic equivalent of the pluton. Two large-scale eruptions of the Hotaka Cauldron produced thick (1500 m+) intracaldera ignimbrites, outflow sheets, and wide spread air-fall tephras (Fig. 15). The total erupted volume is about 700 km^3. The air-fall tephras in shallow marine sediments have been investigated stratigraphically, and their eruption ages of 1.76 Ma and 1.75 Ma were estimated, respectively (Nagahashi *et al.*, 2000). These ages are important constraints (maximum age) for the final emplacement age of the Takidani Granodiorite, because equivalent ignimbrites in the cauldron were intruded and thermally metamorphosed by the pluton. From these facts, I conclude that the maximum age of final emplacement of the Takidani Granodiorite, as well as the eruption age of the ignimbrites, is restricted to 1.76 Ma.

K-Ar mineral dating, zircon fission-track dating and track length analyses for 14 different depth level specimens (0 - 1700m) from the roof contact were performed (Fig. 16). Specimens just below the roof yield concordant K-Ar hornblende (1.4±0.1 Ma) and biotite (1.30±0.03 Ma) ages, and these ages are also consistent with an ion microprobe U-Pb zircon age (1.36±0.23 Ma; Sano *et al.*, 2002). The above consistency with variable closure temperature methods indicates that the final emplacement age is ~1.4 Ma. Hornblende K-Ar ages (1.5 - 2.8 Ma) show weak positive correlations to the depth from the roof with large divergence, and these ages are mostly older than those of the tephrochronological constraints (1.76 Ma). Thus they are deceptive apparent ages and probably affected by excess ^{40}Ar. In contrast to the above, biotite K-Ar ages (1.30 - 1.03 Ma) show a linear negative correlation to depth, and they are cooling ages reflecting their closure temperatures (400 - 370°C).

2.4 Uplift Tectonics and rapid denudation

Bottomward decrease in the biotite ages (Fig. 16) represents the time of leaving from the zone with plastically deformable temperature, because mylonitizations are widely observed in the Takidani Granodiorite (Harayama *et al.* 2003; Fig. 17) and the fluid inclusion microthermometry for the pluton (Bando *et al.*, 2003) revealed that the temperature of a brittle-plastic transition zone ranges from 480°C to 380°C, nearly equal to the biotite closure temperatures. Zircon fission-track ages are 1.00 - 0.88 Ma, and show no correlations to depth (Fig. 16). As no specimens show shortened fission-tracks, the pluton rapidly passed through the partial annealing zone (330 - 230°C) and reached the shallow and lower temperature zone about 1 Ma. Therefore, the second stage uplifting and tilting of the Northern Japan Alps caused rapid denudation of the Takidani Granodiorite as well as the

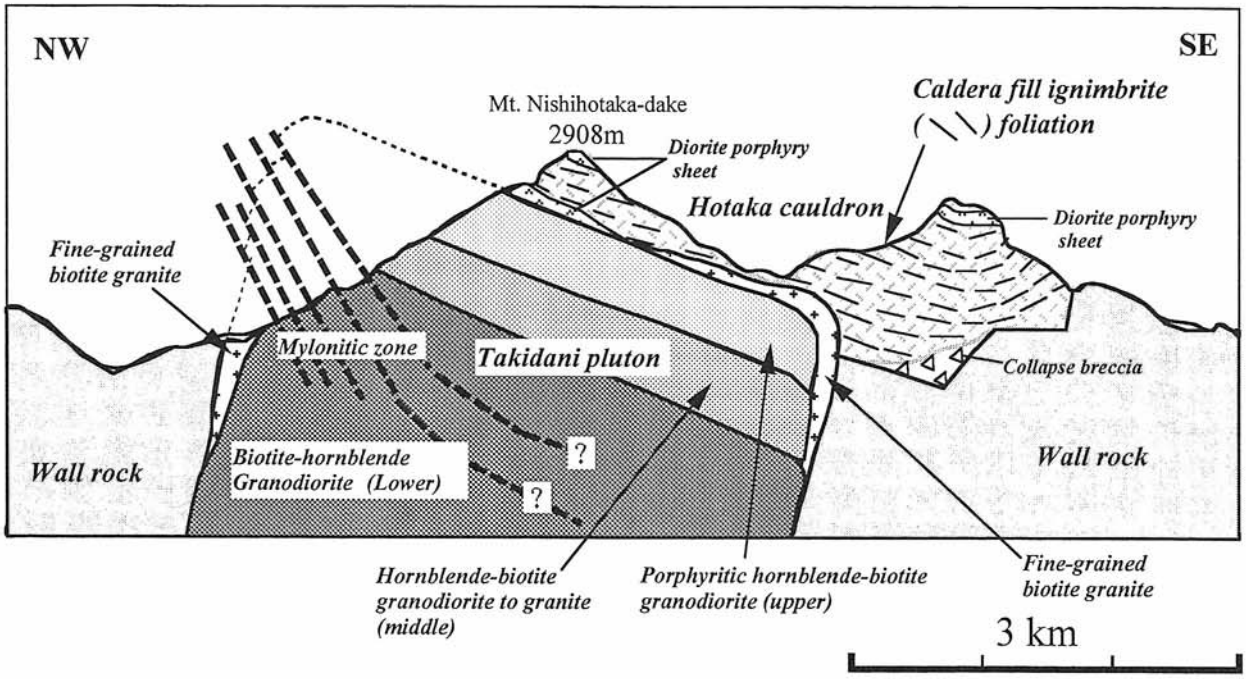

Fig. 14. Schematic geological section of the Takidani Pluton and the Hotaka Cauldron.

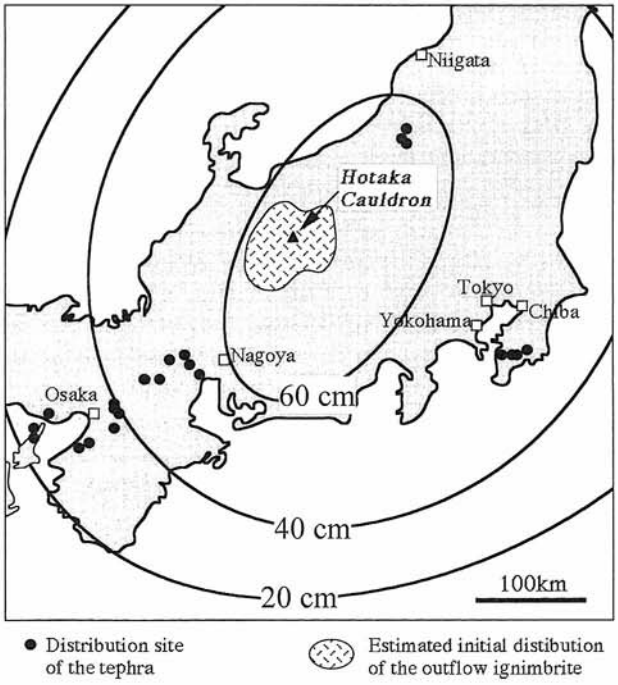

Fig. 15. Outflow ignimbrite and wide spread fall tephra supplied from the Hotaka Cauldron.

Hotaka Cauldron (Fig. 18). The Takidani Granodiorite is unconformably overlain by third stage volcanics (~ 0.1 Ma). However, basal conglomerates of second stage volcanics (~ 0.65 Ma) contain no granodiorite fragments other than thermally metamorphosed clasts of the ignimbrites of Hotaka Cauldron (Harayama, 1990). This suggests that the pluton was first exposed at the surface during Middle Pleistocene time.

3. Excursion

Day 1. (August 28) The Jiigatake Volcanic Rocks

Stop 1: Rhyolite lava, hyaloclastite and stratified clastic sediment of the Jiigatake Volcanic Rocks

The sediment, as well as flow structure of the rhyolite lava, exhibits very steep bedded structure (N32°E 74°E). These volcanic rocks ponded in the Jiigatake Cauldron (*ca.* 2 Ma), and together with the Kurobegawa Pluton, were tilted to the East by second stage uplifting of the Northern Japan Alps after the late Early Pleistocene (1.3 Ma -) (Fig. 19).

Day 2. (August 29) The Kurobegawa Granitic Pluton and the Jiigatake Volcanic Rocks

Stop 2: The boundary between rhyolite welded tuff of the Jiigatake Volcanic Rocks and the upper granite of the Kurobegawa Granitic Pluton at Ohgisawa

The pluton intrudes the Pliocene Jiigatake Volcanic Rocks at the south and east margin and contact metamorphism effects are observable. The granite becomes leucocratic and contains no enclaves at the contact. Elliptic MME with major axis of 10 cm to 2 m appear away from the contacts. MME commonly show quenched textures and often have chilled margin against the host granite. Mixing occasionally occurs restrictedly on a small scale around MME (Figs. 20, 21).

Stop 3: The middle unit of the Kurobegawa Granitic Pluton at Bogoyazawa.

In the middle unit, the contacts between the lower and the upper granites are sharp and truncated. There is no thermal recrystallization in both the granites. MME are in sharp

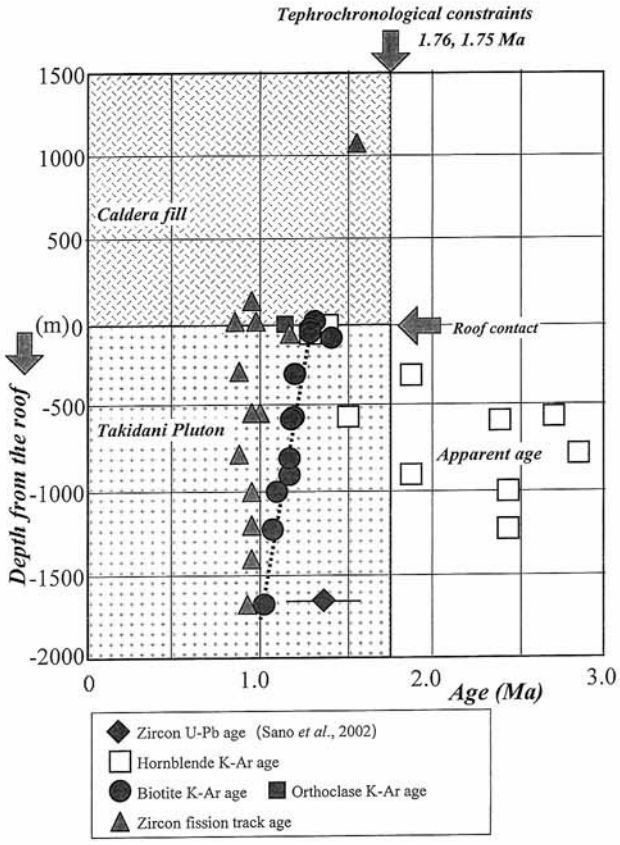

Fig.16. Depth from the roof contact vs. radiometric age of minerals.

contact with the lower and the upper granite. MME are sometimes fringed with the lower granite (Fig. 22).

Stop 4: The middle unit of the Kurobegawa Granitic Pluton at Sakuro.

The occurrence is similar to that of Stop 3 (Figs. 23, 24). See the explanation of Stop 3.

Day 3. (August 30) The Kurobegawa Granitic Pluton

Stop 5: The Jujikyo diorite and the lower granite of the Kurobegawa Granitic Pluton at Sen-nin Dam.

The Jujikyo diorite (medium-grained equigranular biotite hornblende diorite) is intruded by the lower granite (Fig. 25). But the diorite hardly shows a contact aureole. The lower granite here rarely contains the MME while the Jujikyo diorite contains Permian metamorphic rocks as xenoliths and also MME.

Day 4. (August 31) The Kurobegawa Granitic Pluton

Stop 6: The hybrid unit of the Kurobegawa Granitic Pluton at Babadani (Fig. 26).

This unit densely contains MME ranging 10 cm to 2 m in major axis. Generally, chilled crust develops in various degrees in the outermost part of MME. No plagioclase and quartz phenocrysts are found in the area surrounded by the well-developed quenched crust, whereas they are often injected into the interior of MME bounded by very weakly developed chilled margin. Plagioclase and quartz phenocrysts

Fig. 17. Mylonitic texture in the Takidani Pluton.

are enveloped in MME and sometimes seem to be connected with the crystal mush of the exterior (Fig. 27).

Stop 7: The hybrid unit of the Kurobegawa Granitic Pluton at Jijidani.

This granodiorite to granite unit shows a fine- to medium-grained, heterogeneous texture (Fig. 28). The modal proportion of plagioclase and quartz phenocrysts varies in places, This unit is characterized by two contrasting types of biotite occurrence in addition to ovoidal quartz and plagioclase phenocrysts. Typical quartz-amphibole/biotite ocelli are often developed in the fine-grained matrix. Blade-shaped biotite is scattered in the matrix consisting of fine plagioclase, K-feldspar and quartz.

Day 5. (September 1) Takidani Granodiorite and Hotaka Cauldron

Stop 8: Looking northeastward at the roof contact of the volcano-pluton.

The roof contact line between the Takidani Granodiorite and Hotaka Andesite (cauldron) on the western side of the Mt. Nishihotaka-dake, looking northeast from the Nishihotaka-guchi ropeway station (Fig. 29). Mylonitic deformation resulted from the postemplacement tilting are observable on the opposite ridge, and are also recognized widely in the western lower part of the Takidani Pluton.

Outcrops around the station represent the lower facies of the Takidani Granodiorite (equigranular biotite-hornblende granodiorite).

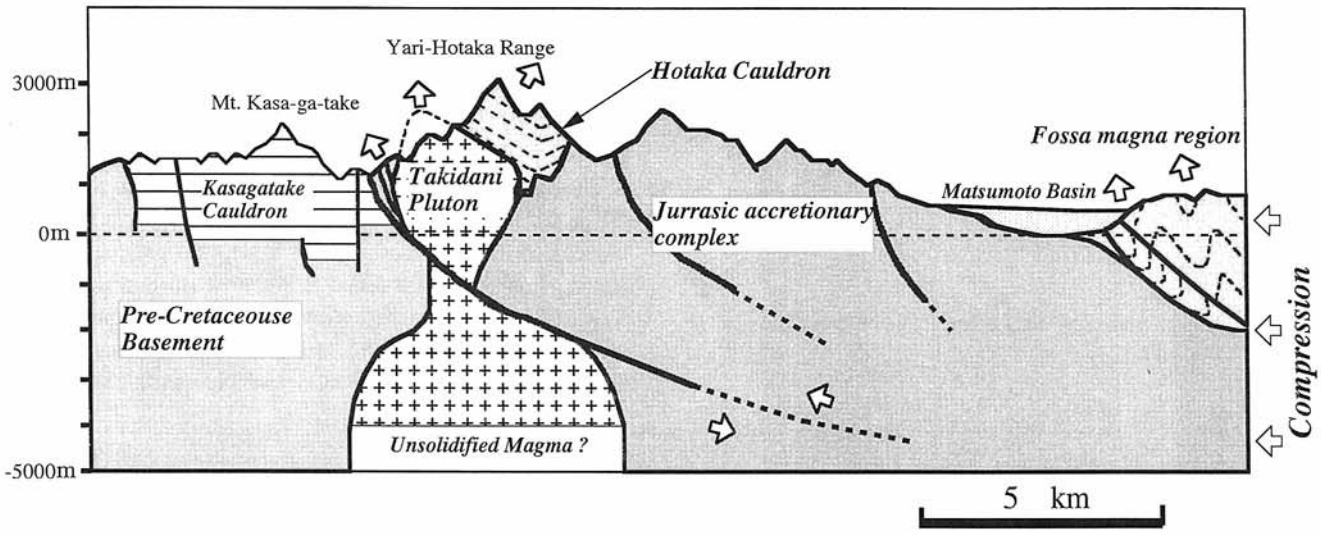

Fig. 18. Pleistocene uplifting and tilting in the southern part of the Northern Japan Alps.

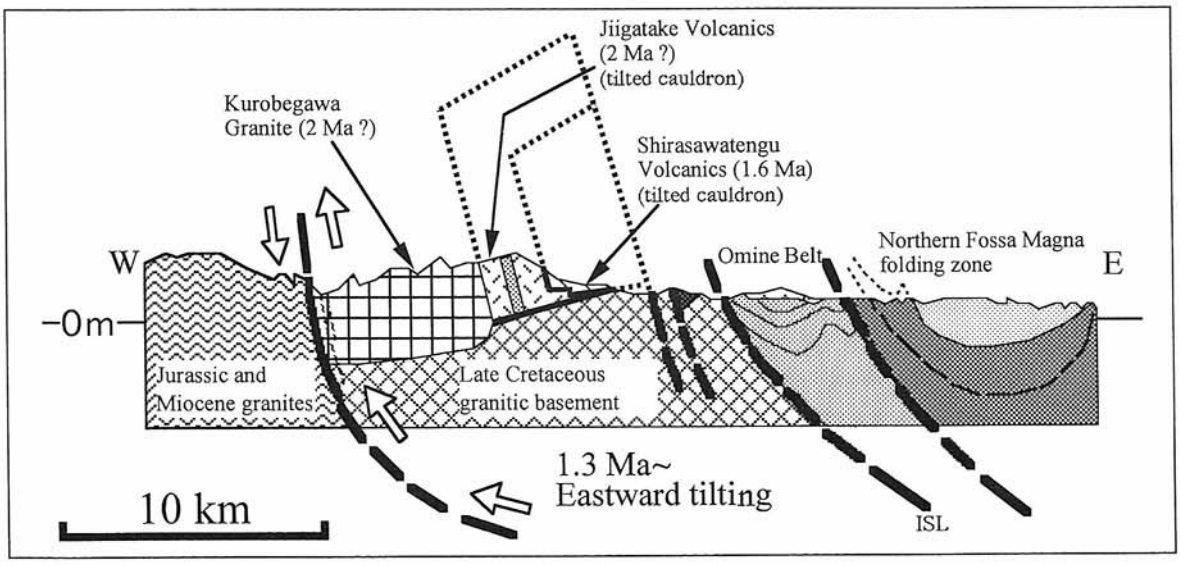

Fig. 19. Schematic geological E-W section of the area of the Kurobegawa Granitic Pluton.

Fig. 20. Photograph of the roof contact between rhyolite welded tuff of the Jiigatake Volcanic Rocks and the upper granite of the Kurobegawa Granitic Pluton at Ohgisawa.

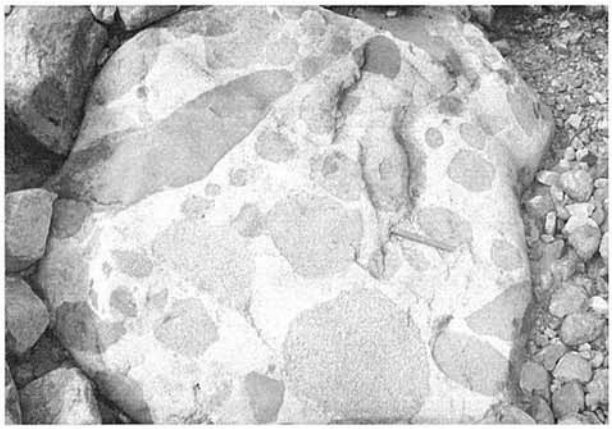

Fig. 21. Photograph of MME in the Kurobegawa Granitic Pluton in a stream bed boulder at Ohgisawa.

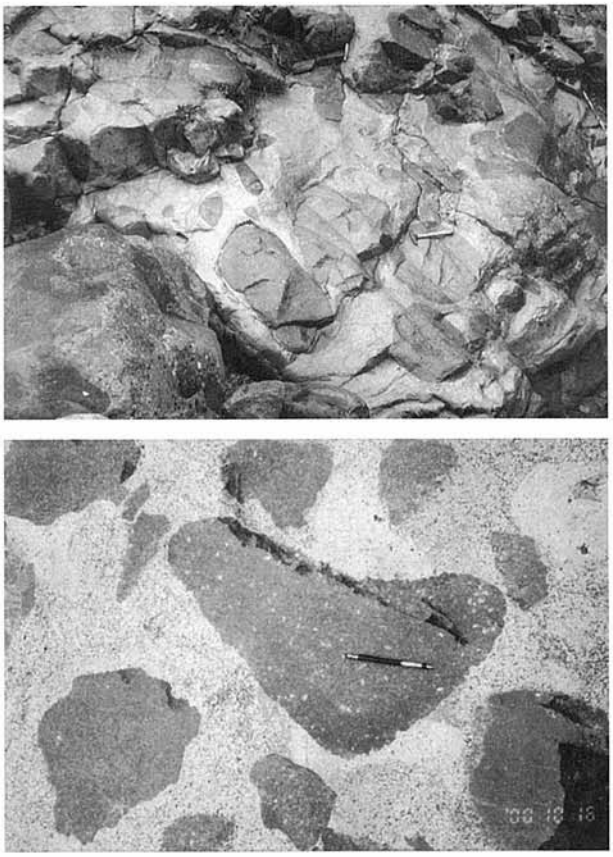

Fig. 22. (upper) Photograph of the middle unit of the Kurobegawa Granitic Pluton at Bogoyazawa.
(lower) Photograph of the middle unit of the Kurobegawa Granitic Pluton at Higashidani.

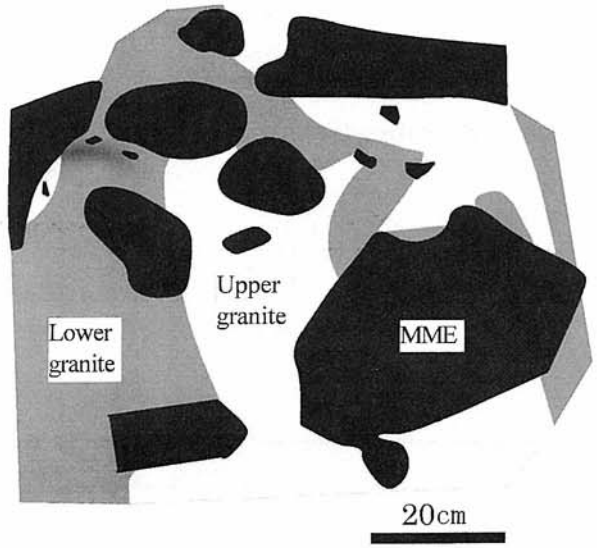

Fig. 23. The middle unit of the Kurobegawa Granitic Pluton at Sakuro.

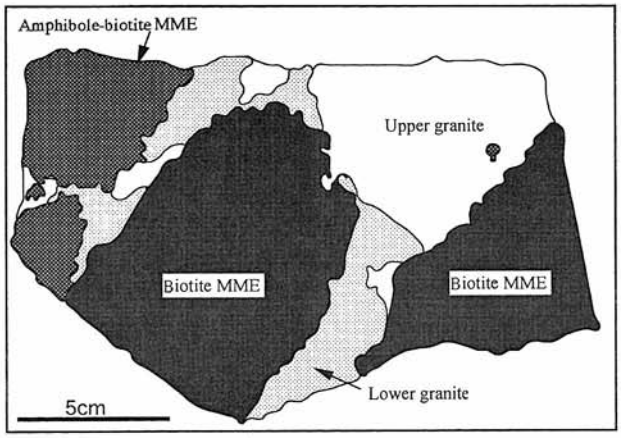

Fig. 24. Sketch of a sawn and polished slab of the middle unit of the Kurobegawa Granitic Pluton.

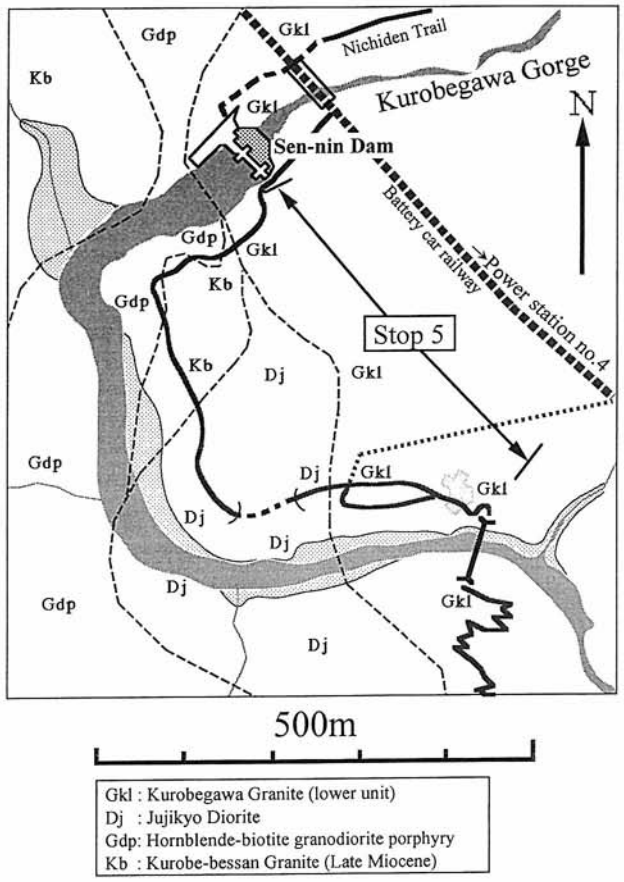

Fig. 25. Geological map of the Sen-nin dam area.

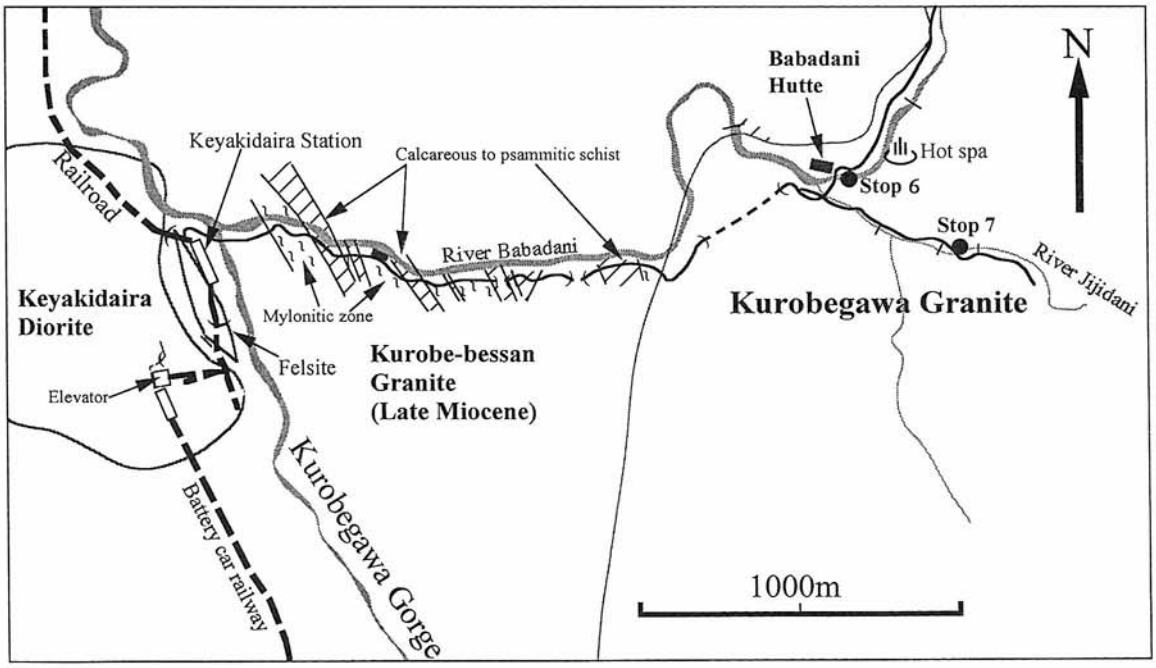

Fig. 26. Geological map of the Babadani area.

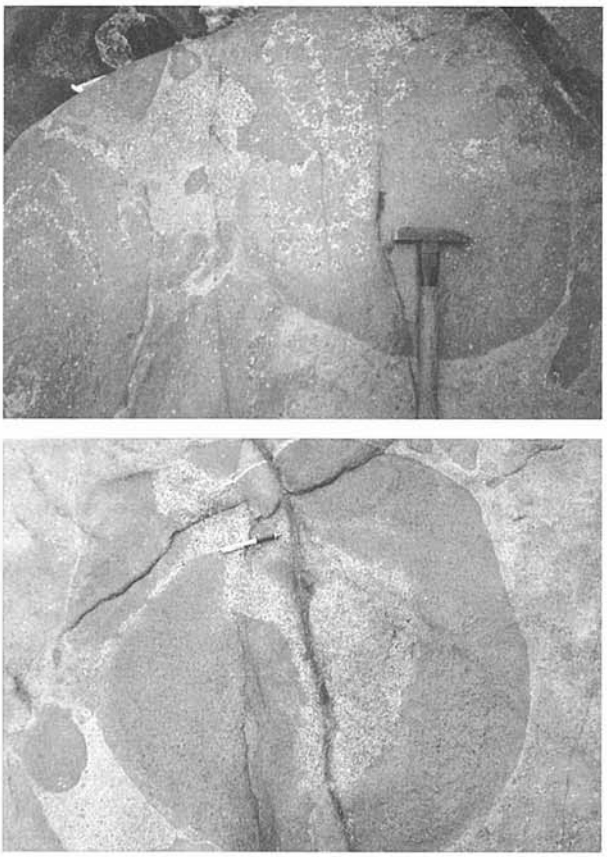

Fig. 27. (upper) Photograph of MME in the hybrid unit of the Kurobegawa Granitic Pluton at Babadani.
(lower) Photograph of MME in the hybrid unit of the Kurobegawa Granitic Pluton at Babadani.

Fig. 28. Photograph of the hybrid unit of the Kurobegawa Granitic Pluton at Jijidani.

Fig. 29. Roof contact between the Takidani Granodiorite and the roof volcanic rocks (Hotaka Cauldron). Mylonitic deformation resulted from the postemplacement tilting is widely recognized in the Takidani Pluton.

References

Bachl, C. A., Miller, C. F., Miller, J. S. and Faulds, J. E. (2001) Construction of a pluton: Evidence from an exposed cross section of the Searchlight pluton, Eldorado Mountains, Nevada. *Bull. Geol. Soc. Amer.*, **113**, 1213-1228.

Bando, M., Bignall, G., Sekine, K. and Tsuchiya N. (2003) Petrography and uplift history of the Quaternary Takidani Granodiorite: could it have hosted a supercritical (HDR) geothermal reservoir? *Jour. Volcanol. Geotherm. Res.*, **120**, 215-234.

Bergantz, G. W. (1999) On the dynamics of magma mixing by reintrusion: implications for pluton assembly processes. *Jour. Struct. Geol.*, **22**, 1297-1309.

Bindeman, I.N. and Bailey, J.C. (1994) A model of reverse differentiation at Dikii Greben' Volcano, Kamchatka: progressive basic magma vesiculation in a silicic magma chamber. *Contrib. Mineral. Petrol.*, **117**, 263-278.

Blake, S. and Fink, J. H. (2000) On the deformation and freezing of enclaves during magma mixing. *Jour. Volcanol. Geotherm. Res.*, **95**, 1-8.

Bottinga, Y. and Weill, D. F. (1970) Densities of liquid silicate systems calculated from partial molar volumes of oxide components. *Amer. Jour. Sci.*, **269**, 169-182.

Burnham, C.W. and Jahns, R.H. (1962) A method for determining the solubility of water in silicate melts. *Amer. Jour. Sci.*, **260**, 721-745.

Burnham, C. W., Holloway, J. R. and Davis, N. F. (1969) Thermodynamic properties of water to 1000°C and 10000 bars. *Geol. Soc. Amer. Spec. Pap.*, **132**, 1-96.

Chesner, C. A. and Ettlinger, A. D. (1989) Composition of volcanic allanite from the Toba Tuffs, Sumatra, Indonesia. *Amer. Mineral.*, **74**, 750-758.

Collins, W. J., Richards, S. R., Healy, B. E. and Ellison, P. I. (2000) Origin of heterogeneous mafic enclaves by two-stage hybridization in magma conduits (dykes) below and in granitic magma chambers. *Trans. Roy. Soc. Edinburgh, Earth Sci.*, **91**, 27-45.

Couch, S., Sparks, R. S. J. and Carroll, M. R. (2001) Mineral disequilibrium in lavas explained by convective self-mixing in open magma chambers. *Nature*, **411**, 1037-

1039.

Eichelberger, J. C. (1980) Vesiculation of mafic magma during replenishment of silicic magma reservoirs. *Nature*, **288**, 446-450.

Ernst, W. G. and Liu, J. (1998) Experimental phase-equilibrium study of Al- and Ti-contents of calcic amphibole in MORB - A semiquantitative thermobarometer. *Amer. Mineral.*, **83**, 952-969.

Green, T. H. (1972) Anatexis of mafic crust and high pressure crystallization of andesite. *In* Thorpe, R. S., ed., *Andesites: Orogenic andesites and related rocks.*, Wiley, Chichester, 465-487.

Harayama, S. (1990) *Geology of the Kamikochi district. With Geological Sheet Map at 1:50,000*. Geol. Surv. Japan, 175 p. *

Harayama, S. (1992) Youngest exposed granitoid pluton on Earth: Cooling and rapid uplift in the Pliocene-Quaternary Takidani Granodiorite in the Japan Alps, central Japan. *Geology*, **20**, 657-660.

Harayama, S. (1994) Cooling history of the youngest exposed pluton in the World - The Plio-Pleistocene Takidani Granodiorite (Japan Alps, central Japan) -. *Mem. Geol. Soc. Japan*, no.43, 87-97. *

Harayama, S., Takeuchi, M., Nakano, S., Sato, T. and Takizawa, F. (1991) *Geology of the Yarigatake district. With Geological Sheet Map at 1:50,000*. Geol. Surv. Japan, 190 p. *

Harayama, S., Takizawa, F., Kato, H., Komazawa, M., Hiroshima, T. and Sudo, S. (1995) *Geological map of Japan 1:200,000, Toyama*. Geol. Surv. Japan.

Harayama, S., Takahashi, Y., Nakano, S., Kariya, Y. and Komazawa, M. (2000) *Geology of the Tateyama district. With Geological Sheet Map at 1:50,000*. Geol. Surv. Japan, 218 p. *

Harayama, S., Ohyabu, K., Miyama, Y., Adachi, H. and Shukuwa, R. (2003) Eastward tilting and uplifting after the late Early Pleistocene in the eastern-half area of Hida Mountain Range. *Quatern. Res.*, **42**, 127-140.*

Hibbard, M. J. (1991) Textural anatomy of twelve magma-mixed granodiorite systems. *In* Didier, J., and Barbarin B., eds., *Enclaves and granite petrology. Developments in petrology 13*, Elsevier, Amsterdam, 431-444.

Huppert, H.E. and Sparks, R. S. J. (1989) Chilled margins in igneous rocks. *Earth Planet. Sci. Lett.*, **92**, 397-405.

Ishizawa, K. (1982) Geology of the igneous rocks in the Mt. Kashimayarigatake-Mt. Eboshidake area, Hida Mountains, central Japan. *Jour. Geol. Soc. Japan*, **88**, 215-230.*

Johnson, M. C., Anderson, A. T., Jr. and Rutherford, M. J. (1994) Pre-eruptive volatile contents of magmas. *In* Carroll, M. and Holloway, J., eds., *Volatiles in Magmas.* Mineral. Soc. Amer. Rev. Mineral., **30**, 281-330.

Kato, H., Sato, T., Mimura, K. and Takizawa, F. (1989) *Geology of the Omachi district. With Geological Sheet map at 1:50,000*. Geol. Surv. Japan, 111 p. *

Marsh, B. D. (1996) Solidification fronts and magmatic evolution. *Mineral. Mag.*, **60**, 5-40.

Murase, T. and McBirney, A. (1973) Properties of some common igneous rocks and their melts at high temperatures. *Bull. Geol. Soc. Amer.*, **84**, 3563-3592.

Nagahashi, Y., Satoguchi, Y. and Yoshikawa, S. (2000) Correlation and stratigraphic eruption age of the pyroclastic flow deposits and wide spread volcanic ashes intercalated in the Pliocene-Pleistocene strata, central Japan. *Jour. Geol. Soc. Japan*, **106**, 51-69. *

Nakada, S. and Motomura, Y. (1997) Magma chamber of Unzen Volcano and origin of phenocrysts and enclaves. *Bull. Volcanol. Soc. Japan*, **42**, 167-174.*

Nakano, S., Takeuchi, M., Yoshikawa, T., Nagamori, H., Kariya, Y., Okumura, K. and Taguchi, Y. (2002) *Geology of the Shiroumadake district. With Geological Sheet Map at 1:50,000*. Geol. Surv. Japan, 105 p. *

Nishimura, S. and Mogi, T. (1986) The interpretation of discordant ages of some granitic bodies. *Jour. Geotherm. Res. Soc. Japan*, **8**, 145-164.

Philpotts, A. R., Shi, J. and Brustman, C. (1998) Role of plagioclase crystal chains in the differentiation of partly crystallized basaltic magma. *Nature*, **395**, 343-346.

Robertson, J. K. and Willey, P. J. (1971) Rock-water systems, with special reference to the water-deficient region. *Amer. Jour. Sci.*, **271**, 252-277.

Rutherford, M. J. and Devine, J. D. (1988) The May 18, 1980, eruption of Mount St. Helens, 3, Stability and chemistry of amphibole in the magma chamber. *Jour. Geophys. Res.*, **93**, 11949-11959.

Sakuyama, M. (1979) Lateral variations of H_2O contents in Quaternary magmas of northeastern Japan. *Earth Planet. Sci. Lett.*, **43**, 103-111.

Sano, Y., Tsutsumi, Y., Terada, K. and Kaneoka, I. (2002) Ion microprobe U-Pb dating of Quaternary zircon: implication for magma cooling and residence time. *Jour. Volcanol. Geotherm. Res.*, **117**, 285-296.

Sato, H. (1975) Diffusion coronas around quartz xenocrysts in andesite and basalt from Tertiary volcanic region in northeastern Shikoku, Japan. *Contrib. Mineral. Petrol.*, **50**, 49-64.

Sparks, R. S. J. and Marshall, L. (1986) Thermal and mechanical constraints on mixing between mafic and felsic magmas. *Jour. Volcanol. Geotherm. Res.*, **29**, 99-124.

Streckeisen, A. (1976) To each plutonic rock its proper name. *Earth Sci. Rev.*, **12**, 1-33.

Tepley, F. J. III, Davidson, J. P. and Clynne, M. A. (1999) Magmatic interactions as recorded in plagioclase phenocrysts of Chaos Crags, Lassen Volcanic Center, California. *Jour. Petrol.*, **40**, 787-806.

Thomas, N., Tait, S. and Koyaguchi, T. (1993) Mixing of stratified liquids by the motion of gas bubbles: application to magma mixing. *Earth Planet. Sci. Lett.*, **115**, 161-175.

Troll, V. R. and Schmincke, H.-U. (2002) Magma mixing and crustal recycling recorded in ternary feldspar from compositionally zoned peralkaline ignimbrite 'A', Gran Canaria, Canary Islands. *Jour. Petrol.*, **43**, 243-270.

Tsuchiya, N. (1986) Cl and F contents of apatite in the

Matsumae plutonic rocks, southwestern Hokkaido, Japan: A useful indicator of vapor saturation. *Jour. Japan. Assoc. Mineral. Petrol. Econ. Geol.*, **81**, 67-76.

Tsuchiyama, A. (1985) Dissolution kinetics of plagioclase in the melt of the system diopside-albite-anorthite, and origin of dusty plagioclase in andesites. *Contrib. Mineral. Petrol.*, **89**, 1-16.

Uchiumi, S., Harayama, S. and Uto, K. (1995) K-Ar dating on age-unknown rocks in the 1:200,000 quadrangle, Toyama. *Bull. Geol. Surv. Japan*, **46**, 375-381.*

Wada, H., Harayama, S. and Yamaguchi, Y. (2003) Mafic enclaves densely concentrated in the upper part of the vertically zoned felsic magma chamber: The Kurobegawa Granitic Pluton, Hida Mountain Range, Central Japan. *Bull. Geol. Soc. Amer.*, (in press).

Wiebe, R. A. (1974) Coexisting intermediate and basic magmas, Ingonish, Cape Breton Island. *Jour. Geol.*, **82**, 74-87.

Wiebe, R. A. and Collins, W. J. (1998) Depositional features and stratigraphic sections in granitic plutons: implications for the emplacement and crystallization of granitic magma. *Jour. Struct. Geol.*, **20**, 1273-1289.

Wiebe, R. A., Frey, H. and Hawkins, D. P. (2001) Basaltic pillow mounds in the Vinalhaven intrusion, Maine. *Jour. Volcanol. Geotherm. Res.*, **107**, 171-184.

Williams, Q. and Tobisch, O. T. (1994) Microgranitic enclave shapes and magmatic strain histories: Constraints from drop deformation theory. *Jour. Geophys. Res.*, **99**, 24359-24368.

Wones, D. R. (1989) Significance of the assemblage titanite+magnetite+quartz in granitic rocks. *Amer. Mineral.*, **74**, 744-749.

Wyllie, P.J. (1977) Crystal anatexis: An experimental review. *Tectonophysics*, **43**, 41-71.

Wyllie, P. J., Cox, K.G. and Biggar, G. M. (1962) The habit of apatite in synthetic systems and igneous rocks. *Jour. Petrol.*, **3**, 238-242.

Yamada, N., Nozawa, T., Harayama, S., Takizawa, F. and Kato, H. (1988) *Geological map of Japan 1:200,000, Takayama*. Geol. Surv. Japan.

Yamada, R. and Harayama, S. (1999) Fission track and K-Ar dating on some granitic rocks of the Hida Mountain Range, Central Japan. *Geochem. Jour.*, **33**, 59-66.

* In Japanese with English abstract.

Received May 20, 2003
Accepted July 10, 2003

Hutton Symposium V, Field Guidebook
Geological Survey of Japan, Interim-Report no.28, p.23－40, 2003

Trip A2

Mid-Cretaceous plutono-metamorphic complex of the Ryoke and San-yo zones in the Iwakuni-Yanai district, SW Japan

Takamoto OKUDAIRA[1], Masaki YUHARA[2], Takeshi IKEDA[3] and Takashi NAKAJIMA[4]

Abstract: The trip will illustrate the cross-section of the Ryoke plutono-metamorphic belt from the non-metamorphic to high-grade (lower granulite facies) rocks. The Ryoke metamorphic belt is a typical low-pressure/high-temperature metamorphic belt formed at a convergent plate margin, and the emplacement mechanisms and geochemical characteristics of the granites of the San-yo and Ryoke zones changed systematically with metamorphic grade. The Older Ryoke granite sheets occur only in the high-grade zones, and they have been considered to be the heat source of the regional Ryoke metamorphism, whereas the San-yo and Younger Ryoke batholiths, with narrow contact aureoles, have huge volume but their thermal effect was local. To understand the mutual relation between regional low *P/T* metamorphism and plutonism at a convergent plate margin, we will examine successively both the metamorphic and granitic rocks at the same crustal depth from shallow to deep crustal levels.

Key words: Cretaceous, field excursion, Hutton symposium, Iwakuni-Yanai district, Plutono-metamorphic complex, Ryoke metamorphic belt, Ryoke and San-yo zones, SW Japan

1. Introduction

Active convergent plate margins are one of the most important granite-forming sites. Before the opening of the Japan Sea during the Miocene, the Japanese Islands were a part of the Eurasian continental margin. The Cretaceous-Paleogene granitoids are exposed all over SW Japan from Kyushu to central Japan, extending for nearly 800 km and is similar in size to that of the Sierra Nevada and Peninsular Ranges batholiths in western North America. As shown in Fig. 1, the Inner Zone defined as a zone on the continental side of the Median Tectonic Line of SW Japan is generally divided, based on granitoids and related mineralizations, into the following three granitoid zones from south to north:

- Ryoke zone with no associated mineral deposits, located along the Seto Inland Sea;
- San-yo zone, with tungsten (copper, etc.) deposits;
- San-in zone, with molybdenum deposits, located along the Japan Sea.

This classification originated from the Kinosaki's (1952) ore provinces and it was refined from the viewpoint of granite mineralogy by Ishihara (1977) with his new categorization of ilmenite-series and magnetite-series. Most granitoids in the San-in zone are of magnetite-series and those from the San-yo and the Ryoke zones are of ilmenite-series. These three zones are not tectonically juxtaposed suspect terranes, but a geologically continuous single unit, because the granitoids of different zones are in intrusive contact. Across-arc variation of the granitoids from San-in, San-yo and Ryoke zones has been studied well, such as magnetic susceptibility (Kanaya and Ishihara, 1973), oxygen isotopes (Honma and Sakai, 1976) and Sr-Nd isotopes (Kagami *et al.*, 1992). Kagami *et al.*(1992) noted the low Sr*I* (= initial $^{87}Sr/^{86}Sr$ isotopic ratio) and high εNd in the San-in zone, middle Sr*I* and εNd in the San-yo zone, and high Sr*I* and low εNd in the Ryoke zone in the Chugoku district. However, this isotopic zonal distribution is likely to be unclear in the other districts of SW Japan (Nakajima, 1996).

Granitoids of the first two zones show similar ages of emplacement (mid-Cretaceous), whereas the San-in granitoids are younger (early Paleogene). It means that the San-yo and Ryoke granitoids constitute a part of the Cretaceous Circum-Pacific granite belt, on the other hand the San-in granitoids may reflect the different tectonic setting of post-Cretaceous rift-drift history of microplates in northwestern Pacific rim. Actually, the age of the youngest San-in granitoid overlaps even the reconnaissance stage of the opening of the Japan Sea. Therefore, it seems better to concentrate our target to the San-yo and the Ryoke granitoids for discussing the Cretaceous granitic magmatism of SW Japan without the noise of post-Cretaceous activity.

Characteristics of the first two granitoid types are summarized in Table 1. Based on their geochemical characteristics, the San-yo and Ryoke granitoids are cogenetic, and they can be called as the Ryoke - San-yo series (Moutte and Iiyama, 1984). Although not well constrained, based on the Al-in-hornblende barometer, the depth of emplacement of granitoids was >400 MPa in the Ryoke zone and <400 MPa in the San-yo zone (Takahashi, 1993). Pressure estimation of associated metamorphic rocks gave similar results as that of the granitoids

[1]Department of Geosciences, Osaka City University, Osaka 558-8585, Japan. E-mail: oku@sci.osaka-cu.ac.jp
[2]Department of Earth System Sciences, Fukuoka University, Fukuoka 814-0180, Japan. E-mail: yuhara@fukuoka-u.ac.jp
[3]Department of Earth and Planetary Sciences, Kyushu University, Fukuoka 812-8581, Japan. E-mail: ikeda@geo.kyushu-u.ac.jp
[4]Geological Survey of Japan, Tsukuba 305-8567, Japan. E-mail: tngeoch.nakajima@aist.go.jp

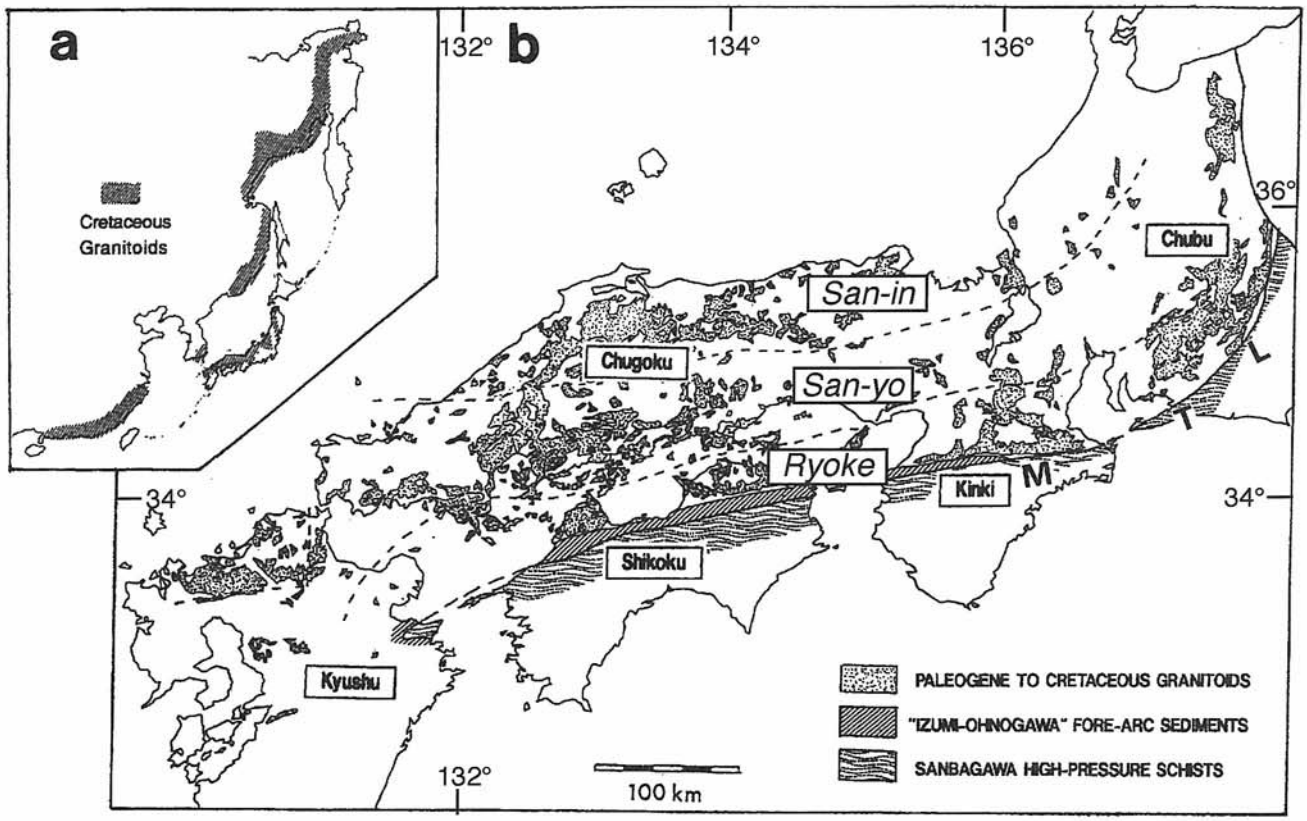

Fig. 1 (a) Cretaceous granitic provinces in the NW Pacific rim including the Japanese Islands. (b) Three granitic provinces in SW Japan (Nakajima, 1996). MTL denotes the Median Tectonic Line, a large strike-slip fault which runs through the center of SW Japan along the arc trend.

Table 1 Characteristics of the granitoids of the San-yo and Ryoke zones, based on Moutte and Iiyama (1984) and Kagami *et al.* (1992).

	San-yo zone	Ryoke zone	
		Younger granitoids	Older granitoids
level of emplacement	shallow (< 0.4 GPa)	intermediate (~ 0.4 GPa)	deep (> 0.4 GPa)
volume	batholith	stock	sill
lithology	massive to porphyritic	gneissose to massive	gneissose
relation with host rock	discordant	discordant	concordant
enclaves	very rare	some	many
major rock type	adamellite + aplite	granodiorite + granite + diorite	granodiorite + tonalite + diorite
mean SiO_2 (wt%)	65 - 75	65 - 75	60 - 70
I/S type	I type	I type	I type
opaque mineral	Ilm > Mt	Ilm >> Mt	Ilm >> Mt
ore deposit	W	none	none
$\delta^{18}O$ quartz	9 - 10‰	12 - 14‰	13 - 15‰
$^{87}Sr/^{86}Sr$ initial ratio	0.706-0.708	0.707-0.709	
Sr (ppm)	12-538 (mean: 176)	13-410 (mean: 203)	

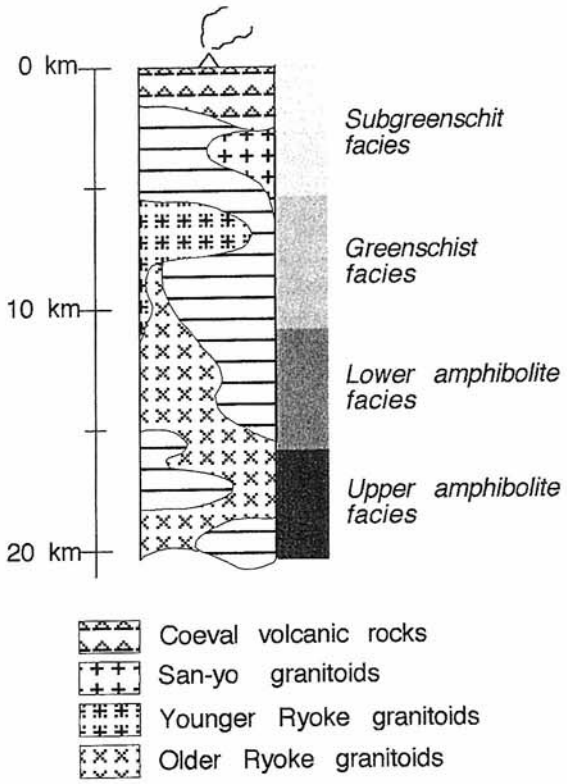

Fig. 2 Schematic cross-section from the San-yo to Ryoke zones exhibiting a crustal cross section down to middle crustal level.

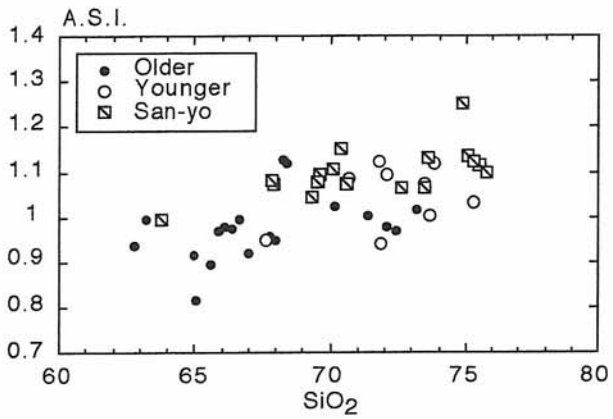

Fig. 3 Positive correlation between ASI and SiO_2 content of the granitoids of the San-yo and Ryoke zones in the Iwakuni-Yanai district. Data source: Honma (1974), Moutte (1990) and Owada *et al.* (1995).

(Ikeda, 2003).

Since early days, Ryoke granitoids have been divided into two groups: Younger Ryoke granitoids and Older Ryoke granitoids. The Younger Ryoke granitoids are nearly unfoliated and intruded as relatively small stock-like bodies cross-cutting the general structure of the weakly-metamorphosed host rocks, whereas the Older Ryoke granitoids are foliated and occur as sheet-like bodies intruding high-grade gneisses concordantly to their gneissose structure. Similar to the Younger Ryoke granitoids, the San-yo granitoids are unfoliated and occur as batholithic large bodies emplaced in the unmetamorphosed sedimentary rocks. This geological succession from the San-yo to Ryoke zones exhibits a crustal cross section down to middle crustal level (Nakajima, 1994, 1996; Fig. 2). This is a part of the Circum-Pacific Cordilleran-type orogenic belt formed at an ancient arc-trench system or active continental margin (*e.g.* Miyashiro, 1994; Nakajima, 1994; Brown, 1998; Okudaira *et al.*, 2000).

For the San-yo and Ryoke granitoids, the aluminium saturation index (ASI) and SiO_2 show a positive correlation (Fig. 3) with other I-type granitoids in the world (Nakajima, 1996), implying that the major source of these granitoids are mafic magmatic rock or its metamorphosed equivalent, as also suggested by Kagami *et al.* (1992). Kutsukake (2002) showed REE pattern of the I-type granitoids (Fig. 4) and discussed that they were generated by the dehydration melting of amphibolite or hydrous melting of tholeiite at 1 GPa or higher pressure. Furthermore, these granitoids are designated as arc-type granitoids in terms of minor element chemistry (Kagami *et al.*, 1992; Kutsukake, 1993, 2002; Nakajima, 1996; Fig. 5). On the initial εSr vs. εNd diagram, the Ryoke granitoids are plotted in high Sr*I* and low εNd region (Yuhara *et al.*, 2000; Fig. 6), and the contribution of upper crustal recycled materials seems to be small (Kagami *et al.*, 1992).

The Ryoke granitoid zone is equivalent to the low-*P*/high-*T* Ryoke metamorphic belt which has been considered to be a typical example of Miyashiro's (1961) low-*P* facies series or andalusite-sillimanite type. The Ryoke metamorphic belt and the high-*P* Sambagawa metamorphic belt are typical example of paired metamorphic belt, (*e.g.* Miyashiro, 1961, 1994). They are considered to have formed at different *P-T* conditions and geological settings. The former formed beneath volcanic arc or fore arc at a depth of 15-20 km, whereas the latter formed near trench zone at *ca.* 30 km deep (*e.g.* Miyashiro, 1994; Iwamori, 2000; Okudaira *et al.*, 2000). The process of

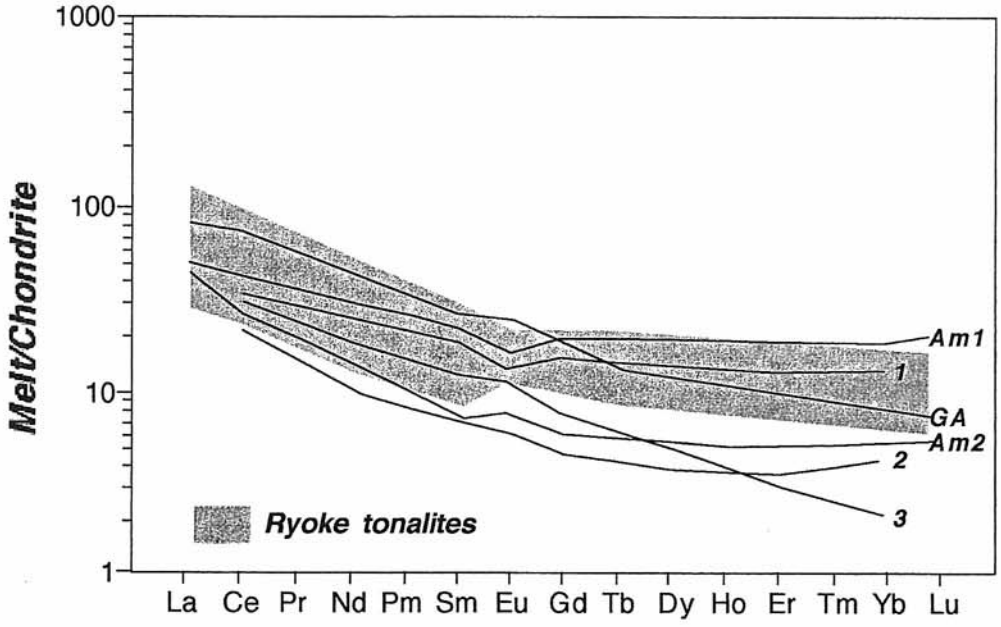

Fig. 4 Chondrite-normalized REE patterns for the Ryoke tonalites and the tonalitic modeled melts (Kutsukake, 2002). 1-3: Tholeiitic sources (1 gabbroic residue, 2 amphibolitic residue, 3 eclogitic residue; Gromet and Silver, 1987), Am1 and Am2: Amphibolitic source (Leake, 1990), GA: Garnet amphibolite source (Anderson and Cullers, 1990).

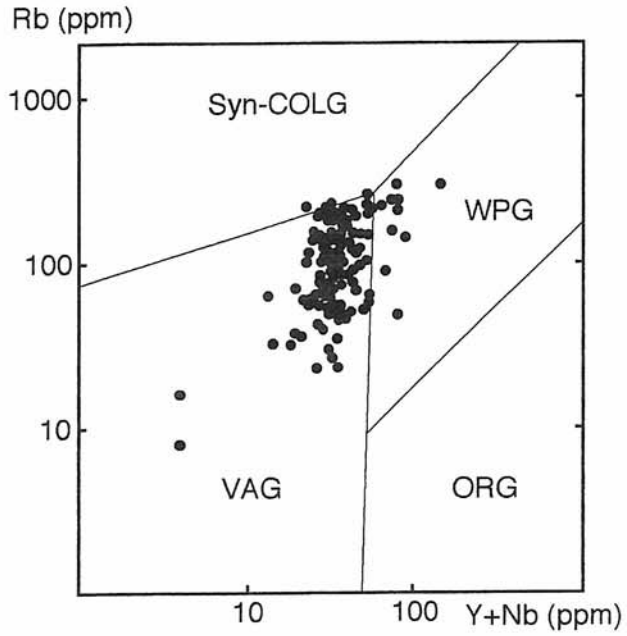

Fig. 5 Rb versus Y + Nb diagram (simplified from Nakajima, 1996). syn-COLG: syn-collision granites, WPG: within plate granites, ORG: ocean ridge granites, VAG: volcanic arc granites (discrimination lines from Pearce *et al.*, 1984).

exhumation and juxtaposition of different types of metamorphic belts are important to clarify continental margin processes and geological evolution of the Japanese Islands.

The Cretaceous granitic magmatism in SW Japan has been ascribed to the interaction of mid-oceanic ridge to the trench of the Eurasian continental margin (Uyeda and Miyashiro, 1974; Kinoshita and Ito, 1986; Nakajima *et al.*, 1990; Nakajima, 1994; Kinoshita, 1995; Brown, 1998; Iwamori, 2000). Along-arc, eastward younging variation of the ages (K-Ar ages and Rb-Sr mineral isochron ages) of granitoids is considered to be the evidence for the ridge subduction model. Based on the CHIME U-Th-total Pb monazite age data, Suzuki and Adachi (1998) argued that the eastward younging ages of the Ryoke granitoids so far documented reflect the differential uplift of the Ryoke belt rather than lateral migration of magmatism. Based on the Rb-Sr whole-rock isochron ages, Yuhara *et al.* (2000) considered the outbreak of magmatism all over SW Japan to be around 120 Ma. However, it should be noted that the magmatic ages of the San-yo granitoids given by SHRIMP U-Pb zircon ages, well-defined Rb-Sr whole rock isochron ages, Th-Pb thorite and U-Pb uraninite ages show the eastward younging trend approximately from 100 Ma at western Chugoku to 70 Ma at central Japan. It seems that this problem has not yet been settled with a convincing conclusion for all.

To discuss the shallow to mid-crustal process during the mid-Cretaceous, this field trip focuses on the shallow- to deep-seated granitic rocks, such as San-yo and Ryoke granitoids and related low-*P*/high-*T* metamorphic rocks in the Iwakuni-Yanai district, Yamaguchi Prefecture. Route map and locations of stop points in the Yanai-Iwakuni district is available in Appendix.

2. Geology of the Iwakuni-Yanai district

As the Iwakuni-Yanai area includes the San-yo and Ryoke zones (Fig. 7a), we can enjoy a variety of the San-yo and Ryoke granitoids with host metamorphic rocks of various metamorphic grades from virtually unmetamorphosed to lower granulite grade. Roughly, the San-yo zone represents the shallow level of the orogen and it goes to deep in the crust as we traverse this area to the south in the Ryoke zone.

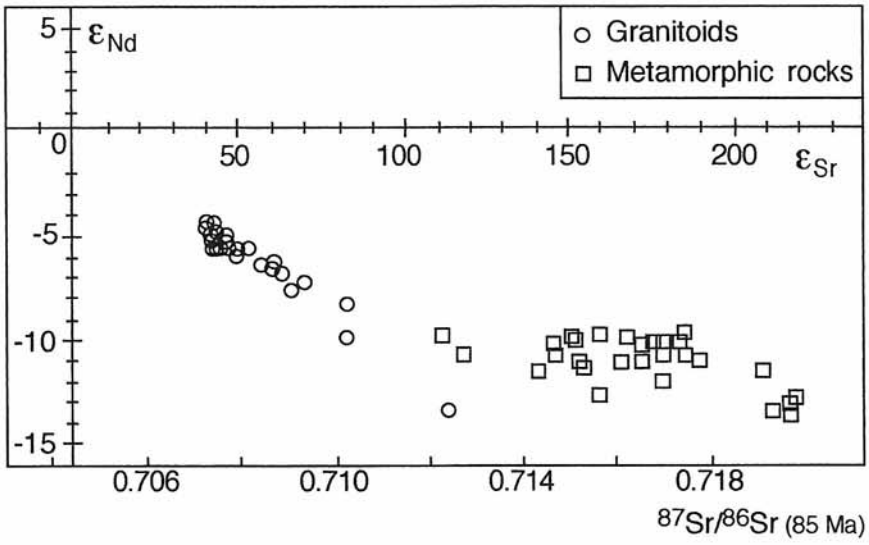

Fig. 6 Initial εSr versus εNd diagram for Ryoke granitic and metamorphic rocks (partly modified from Yuhara *et al.*, 2000). Chondritic uniform reservoir (CHUR) parameters for calculation of initial εSr versus εNd are: $^{87}Sr/^{86}Sr$ (present) = 0.7045, $^{87}Rb/^{86}Sr$ (present) = 0.0827, $^{143}Nd/^{144}Nd$ (present) = 0.512638, $^{144}Sm/^{144}Nd$ (present) = 0.1966.

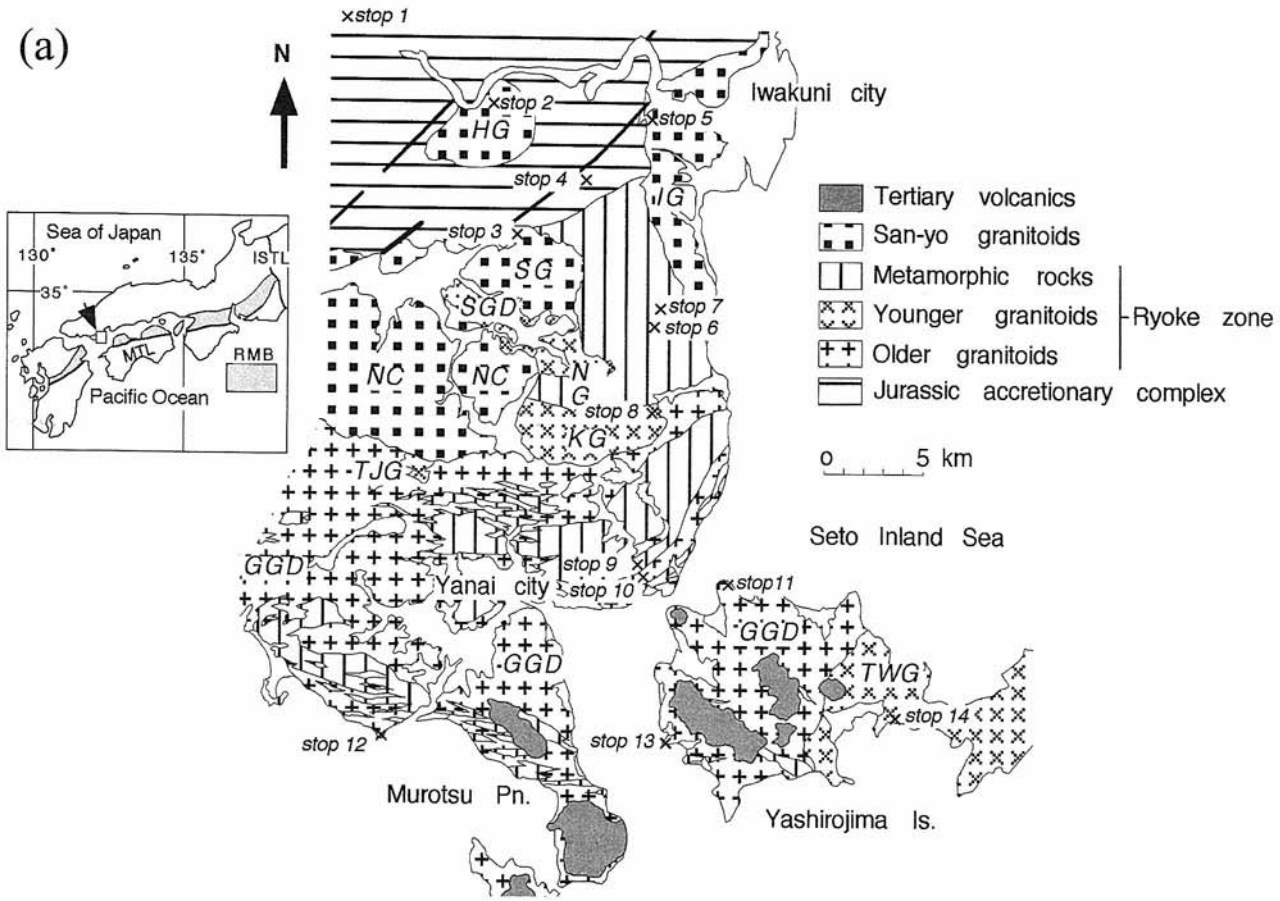

Fig. 7 (a) Geological map of the Iwakuni-Yanai district (modified from Higashimoto *et al.*, 1983). Individual granite bodies are identified as HG (Habu granodiorite), IG (Iwakuni granite), SG (Shimokubara granite), NC (Nakayamagawa complex), SGD (So-o granodiorite), NG (Namera granite), KG (Kibe granite), TJG (Tajiri granite), TWG (Towa granite), and GGD (Gamano granodiorite). RMB (Ryoke Metamorphic Belt) in Index map.

The host rocks in this area are Jurassic accretionary complex of the Mino-Tamba belt. Radiolarian fossils in the complex suggest a pre-Early Cretaceous stratigraphic age for the protolith of the metamorphic belt (*e.g.* Takami *et al.*, 1990; Takami and Itaya, 1996). These protoliths were regionally metamorphosed under low-*P*/high-*T* conditions during mid-Cretaceous. They show a distinct tectonic foliation which appears to be commonly parallel to their bedding planes. The metamorphic grade increases southward, except in the southernmost area where it decreases, whereas the highest-grade zone is located in the central region of the district. Therefore, the order of increasing metamorphic grade does not agree with the order of increasing structural level. There is, however, still controversy regarding their pressure estimation (Ikeda, 2003). In the southern part of the Iwakuni-Yanai district, Miocene high-Mg andesite covers the Ryoke granitic and metamorphic rocks sporadically.

2.1 Granitic rocks

In the Iwakuni-Yanai district, the San-yo granitoids are exposed in the northern part, the Older Ryoke granitoids occur in the southern part of the area, and the Younger Ryoke granitoids mostly constitute the middle part but some are also exposed in the San-yo granitoid area (Fig. 7b). The San-yo granitoids intrude the Younger Ryoke granitoids, and the Younger Ryoke granitoids intrude the Older Ryoke granitoids where the intrusive contact is observed. The CHIME ages of the granitoids (Suzuki and Adachi, 1998) seem to be concordant with the intrusive relationships (Fig. 8).

The granitoids of the San-yo zone include Iwakuni granite, Habu granodiorite, Shimokubara granite and Nakayamagawa complex (Fig. 7a). They are mostly unfoliated coarse-grained biotite adamellite to granodiorite associated with hornblende-bearing varieties. Some adamellites have pink or pale brown K-feldspars. Most of the San-yo granitoids are equigranular and homogeneous, but some of them are porphyritic with K-feldspar megacrysts of 2 to 5 cm in size. The San-yo granitoids are mostly felsic with 70-75 wt% SiO_2. The San-yo granitoids often have contact aureole of max. *ca.* 500 m. Hornfels with cordierite porphyroblasts occur near the contact boundary of the Iwakuni granite.

The Ryoke granitoids are mostly of I-type, but have been known to include S-type-like granitoids, such as garnet- and/or muscovite-bearing granitoids (without magmatic cordierite nor sillimanite). This S-type-like character was often too much emphasized and the Ryoke granitoids are categorized as I'-type in some papers (*e.g.* Pitcher, 1983). However, the amount of these S-type-like granitoids is small

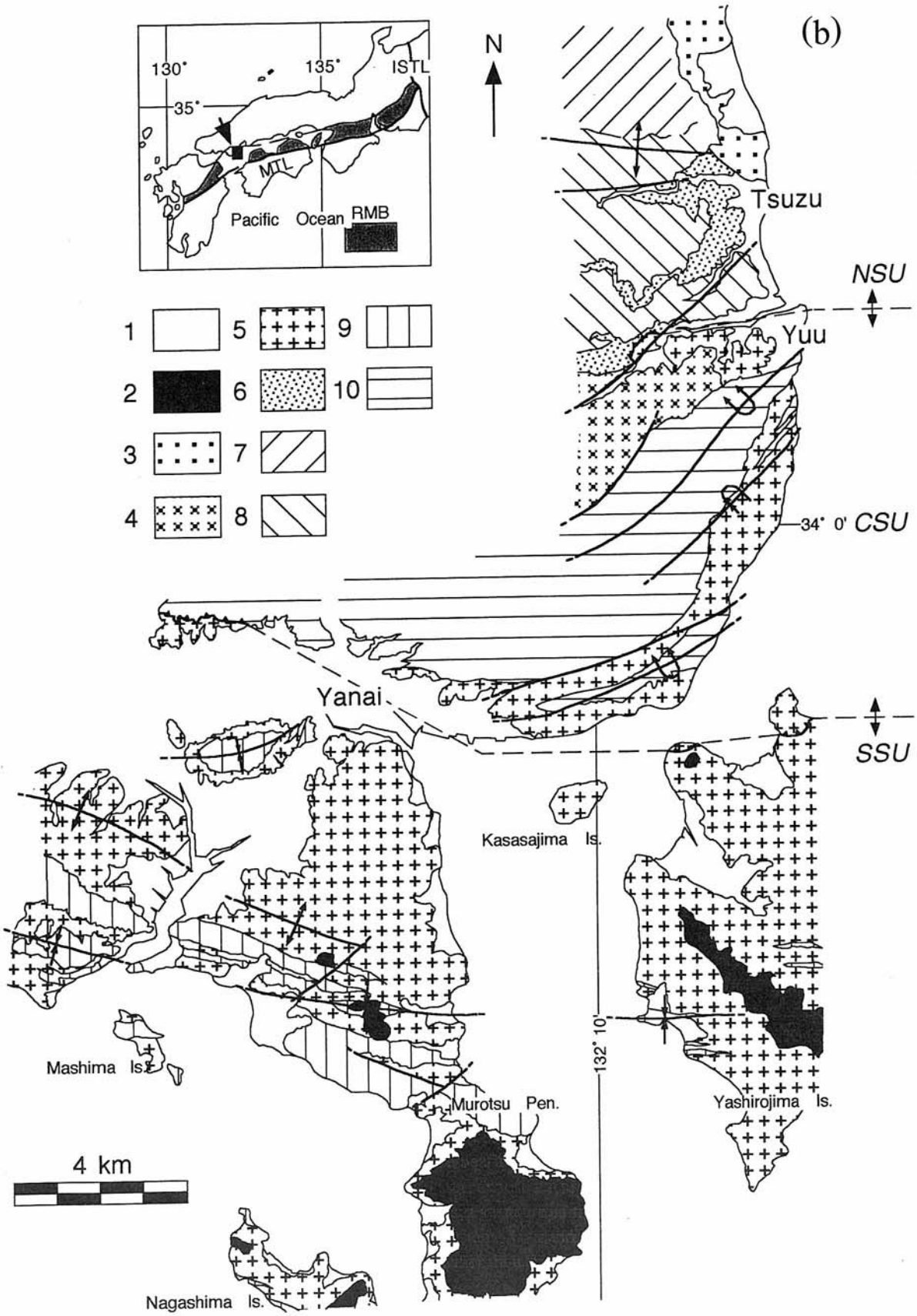

Fig. 7 (b) Geological map of the Yanai district (Okudaira *et al.*, 2001). 1: alluvium. 2: Tertiary volcanics. 3: Iwakuni granite. 4: Younger Ryoke granitoid (Kibe granite). 5 and 6: Older Ryoke granitoids (5 Gamano granodiorite, 6 Tengatake-Nagano migmatite). 7-10 : Ryoke metamorphic rocks (7 biotite zone, 8 cordierite zone, 9 sillimanite zone, 10 garnet-cordierite zone). NSU: Northern structural unit, CSU: Central structural unit, SSU: Southern structural unit.

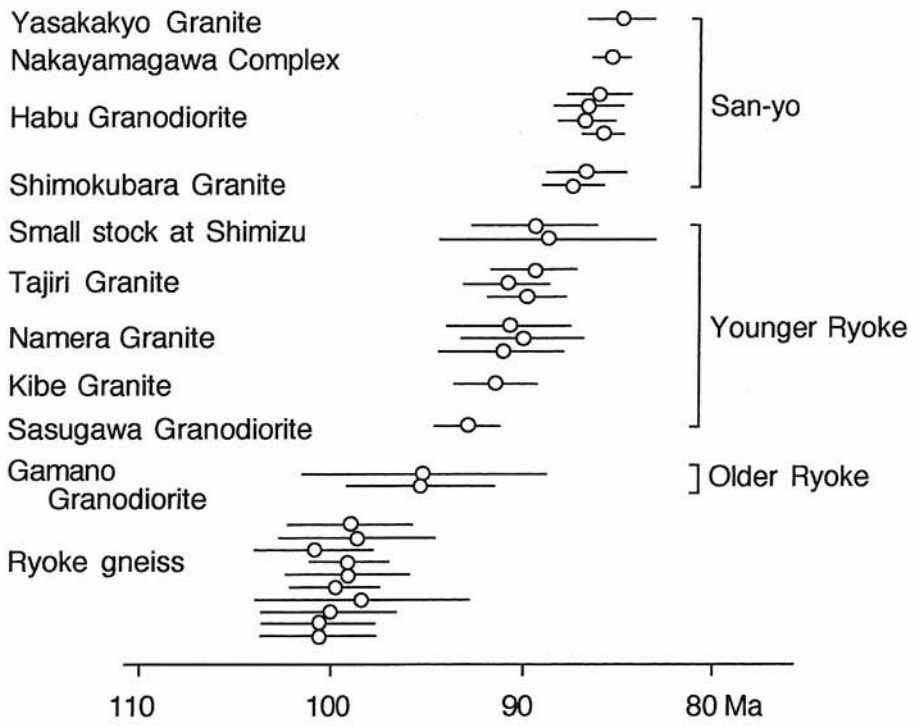

Fig. 8 Summary of CHIME monazite ages for gneisses and granitoids (partly modified from Suzuki and Adachi, 1998).

and their total surface exposure area is nearly 5% of the whole area of the Ryoke granitoids in SW Japan. All these S-type-like granitoids belong to the Younger Ryoke granitoids, whereas the Older Ryoke granitoids do not have such peraluminous minerals.

The Younger Ryoke granitoids in this area include Namera granite, Tajiri granite, Kibe granodiorite, So-o granodiorite and Towa granite. Tajiri granite, a fine-grained leucocratic granite of a few kilometers in size, is the only two-mica granite in this area. Namera granite is a coarse-grained biotite granite stock and partly contains garnet. Other bodies are all free from garnet and muscovite. Cordierite has been reported in some old literatures but not confirmed. Contact metamorphism around the Younger Ryoke granitoids is not observed well, presumably because, most of them intrude the regional metamorphic rocks of higher metamorphic grade than the biotite zone.

The widespread foliated Older Ryoke granitoids in this area is called Gamano granodiorite. It has a lithological variation from foliated coarse-grained hornblende-biotite tonalite to hornblende-bearing biotite granodiorite. The Gamano granitoids are exposed in an area elongated concordantly to the general structure of the wall rocks and the foliation is parallel to them. Gamano granodiorite is less silicic (SiO_2 = 65-70 wt%) than the Younger Ryoke and the San-yo granitoids.

2.2 Metamorphic rocks

2.2.1 Mineral zonation and *P-T* conditions

Using pelitic mineral assemblages, the progressive metamorphism can be described as a sequence of seven zones from north to south, *i.e.* chlorite, chlorite-biotite, biotite, muscovite-cordierite, K-feldspar-cordierite, garnet-cordierite and sillimanite-K-feldspar zones (Ikeda, 1993, 1998a,b; Fig. 9). However, the metamorphic zones different from Ikeda's zones have been proposed by Okudaira *et al.* (1993, 2001) and Nakajima (1994). In order to avoid confusion about these different zones, correlation among them are illustrated as below:

Ikeda (1993, 1998a,b)	**Okudaira *et al.* (1993, 2001)**	**Nakajima (1994, 1996)**
chlorite	—	chlorite
chlorite-biotite	—	chlorite
biotite	biotite	biotite
muscovite-cordierite	biotite	cordierite
K-feldspar-cordierite	cordierite	sillimanite-I
garnet-cordierite	garnet-cordierite	sillimanite-II
sillimanite-K-feldspar	sillimanite	sillimanite-I

The locations of the zone boundaries also differ slightly. The difference in the metamorphic zonation may be due to the difference in the identification of the stable mineral parageneses in each zone during peak regional metamorphism. For avoiding confusion, the metamorphic rocks in this paper are described based on Ikeda's classification.

The areas in the chlorite-biotite, biotite and the muscovite-cordierite zones locally overlap with contact aureoles of the San-yo granitoids. Even though the extent of the contact aureoles is difficult to discern, cordierite with trilling and randomly oriented muscovite are taken as evidence for

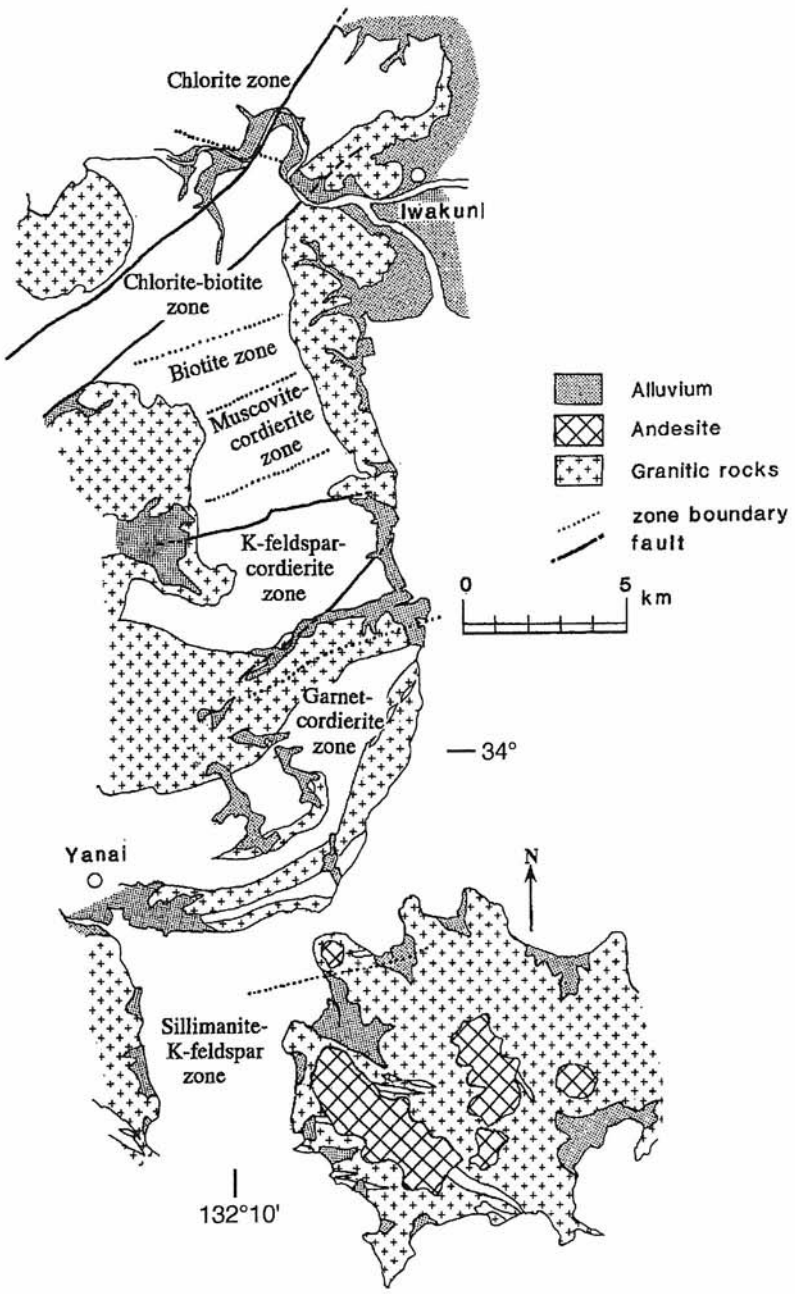

Fig. 9 Metamorphic zonation map of the Iwakuni-Yanai district (Ikeda, 1993, 1998a).

contact metamorphism. The arrangement of the metamorphic zones does not represent progressive changes in metamorphic grade, i.e. the highest-grade garnet-cordierite zone occurs between the K-feldspar-cordierite and sillimanite-K-feldspar zones (Ikeda, 1993, 1998a.b; Okudaira *et al*., 1993; Nakajima, 1994; Okudaira, 1996b).

According to Okudaira (1996b), estimated *P-T* conditions for the mineral zones are 460-590°C at ca 300 MPa (K-feldspar-cordierite zone), 630-690°C at 300-500 MPa (sillimanite-K-feldspar zone), and 730-770°C at 550-650 MPa (garnet-cordierite zone). However, the pressure estimates for the sillimanite-K-feldspar zone and garnet-cordierite zone were calculated based on different geobarometry, still uncertainty persists in the fact that the pressure condition of the garnet-cordierite zone is higher than that of the sillimanite-K-feldspar zone. Recently, based on internally consistent *P-T* estimation, Ikeda (2003) indicated the *P-T* conditions of each zone to be *ca.* 470°C at 20-50 MPa (chlorite-biotite zone), 450°C at 90-120 MPa (biotite zone), 520-550°C at 40-100 MPa (muscovite-cordierite zone), 600-680°C at 120-370 MPa (K-feldspar-cordierite zone), 700-760 °C at 500-640 MPa (sillimanite-K-feldspar zone), and 790-860 °C at 460-760 MPa (garnet-cordierite zone). Inferred metamorphic field gradient of the metamorphic belt is of 40-50°C/km. It has been suggested that the 'regional' low-*P* metamorphism resulted from the thermal effect of intrusion of the Gamano granodiorite (Okudaira *et al*., 1993; Okudaira, 1996a,b; Ikeda, 1998a,b).

The following description for each mineral zone is essentially after Ikeda (1998a,b).

Chlorite zone This zone is defined by absence of biotite in pelitic rocks. Dominant pelitic assemblage is chlorite + muscovite + albite together with quartz. K-feldspar locally occurs in siliceous rocks.

Chlorite-biotite zone This zone is characterized by the occurrence of biotite coexisting with chlorite and muscovite. Near the biotite isograd, biotite is fine-grained (< 50 mm long) and occurs only sporadically as a constituent of the schistosity. In the higher-grade part, biotite occurs not only as single grains parallel to schistosity but also as ovoidal aggregates with long axes of 0.1-0.2 mm. Such aggregates are composed of biotite grains that are coarser (0.1 mm in maximum) than those forming the schistosity, and are locally associated with quartz grains in their centers. Such aggregates persist into the biotite zone. The dominant assemblage in pelitic rocks is Chl + Bt + Ms + Pl. K-feldspar occurs only rarely in pelitic rocks but is common in siliceous rocks.

Biotite zone The disappearance of chlorite from most pelitic rocks defines the start of the biotite zone. Both biotite and muscovite are coarse-grained (0.1 mm long) compared with those in the chlorite-biotite zone. In this zone, the dominant mineral assemblage is Bt + Ms + Pl.

Muscovite-cordierite zone The coexistence of cordierite and muscovite defines the zone. Cordierite is minor, < 5% in modal amount, and now occurs as fine-grained pinite in the assemblage of Crd + Bt + Ms + Pl. However, this assemblage is uncommon and the most frequent assemblage in the pelitic rocks are same as that of the biotite zone. The grain sizes of muscovite and biotite are similar to those in the biotite zone and increase up to 0.3 mm.

However, according to Okudaira *et al.* (1993), the muscovite-cordierite zone cannot be distinguished from the biotite zone, since the mineral characteristics of both the zones are essentially the same.

K-feldspar-cordierite zone The first appearance of cordierite that coexists with K-feldspar defines the start of this zone. There is a marked reduction in the preferred orientation of muscovite and biotite, and the development of compositional banding composed of quartzo-feldspathic and micaceous layers occurs in this zone. The first appearance of andalusite, which is poikiloblastic including biotite and carbonaceous materials, coincides approximately with this isograd. In the southern part of this zone, andalusite with its armor of cordierite is partly or completely transformed to sillimanite. Most pelitic and siliceous rocks contain muscovite which occurs either as coarse (0.3 mm long) tabular grains in the matrix, or as aggregates replacing the cordierite rimming andalusite and sillimanite. The muscovite in this zone and at higher metamorphic grades is thought to be of retrograde origin. However, there is a possibility that some of the muscovite was stable at the peak metamorphism. The representative mineral assemblages in pelitic rocks are:

- andalusite and/or sillimanite + cordierite + biotite + K-feldspar + plagioclase
- cordierite + biotite + K-feldspar + plagioclase
- garnet + biotite + K-feldspar + plagioclase.

A tourmaline-out isograd that is defined by the disappearance of tourmaline is delineated within this zone (Kawakami and Ikeda, 2003).

Sillimanite-K-feldspar zone The sillimanite-K-feldspar zone is defined by the occurrence of sillimanite and K-feldspar in the matrix assemblage. Sillimanite occurs as fibrous or columnar grains and is commonly associated with biotite. The assemblages of Sil + Bt + Kfs + Pl and Sil + Grt + Bt + Kfs + Pl are dominant in pelitic and siliceous rocks. Cordierite is less common in this zone compared to the K-feldspar-cordierite zone, coexisting with sillimanite, biotite and K-feldspar while no coexisting garnet is found.

Garnet-cordierite zone The coexistence of garnet and cordierite is characteristic in this zone. The dominant mineral assemblages in pelitic rocks are:

- cordierite + biotite + K-feldspar + plagioclase
- garnet + biotite + K-feldspar + plagioclase
- garnet + cordierite + biotite + K-feldspar + plagioclase

The garnet + biotite + K-feldspar + plagioclase assemblage is dominant in both pelitic and siliceous rocks. Cordierite locally includes fibrous or rounded sillimanite in the center of a single grain. Spinel is observed only in this zone. The spinel is rare and occurs along grain boundaries within cordierite clusters and coexists with biotite and K-feldspar. Orthopyroxene occurs only in basic rocks of this zone and coexists with hydrous minerals such as biotite, hornblende (Ikeda, 2002).

2.2.2 Metamorphic *P-T* path

Metamorphic *P-T* paths for the rocks in the Iwakuni-Yanai district have been estimated petrologically (Ikeda, 1998a,b; Brown, 1998). As shown in Fig. 10, the prograde *P-T* paths for the K-feldspar-cordierite zone and garnet-cordierite zone are nearly isobaric, suggesting the possibility that the heat source for the low-*P*/high-*T* Ryoke metamorphism was caused by the intrusion of the Older granitoids (*e.g.* Okudaira *et al.*, 1993).

2.3 Deformation

2.3.1 Large-scale structures

The Older granitoids and metamorphic rocks occurring in the Yanai district were folded together, and they are divided into three structural units: the northern, central and southern units (Okudaira *et al.*, 1993, 2001; Fig. 7b). The geological structure of the northern unit is characterized by gentle upright folds with fold axis gently plunging toward ESE. The geological structure of the southern unit is also characterized by gentle folds of upright fashion and of WNW-ESE to E-W trend. In contrast to the structures of the northern and southern units, the geological structure of the central unit is characterized by overturned folds facing toward the southeast direction with NNE-NE plunging fold axes. Although the boundaries among the structural units can be recognized in the limited areas, they have a east-west strike and a northward dip.

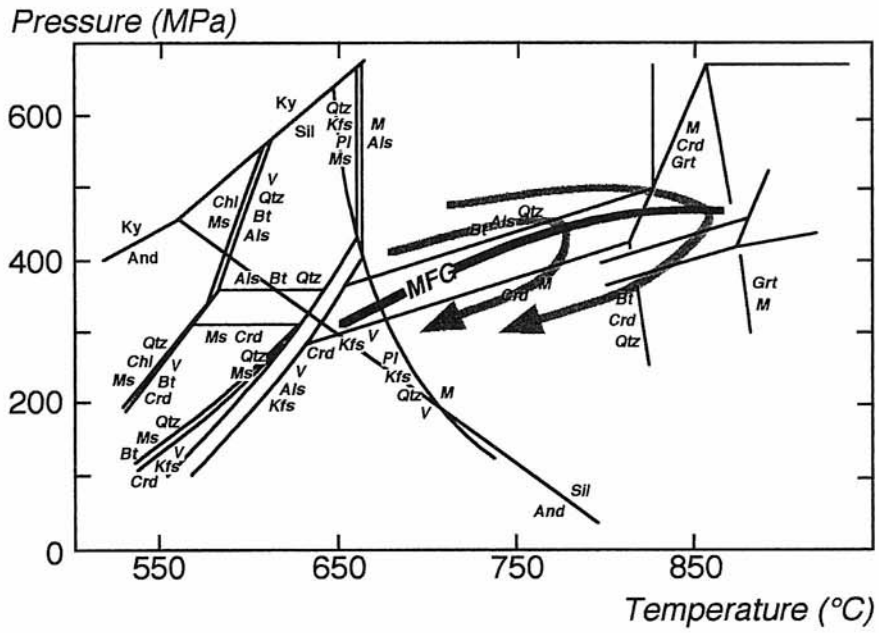

Fig. 10 *P-T* paths of the highest grade rocks of the Ryoke metamorphic belt (partly modified from Brown, 1998).

2.3.2 Deformation events

In the Older granitoids and metamorphic rocks, deformation structures caused by three different phases (D1, D2 and D3) of high-*T* ductile deformation have been recognized (Okudaira *et al.*, 1993, 1995a,b). Deformation structures resulting from D1 and D3 are penetratively observed, while the occurrence of D2 structure is limited. In all the rocks, D1 structure is characterized by a distinct foliation (S1-foliation) parallel to lithologic boundaries. In some metapelites, there are many kinds of asymmetric deformation structures. Judging from the asymmetric structures, the overall movement picture of D1 is top to the north. The emplacement of the Older granitoids partly occurred during D1. D2 is related to the formation of large-scale overturned folds and their parasitic folds (F2-folds), which are facing toward SE with NNE-NE plunging fold axes in the central unit, and of distinct shear zones (D2-shear zones) truncating S1-foliation. D2-shear zones are well observed near the boundary between the central and southern units, while it is not clear near the boundary between the northern and central units. In the northern part of Yashirojima Island, where the boundary between the central and southern units is located, many fine-grained layers with distinct foliation (S2-foliation) are recognized as D2-shear zones truncating S1-foliation in the coarse-grained granodiorite. The fine-grained layers consist of fine grains produced by dynamic recrystallization of constituent minerals of the coarse-grained granodiorite. The asymmetric structures in the D2-shear zones near the boundary between the central and southern units indicate the shear sense of top to the WSW-SW. D3 is responsible for the formation of gentle upright folds (F3-folds) with E-W trending axes. D1 and D2 structures are folded by F3-folds.

2.3.3 Tectonic perspective

Tectono-metamorphic processes of the Ryoke metamorphic belt in the Iwakuni-Yanai district have been summarized as follows (Okudaira *et al.*, 2001; Fig. 11).

・The accretion of the sedimentary rocks of the Mino-Tamba belt at the eastern margin of the Eurasian continent, from Early to Late Jurassic.

・The northward dipping large-scale extensional fracture zones which appear to have top to the NNE-NE sense of shear occurred at intermediate to shallow crustal levels. The Older Ryoke granitoids ascended along the northward dipping large-scale extensional fracture zones from the lower to middle crust (*ca.* 95 Ma). The emplacement of the Gamano granodiorite resulted in the low-*P* metamorphism in the upper and middle crust (Fig. 11a).

・Immediately after the emplacement of the granodiorite, the metamorphic sequence was modified by D2 low-angle faults and large-scale recumbent folds (Fig. 11b,c). The mylonite zones developed along the MTL also represent this tectonic event (*e.g.* Hara *et al.*, 1991; Ohtomo, 1993; Okudaira *et al.*, 1993). The D3 upright folds with E-W trending axes were formed. After D3, a large amount of granite (Younger Ryoke and San-yo granitoids) intruded as stocks. The intrusion of the granite stocks resulted in a narrow contact metamorphism of the wall rocks.

3. Description of field stops

Day 1 (August 30)

Stop 1 : Weakly metamorphosed protolith of the Ryoke metamorphic rocks (Gonomoto, Mikawa Town)

This outcrop is dominated by low-grade metamorphic rocks, belonging to a Jurassic accretionary complex of the Mino-Tamba belt. Early Jurassic radiolarian fossils included

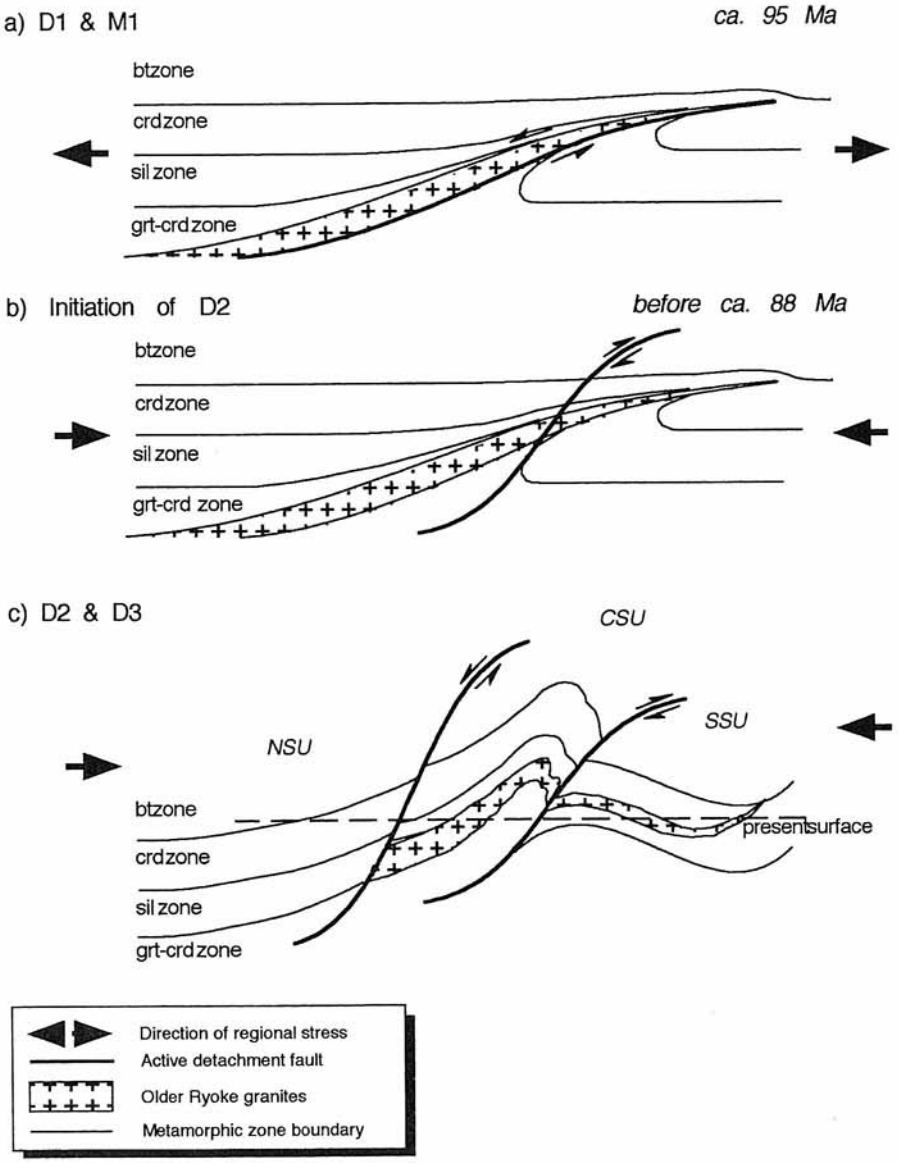

Fig. 11 A possible tectonic model for the Ryoke metamorphic belt in the Yanai district during Cretaceous time (Okudaira *et al.*, 2001).

in the pelitic rocks represent its accretion at a trench around 200 Ma (Takami and Itaya, 1996).

There is a schistosity defined by the preferred orientation of fine-grained muscovite and chlorite. Crenulation cleavages also develop. The fine-grained muscovite and chlorite are not of detritus grains, but recrystallized grains. The muscovite K-Ar ages of 176-165 Ma suggest that the rocks of this outcrop were metamorphosed at a subduction zone before the Ryoke metamorphism (Takami and Itaya, 1996). The basic rocks involve the mineral assemblages of chlorite + pumpellyite + epidote + stilpnomelane, chlorite + pumpellyite + actinolite or chlorite + epidote + muscovite, suggesting the high-*P*/low-*T* metamorphism (upper prehnite-pumpellyite to pumpellyite-actinolite facies: Takami and Itaya, 1996).

Stop 2 : Habu granodiorite (Habu, Iwakuni City)

At this stop we observe an example of the San-yo granitoid. The Habu granite is composed of two lithological unit; medium-grained biotite granite of main facies and medium-grained hornblende-biotite tonalite to granodiorite of marginal facies. These two units have distinctly different Sr*I* confirmed by apatite work, indicating to be derived from two different magmas (Tsuboi and Suzuki, 2003). They obtained Rb-Sr mineral isochron ages of 90 Ma (marginal granodiorite) and 91 Ma (central granite). The CHIME ages of 87-86Ma (Suzuki and Adachi, 1998) and SHRIMP zircon age of 90 Ma (Tsuboi *et al.*, 2001) on the Habu granodiorite are concordant with them. There is, however, still controversy regarding the age of the granodiorite, such as a whole-rock isochron age of 124 Ma (Owada *et al.*, 1995), hornblende K-Ar age of 104 Ma (Yuhara *et al.*, 1999) and biotite K-Ar ages of 103 Ma and 99 Ma (Higashimoto *et al.*, ages 1983). This stop stands in the main biotite granite facies of this body. Representative whole-rock chemistries of the

Table 2 Whole-rock analyses of the Habu granodiorite (Owada *et al.*, 1995; Yuhara *et al.*, 1999).

	Marginal facies			Central facies			
	HB-04	HB-07	HB-08	HB-05	HB-11	HB-12	HB-101
SiO_2	67.84	63.77	63.77	69.59	70.60	69.57	—
TiO_2	0.41	0.56	0.58	0.29	0.24	0.30	—
Al_2O_3	16.36	16.82	16.97	15.77	15.59	15.95	—
Fe_2O_3	4.16	5.66	5.38	3.23	3.08	3.36	—
MnO	0.09	0.10	0.11	0.08	0.07	0.07	—
MgO	1.40	2.08	2.12	0.96	0.79	0.95	—
CaO	3.56	4.72	4.72	2.69	2.44	2.69	—
Na_2O	3.23	3.34	3.36	3.51	3.77	3.58	—
K_2O	3.07	2.65	2.71	3.48	3.59	3.73	—
P_2O_5	0.14	0.16	0.15	0.11	0.09	0.11	—
Total	100.26	99.86	99.87	99.71	100.26	100.31	—
Rb	111	94	90	140	146	139	115
Sr	270	306	305	208	191	222	257
SrI*	—	—	—	—	—	—	0.70607
ASI	1.08	0.99	1.00	1.09	1.07	1.08	—

* Estimated by whole-rock-mineral isochron

Habu granodiorite by Owada *et al.* (1995) and Yuhara *et al.* (1999) are shown in Table 2.

Stop 3 : Shimokubara granite (Kinmeiji, Kuga Town)

Coarse-grained porphyritic biotite granite is predominant. Existence of porphyritic K-feldspar up to 5 cm is a characteristic feature. This granite consists of quartz, plagioclase, K-feldspar and biotite, with small amounts of apatite, zircon, monazite, allanite and ilmenite. K-Ar biotite age and CHIME monazite ages of this granite have been estimated to be 88 Ma (Kawano and Ueda, 1966), and 86.6±2.1 and 87.3±1.6 Ma (Suzuki *et al.*, 1996), respectively. Bulk-rock chemistry of the granite is homogeneous (Table 3). The homogeneity may be considered as indicating the emplacement of the granite as a largely molten mass and a differentiation before emplacement and not in situ (Moutte, 1990).

Stop 4 : Metamorphic rocks of the Bt zone (Hashirano, Iwakuni City)

A large quarry of weakly metamorphosed rocks mainly derived from pebbly shale. This outcrop is located near the cordierite isograd which defines the upper limit of biotite zone marked by the absence of both chlorite and cordierite. The common mineral assemblage is muscovite + biotite. Pressure-temperature conditions of the zone was calculated to be *ca.* 90-120 MPa and 450°C (Ikeda, 2003).

Stop 5 : (This stop will be visited, if possible) : Iwakuni granite (Kawanishi, Iwakuni City)

This stop presents another example of the San-yo granitoid. The Iwakuni granite is exposed in a wide area along the seashore extending from Iwakuni to Tsuzu. It consists of hornblende-bearing and hornblende-free coarse-grained biotite adamellite. The hornblende-bearing adamellite occurs at the central part and the hornblende-free adamellite

Table 3 Whole-rock analyses of the Shimokubara granite (Moutte, 1990).

sample	817 Aplite	1101	1135	1114	1126
SiO_2	74.90	69.30	70.40	70.10	67.90
TiO_2	0.018	0.202	0.230	0.226	0.197
Al_2O_3	13.4	15.2	14.5	15.5	16.6
Fe_2O_3	0.74	2.25	2.29	2.41	2.11
MnO	0.133	0.072	0.068	0.077	0.066
MgO	0.046	0.456	0.325	0.54	0.44
CaO	0.44	2.15	2.09	2.52	2.33
Na_2O	3.50	3.89	3.05	3.46	3.77
K_2O	3.85	3.90	3.50	3.43	4.65
P_2O_5	0.08	0.02	0.07	0.09	0.07
Total	97.1	97.4	96.5	98.4	98.1
Li	20	51	63	98	74
Rb	310	157	155	181	173
Cs	33.6	12	14	16	14
Be	6.5	3.1	4.6	4.5	4.0
Sr	14	170	130	141	162
Ba	34	430	280	215	300
Zr	33	98	79	81	81
Hf	—	2.7	3.0	2.8	3.4
Nb	12.5	14.2	13	16.6	14
Ga	18.1	17.6	17.2	17.4	19.2
Pb	16.3	23	19	24	29
Sn	18.2	9.2	12	13	12
Sc	3.0	3.8	3.6	3.4	2.8
V		9.4	7.6	10.5	9.1
Co	0.20	—	—	2.8	2.9
Cu	30	—	244	—	—
Zn	12.5	53	41	58	54
Ce	23	57	51	48	48
Eu	—	0.68	0.55	0.59	0.67
Y	9.7	23.3	23.0	26.0	32.0
Th	1.0	6.1	5.1	7.0	6.5
ASI	1.25	1.05	1.15	1.11	1.07
Sr/Y	1.44	7.30	5.65	5.42	5.06

at the northern and southern part of the N-S trending body. This stop is an area of hornblende-free biotite adamellite. K-feldspar looks slightly pinkish.

Day 2 (August 31)

Stop 6 : Metamorphic rocks of the Kfs-Crd zone (Tsuzu, Iwakuni City)

The K-feldspar-cordierite zone is defined by the assemblage of cordierite + K-feldspar. Occasionally, andalusite coexists with K-feldspar and cordierite. Temperature condition of this zone was calculated to be *ca.* 460-590°C, based on two feldspar thermometry (Okudaira *et al.*, 1995a; Okudaira, 1996b), whereas Ikeda (2003) estimated the *P-T* conditions of this zone using Gibbs' method to be *ca.* 120-370 MPa and 600-680°C.

Stop 7 : Tengatake-Nagano migmatite (Tsuzu, Iwakuni City)

Tengatake-Nagano migmatite is a strange small body

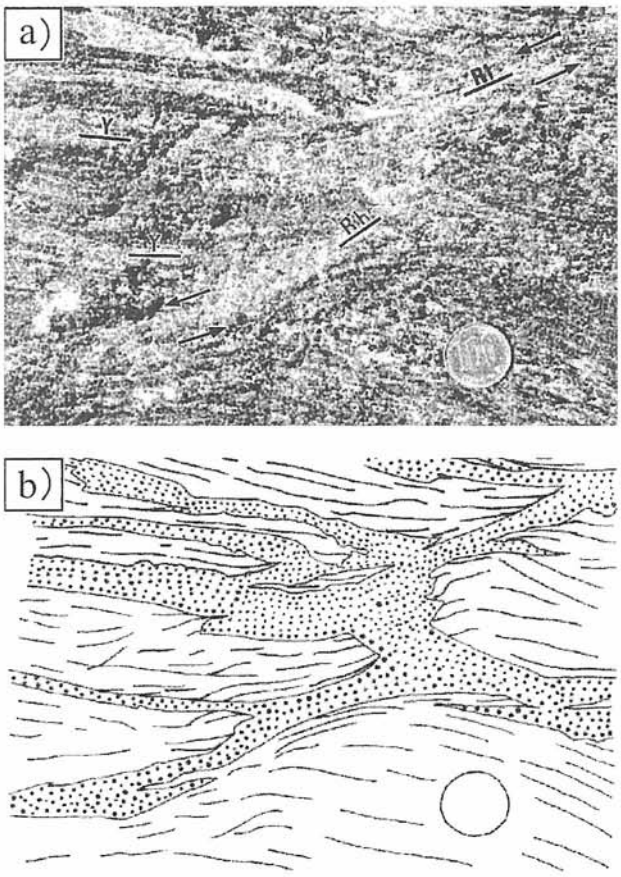

Fig. 12 (a) Photograph showing structure of the melt (fluid ?)-filled fractures around the Nagano migmatite. (b) Sketched profile of photograph (dot: granitic part, strip: metapelite).

designated so far as the Older Ryoke granitoids. The zone of the agmatitic migmatite occurs in the K-feldspar-cordierite zone of the metamorphic sequence where partial melting did not take place extensively. As shown in Figure 12, it is composed mainly of agmatitic metamorphic blocks with matrix of leucocratic rocks which intruded along non-coaxial shear fractures.

Stop 8 : Kibe granite (Nagata, Yuu Town)

This granite is predominantly coarse-grained biotite granite and characterized by preferential alignment of porphyritic K-feldspar. Marginal facies of this granite is medium- to fine-grained without porphyritic K-feldspar. Modal compositions of this granite is: 28.6 % plagioclase, 36.3 % K-feldspar, 26.9 % quartz, 8.2 % biotite (Okamura, 1960). They have weak foliation striking EW, defined by preferential alignment of biotite and porphyritic K-feldspar. K-Ar biotite age and CHIME monazite age of this granite have been estimated to be 86.3±4.3 Ma (Higashimoto *et al.*, 1983) and 87 Ma (Kawano and Ueda, 1966), and 91.3±2.1 Ma (Suzuki and Adachi, 1998), respectively. Representative chemical compositions of the Kibe granite are shown in Table 4.

Table 4 Whole-rock analyses of the Kibe granite (Moutte, 1990).

sample	1292	1295	828	914	1000
SiO_2	73.8	75.3	73.7	70.7	73.5
TiO_2	0.017	0.073	0.042	0.356	0.290
Al_2O_3	12.7	12.7	14.0	14.3	13.8
Fe_2O_3	0.801	0.405	0.37	2.54	2.14
MnO	0.10	0.018	0.006	0.044	0.040
MgO	0.055	0.154	0.107	0.74	0.62
CaO	1.26	0.91	1.14	1.75	1.38
Na_2O	2.06	3.25	2.72	2.6	3.05
K_2O	5.25	4.9	6.85	5.3	4.95
P_2O_5	—	—	0.03	0.13	0.11
Total	96.0	97.7	99.0	98.5	99.9
Li	16	62	18	61	86
Rb	142	136	270	275	300
Cs	19	13	—	—	12.3
Be	—	5.2	1.8	2.2	3.5
Sr	84	72	120	130	95
Ba	210	270	270	480	350
Zr	94	66	44.7	166	135
Hf	3.4	3.0	—	4.5	5.6
Nb	2.0	4.6	3.1	17.8	19.7
Ga	12.5	12.6	14.2	15.8	16.0
Pb	30	32	36.6	31.7	35.8
Sn	—	3.2	—	—	3.4
Sc	3.2	1.05	0.90	6.8	5.5
V	3.5	3.0	1.4	25.6	18.3
Co	0.60	0.90	1.1	3.05	2.45
Cu	—	—	—	—	—
Zn	10	11.2	7.9	59	59
Ce	29	13	15	111	80.4
Eu	0.50	0.40	0.60	0.78	0.63
Y	45	5.3	22.1	24.1	18.0
Th	4.5	3.1	4.6	32	20.5
ASI	1.12	1.03	1.00	1.08	1.07
Sr/Y	1.87	13.58	5.43	5.39	5.28

Stop 9 : Metamorphic rocks of the Grt-Crd zone (Obatake, Obatake Town)

The garnet-cordierite zone is defined by the assemblage of garnet + cordierite + K-feldspar in the pelitic rocks. *P-T* conditions have been estimated to be 730-770°C, 550-650 MPa (Okudaira, 1996b), whereas according to Ikeda (1998a,b, 2003), *P-T* conditions of this zone were calculated to be 790-860°C at 460-760 MPa.

Stop 10 : Gamano granodiorite (Obatake, Obatake Town)

The Gamano granodiorite concordantly intruded into the high-grade metamorphic rocks at *ca.* 100-95 Ma (SHRIMP zircon: Nakajima *et al.*, 1993; CHIME monazite: Suzuki *et al.*, 1994; Suzuki and Adachi, 1998), and its foliation, defined by the preferred shape orientation of plagioclase, biotite and hornblende is harmonic in trend with that of the surrounding metamorphic rocks. Representative chemical compositions of the Gamano granodiorite are shown in Table 5.

Table 5 Whole-rock analyses of the Gamano granodiorite (Moutte, 1990; Nakajima, unpub. data).

sample	1176	1413	92072405	92072301
SiO_2	66.1	68.0	67.90	69.38
TiO_2	0.605	0.461	0.73	0.42
Al_2O_3	15.4	14.0	15.52	16.85
Fe_2O_3	4.91	4.08	5.42	2.94
MnO	0.057	0.076	0.10	0.04
MgO	1.01	0.874	1.27	0.91
CaO	3.94	3.22	3.92	4.76
Na_2O	4.0	3.3	3.11	3.31
K_2O	1.88	3.21	2.69	1.63
P_2O_5	0.34	0.27	0.19	0.06
Total	98.2	97.5	100.84	100.29
Li	78	36	—	—
Rb	117	115	138	60
Cs	12	10	6.9	2.7
Be	2.1	2.6	—	—
Sr	250	240	266	306
Ba	180	590	1142	370
Zr	122	132	196	146
Hf	3.9	3.5	5.8	4.6
Nb	22	14.7	21	12
Ga	21.3	19.7	—	—
Pb	16	19	—	—
Sn	8.0	6.0	—	—
Sc	6.8	8.6	12	6.3
V	33	31	33	31
Co	5.9	6.0	11	6.0
Cu	5.0	15.1	15	2.4
Zn	98	81	96	52
Ce	42	71	105	37
Eu	1.3	1.25	1.1	1.4
Y	15	22.0	14	12
Th	2.7	8.1	17.0	5.7
Ni	—	—	7.6	4.8
Cr	—	—	16	18
ASI	0.98	0.95	1.02	1.06
Sr/Y	16.7	10.9	19.6	24.9

Stop 11 : Gamano (Kita-Oshima) granodiorite (Hirarehana cape, Oshima Town)

A kilometer-sized granodiorite block exposed at the northernmost part of Yashirojima Island is very coarse-grained and strongly foliated compared to the Gamano granodiorites around it. In old days it was considered to be a fragment of the ancient "geosynclinal basement" of SW Japan (Kojima and Okamura, 1968). Since isotopic and U-Th-Pb ages of the Kita-Oshima granodiorite are not old but similar to the Gamano granodiorite (Honma and Sakai, 1975; Shigeno and Yamaguchi, 1976; Suzuki *et al.*, 1994; Herzig *et al.*, 1998), they have now been regarded as a part of the Gamano granodiorite. However, the name of Kia-Oshima granodiorite is often used for this characteristic block.

The Rb-Sr whole rock-mineral (biotite, plagioclase and K-feldspar) ages of the granodiorite fall in a range of ca 89-87 Ma. The fission-track zircon and apatite ages are 68.9±2.6 Ma and 57.4±2.5 Ma, respectively (Okudaira *et al.*, 2001). As shown in Figure 13, two distinctive cooling stages have been revealed; 1) a rapid cooling (> 40°C/Myr) for a period (~10 Myrs) soon after the thermal peak of the Cretaceous Ryoke metamorphism (~98 Ma) and 2) the subsequent slow cooling stage (~10°C/Myr) after *ca.* 85 Ma.

Around this outcrop, where the boundary between the central and southern units is located, many fine-grained layers with distinct foliation (S2-foliation) are recognized as D2-shear zones truncating S1-foliation in the coarse-grained granodiorite. The fine-grained layers consist of fine grains (*e.g.* quartz and feldspar) produced by dynamic recrystallization of constituent minerals of the coarse-grained granodiorite. The asymmetric structures in the D2-shear zones near the boundary between the central and southern units indicate the shear sense of top to the WSW-SW.

Stop 12 : (This stop will be visited, if possible) : Metamorphic rocks of the Sil-Kfs zone (Kandori-misaki, Hikari City)

This outcrop is dominated by metapelites of the Sil-Kfs zone. Metamorphic mineral assemblage in the metapelites is sillimanite + cordierite + biotite + K-feldspar. Prismatic sillimanite needles (up to 2-3 cm long) can be observed by naked eyes. Complete boudinages, so-called "pencil structure", resulted from the D3-upright folding are also observed.

Day 3 (September 1)

Stop 13 : Migmatite of the Sil-Kfs zone (Himisaki cape, Oshima Town)

Spectacular migmatite outcrop on the seashore. We can enjoy various lithologies of hybrid "migma" flowing and folded (Fig. 14). Metamorphic mineral assemblages in metapelite blocks and melanosome of the migmatite are sillimanite + cordierite or sillimanite + garnet with K-feldspar. *P-T* conditions have been estimated to be 630-690°C at 300-500 MPa (Okudaira, 1996b) and to be 700-760°C at 500-640 MPa (Ikeda, 2003). We can observe tourmaline boudinages in naked eyes.

On the approach to the Himisaki cape, beautiful outcrops of metamorphosed bedded chert are exposed along the seashore promenade. In the sillimanite zone, metamorphic rocks are less abundant than the cordierite-garnet zone and the percentage of metachert in the metamorphic rocks is larger than in the other zones.

Stop 14: (This stop will be visited, if possible): Towa granite (Tateiwa, Tachibana Town)

Towa granite which is one of the Younger Ryoke granitoids varies petrographically ranging from granodiorite (Pl 40.8%, Qtz 37.2%, Kfs 14.1%, Bt 7.5%, Hbl 0.4%) to adamellite (Pl 34.8%, Kfs 34.6%, Qtz 23.8%, Bt 6.2%, Hbl 0.1%). Its modal composition becomes gradually adamellitic toward the east. The granodiorite is most widespread in the metamorphic belt on the scale of batholithic dimension. This granodiorite is weakly foliated, coarse-grained hornblende-

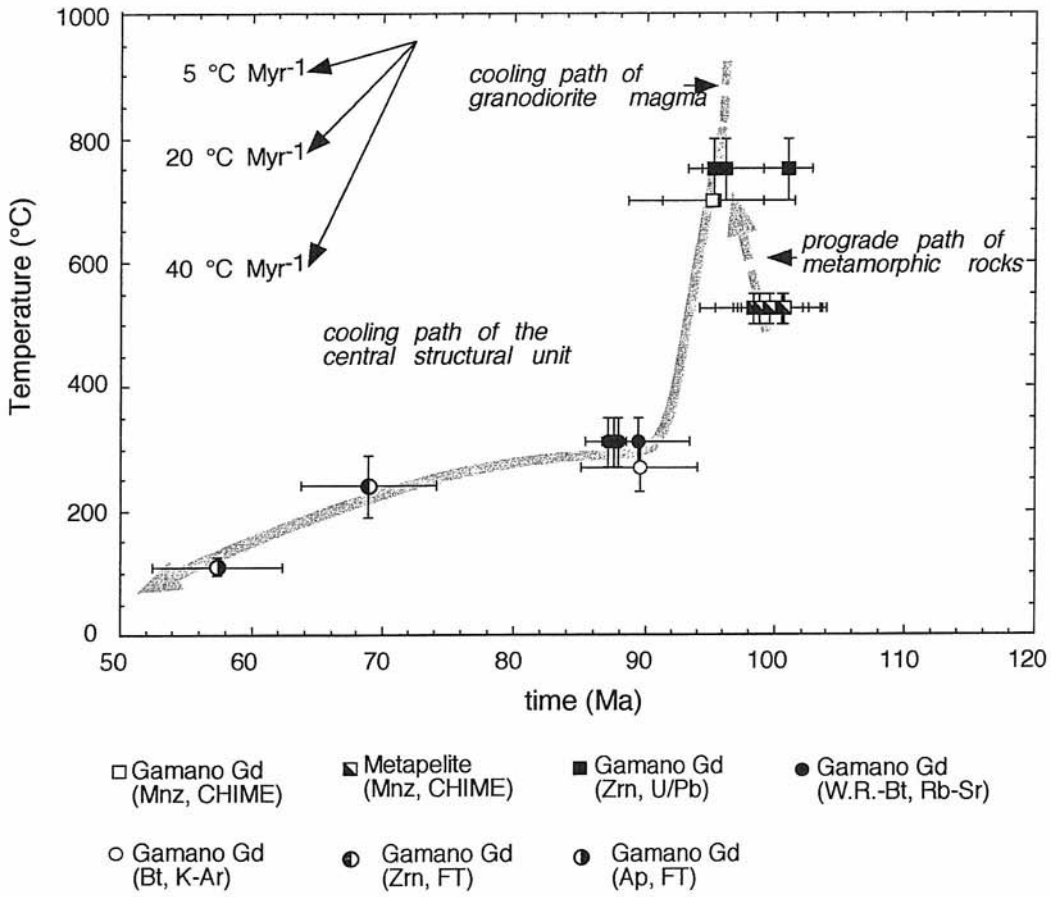

Fig. 13 Cooling history of the central unit of the Ryoke metamorphic belt in the Yanai district (Okudaira *et al.*, 2001 and references therein). In this figure, the range of age represented by the length of the bar reflects the two sigma error. Arrows indicate a possible temperature-time path (cooling history) of the rocks of the central structural unit. Two distinctive cooling stages can be recognized as; 1) a rapid cooling (>40 °C/Myr) for a period (~10 Myrs) soon after the thermal peak (~98 Ma) and 2) subsequently the slow cooling stage (~10°C/Myr) after ca 85 Ma.

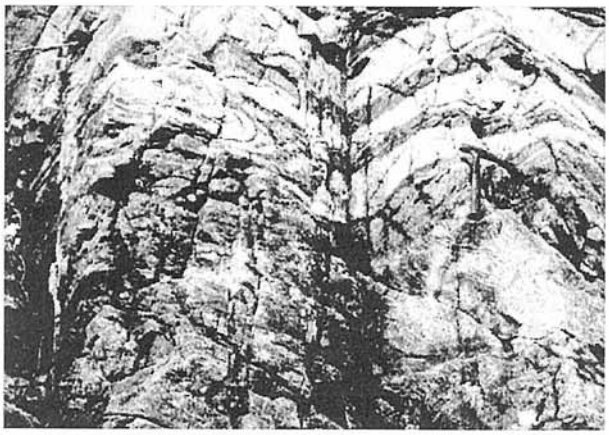

Fig. 14 Photograph of layered migmatite (sillimanite-K-feldspar zone) at Himisaki Cape.

biotite granodiorite. Quartz grains occasionally show undulatory extinction under microscope. Plagioclase composition ranges from An_{28} to An_{34}.

Acknowledgments: We thank M. Tsuboi for providing his paper in press. M. Owada and T. Shimura are thanked for his careful review and his editorial handling, respectively.

References

Anderson, J. L. and Cullers, R. L. (1990) Middle to upper crustal plutonic construction of a magmatic arc: an example from Whipple Mountains metamorphic core complex. *Mem. Geol. Soc. Amer.*, **174**, 47-69.

Brown, M. (1998) Unpairing metamorphic belts: P-T paths and a tectonic model for the Ryoke belt, southwest Japan. *Jour. Metamorphic Geol.*, **16**, 3-22.

Gromet, L. P. and Silver, L. T. (1987) REE variations across

the Peninsular Ranges batholith: implications for batholithic petrogenesis and crustal growth in magmatic arc. *Jour. Petrol.*, **28**, 75-125.

Hara, I., Sakurai, Y., Okudaira, T., Hayasaka, Y., Ohtomo, Y. and Sakakibara, N. (1991) Tectonics of the Ryoke belt. *In* Excursion Guidebook, *98th Ann. Meet. Geol. Soc. Japan*, 1-20.**

Herzig, C. T., Kimbrough, D. L., Tainosho, Y., Kagami, H., Iizumi, S. and Hayasaka, Y. (1998) Late Cretaceous U/Pb zircon ages and Precambrian crustal inheritance in Ryoke granitoids, Kinki and Yanai districts, Japan. *Geochem. Jour.*, **32**, 21-31.

Higashimoto, S., Nureki, T., Hara, I., Tsukuda, E. and Nakajima, T. (1983) *Geology of the Iwakuni district. With Geological Sheet map at 1:50,000.* Geol. Surv. Japan, 79p.*

Honma, H. (1974) Major element chemistry of metamorphic and granitic rocks of the Yanai district in the Ryoke belt. *Jour. Japan. Assoc. Mineral. Petrol. Econ. Geol.*, **69**, 193-204.

Honma, H. and Sakai, H. (1976) Oxygen isotope study of metamorphic and granitic rocks of the Yanai district in the Ryoke belt, Japan. *Contrib. Mineral. Petrol.*, **52**, 107-120.

Ikeda, T. (1993) Compositional zoning patterns of garnet during prograde metamorphism from the Yanai district, Ryoke metamorphic belt, southwest Japan. *Lithos*, **30**, 109-122.

Ikeda, T. (1998a) Progressive sequence of reactions of the Ryoke metamorphism in the Yanai district, southwest Japan: the formation of cordierite. *Jour. Metamorphic Geol.*, **16**, 39-52

Ikeda, T. (1998b) Phase equilibria and the pressure-temperature path of the highest-grade Ryoke metamorphic rocks in the Yanai district, SW Japan. *Contrib. Mineral. Petrol.*, **132**, 321-335.

Ikeda, T. (2002) Regional occurrence of orthopyroxene-bearing basic rocks in the Yanai district, SW Japan: evidence for granulite-facies Ryoke metamorphism. *Island Arc*, **11**, 185-192.

Ikeda, T. (2003) Pressure-temperature conditions of the Ryoke metamorphic rocks in the Yanai district, SW Japan. *Contrib. Mineral. Petrol.* (submitted).

Ishihara, S. (1977) The magnetite-series and ilmenite-series granitic rocks. *Mining. Geol.*, **27**, 293-305.

Iwamori, H. (2000) Thermal effects of ridge subduction and its implications for the origin of granitic batholith and paired metamorphic belts. *Earth Planet. Sci. Lett.*, **181**, 131-144.

Kagami, H., Iizumi, S., Tainosho, Y. and Owada, M. (1992) Spatial variation of Sr and Nd isotope ratios of Cretaceous-Paleogene granitoid rock, Southwest Japan. *Contrib. Mineral. Petrol.*, **112**, 165-177.

Kanaya, H. and Ishihara, S. (1973) Regional variation of magnetic susceptibility of the granitic rocks in Japan. *Jour. Japan. Assoc. Mineral. Petrol. Econ. Geol.*, **68**, 211-224.*

Kawakami, T. and Ikeda, T. (2003) Boron in metapelites controlled by the breakdown of tourmaline and retrograde formation of borosilicates in the Yanai area, Ryoke metamorphic belt, SW Japan. *Contrib. Mineral. Petrol.*, **145**, 131-150.

Kawano, Y. and Ueda, Y. (1966) K-Ar dating on the igneous rocks in Japan (V) - Granitic rocks southwestern Japan. *Jour. Japan. Assoc. Mineral. Petrol. Econ. Geol.*, **56**, 191-211.

Kinosaki, Y. (1952) On the granitic rocks in Chugoku, and the molybdenite and wolframite deposits in them. *Geol. Rept. Hiroshima Univ.*, **3**, 61-75.

Kinoshita, O. (1995) Migration of igneous activity related to ridge subduction in southwest Japan and the East Asian continental margin from the Mesozoic to the Paleogene. *Tectonophysics*, **245**, 25-35.

Kinoshita, O. and Ito, H. (1986) Migration of Cretaceous igneous activity in southwest Japan related to ridge subduction. *Jour. Geol. Soc. Japan*, **92**, 723-735.

Kojima, G. and Okamura, Y. (1968) On the Kitaoshima granite gneiss complex. *Jour. Sci. Hiroshima Univ.*, **C5**, 295-306.

Kutsukake, T. (1993) An initial continental margin plutonism-Cretaceous Older Ryoke granitoids, southwest Japan. *Geol. Mag.*, **130**, 15-28.

Kutsukake, T. (2002) Geochemical characteristics and variations of the Ryoke granitoids, southwest Japan: Petrogenetic implications for the plutonic rocks of a magmatic arc. *Gondwana Res.*, **5**, 355-372.

Leak, B. E. (1990) Granitic magmas: their sources, initiation and consequences of emplacement. *Jour. Geol. Soc. London*, **147**, 587-597.

Miyashiro, A. (1961) Evolution of metamorphic belts. *Jour. Petrol.*, **2**, 277-311.

Miyashiro, A. (1994) *Metamorphic Petrology.* Oxford Univ. Press, New York, 404p.

Moutte, J. (1990) Geochemical study of Cretaceous granitic rocks from Yanai district, southwest Japan. *Nature and Culture, Univ. Museum, Univ. Tokyo*, no. 2, 49-66.

Moutte, J. and Iiyama, J. T. (1984) The Ryoke-Sanyo granitic series in Iwakuni-Yanai district, Southwest Honshu, Japan. *Mining. Geol.*, **34**, 425-436.

Nakajima, T. (1994) The Ryoke plutonometamorphic belt: crustal section of the Cretaceous Eurasian continental margin. *Lithos*, **33**, 51-66.

Nakajima, T. (1996) Cretaceous granitoids in SW Japan and their bearing on the crust-forming process in the eastern Eurasian margin. *Trans. Roy. Soc. Edinburgh, Earth Sci.*, **87**, 183-191.

Nakajima, T., Shirahase, T. and Shibata, T. (1990) Along-arc lateral variation of Rb-Sr and K-Ar ages of Cretaceous granitic rocks in Southwest Japan. *Contrib. Mineral. Petrol.*, **104**, 381-389.

Nakajima, T., Williams, I. S. and Watanabe, T. (1993) SHRIMP U-Pb ages of the Ryoke and Sanyo granitoids in Southwest Japan. *Abstr. 100th Ann. Meet. Geol. Soc. Japan*, 584.**

Ohtomo, Y. (1993) Origin of the Median Tectonic Line. *Jour. Sci. Hiroshima Univ.*, **C9**, 611-669.

Okamura, Y. (1960) Structural and petrological studies on the Ryoke gneiss and granodiorite complex of the Yanai district, Southwest Japan. *Jour. Sci. Hiroshima Univ.*, **C3**, 143-213.

Okudaira, T. (1996a) Temperature-time path for the low-pressure Ryoke metamorphism, Japan, based on chemical zoning in garnet. *Jour. Metamorphic Geol.*, **14**, 427-440.

Okudaira, T. (1996b) Thermal evolution of the Ryoke metamorphic belt, southwestern Japan: Tectonic and numerical modeling. *Island Arc*, **5**, 373-385.

Okudaira, T., Hara, I., Sakurai, Y. and Hayasaka, Y. (1993) Tectono-metamorphic processes of the Ryoke belt in the Iwakuni-Yanai district, southwest Japan. *Mem. Geol. Soc. Japan*, no. 42, 91-120.

Okudaira, T., Hara, I. and Takeshita, T. (1995a) Emplacement mechanism of the Older Ryoke granites in the Yanai district, southwest Japan, with special reference to extensional deformation in the Ryoke metamorphic belt. *Jour. Sci. Hiroshima Univ.*, **C10**, 357-366.

Okudaira, T., Takeshita, T., Hara, I. and Ando, J. (1995b) A new estimate of the conditions for transition from basal <*a*> to prism [*c*] slip in naturally deformed quartz. *Tectonophysics*, **250**, 31-46.

Okudaira, T., Ohtomo, Y. and Hayasaka, Y. (2000) Cretaceous tectonics of southwest Japan in light of the studies for Ryoke metamorphic belt. *Monogr. Assoc. Geol. Collab. Japan*, no. 49, 67-80.*

Okudaira, T., Hayasaka, Y., Himeno, O., Watanabe, K., Sakurai, Y. and Ohtomo, Y. (2001) Cooling and inferred exhumation history of the Ryoke metamorphic belt in the Yanai district, south-west Japan: constraints from Rb-Sr and fission-track ages of gneissose granitoid and numerical modeling. *Island Arc*, **10**, 98-115.

Owada, M., Tanaka, S., Yuhara, M. and Kagami, H. (1995) Rb-Sr whole-rock isochron age of the Habu granodiorite in the eastern Yamaguchi Prefecture. *Jour. Mineral. Petrol. Econ. Geol.*, **90**, 358-364.*

Pearce, J.A., Harris, N.B.W. and Tindle, A.G. (1984) Trace element discrimination diagrams for the tectonic interpretation of granitic rocks. *Jour. Petrol.*, **25**, 956-983.

Pitcher, W. S. (1983) Granite type and tectonic environment. *In* Hsu, K., ed., *Mountain Building Processes*, Academic Press, London, 19-40.

Shigeno, H. and Yamaguchi, M. (1976) A Rb-Sr isotopic study of metamorphism and plutonism in the Ryoke belt, Yanai district. *Jour. Geol. Soc. Japan*, **82**, 687-698.*

Suzuki, K. and Adachi, M. (1998) Denudation history of the high *T/P* Ryoke metamorphic belt, southwest Japan: constraints from CHIME monazite ages of gneisses and granitoids. *Jour. Metamorphic Geol.*, **16**, 23-38.

Suzuki, K., Adachi, M. and Kajizuka, I. (1994) Electron microprobe observations of Pb diffusion in metamorphosed detrital monazites. *Earth Planet. Sci. Lett.*, **128**, 391-405.

Suzuki, K., Adachi, M. and Nureki, T. (1996) CHIME age dating of monazites from metamorphic rocks and granitic rocks of the Ryoke belt in the Iwakuni area, Southwest Japan. *Island Arc*, **5**, 43-55.

Takahashi, Y. (1993) Al in hornblende as a potential geobarometer for granitoids.: A review. *Bull. Geol. Surv. Japan*, **44**, 597-608.*

Takami, M. and Itaya, T. (1996) Episodic accretion and metamorphism of Jurassic accretionary complex based on biostratigraphy and K-Ar geochronology in the western part of the Mino-Tanba Belt, Southwest Japan. *Island Arc*, **5**, 321-336.

Takami, M., Isozaki, Y., Nishimura, Y. and Itaya, T. (1990) Geochronology of weakly metamorphosed Jurassic accretionary complex (the Kuga Group) in eastern Yamaguchi Prefecture, Southwest Japan. *Jour. Geol. Soc. Japan*, **96**, 669-681.*

Tsuboi, M. and Suzuki, K. (2003) Heterogeneity of initial $^{87}Sr/^{86}Sr$ ratios within a single pluton: evidence from apatite strontium isotopic study. *Chem. Geol.*, **199**, 189-197.

Tsuboi, M., Suzuki, K., Sakashima, T., Terada, K. and Sano, Y. (2001) Dating of the habu Granodiorite in the Iwakuni area, southwest Japan, using CHIME, SHRIMP and Rb-Sr methods. *Abstr. 108th Ann. Meet. Geol. Soc. Japan*, 14.**

Uyeda, S. and Miyashiro, A. (1974) Plate tectonics and the Japanese islands: a synthesis. *Bull. Geol. Soc. Amer.*, **85**, 1159-1170.

Yuhara, M., Ohira, H., Owada, M., Kamei, A. and Kagami, H. (1999) Geochronological study of the Habu Granodiorite in the northern Yamaguchi Prefecture, Southwest Japan. *Mem. Geol. Soc. Japan*, no. 53, 323-331.*

Yuhara, M., Kagami, H. and Nagao, K. (2000) Geochronological characterization and petrogenesis of granitoids in the Ryoke belt, Southwest Japan Arc: constraints from K-Ar, Rb-Sr and Sm-Nd systematics. *Island Arc*, **9**, 64-80.

*: in Japanese with English abstract.
**: in Japanese.

Received May 20, 2003
Accepted July 3, 2003

Appendix. Route map and locations of stop points in the Iwakuni-Yanai district.

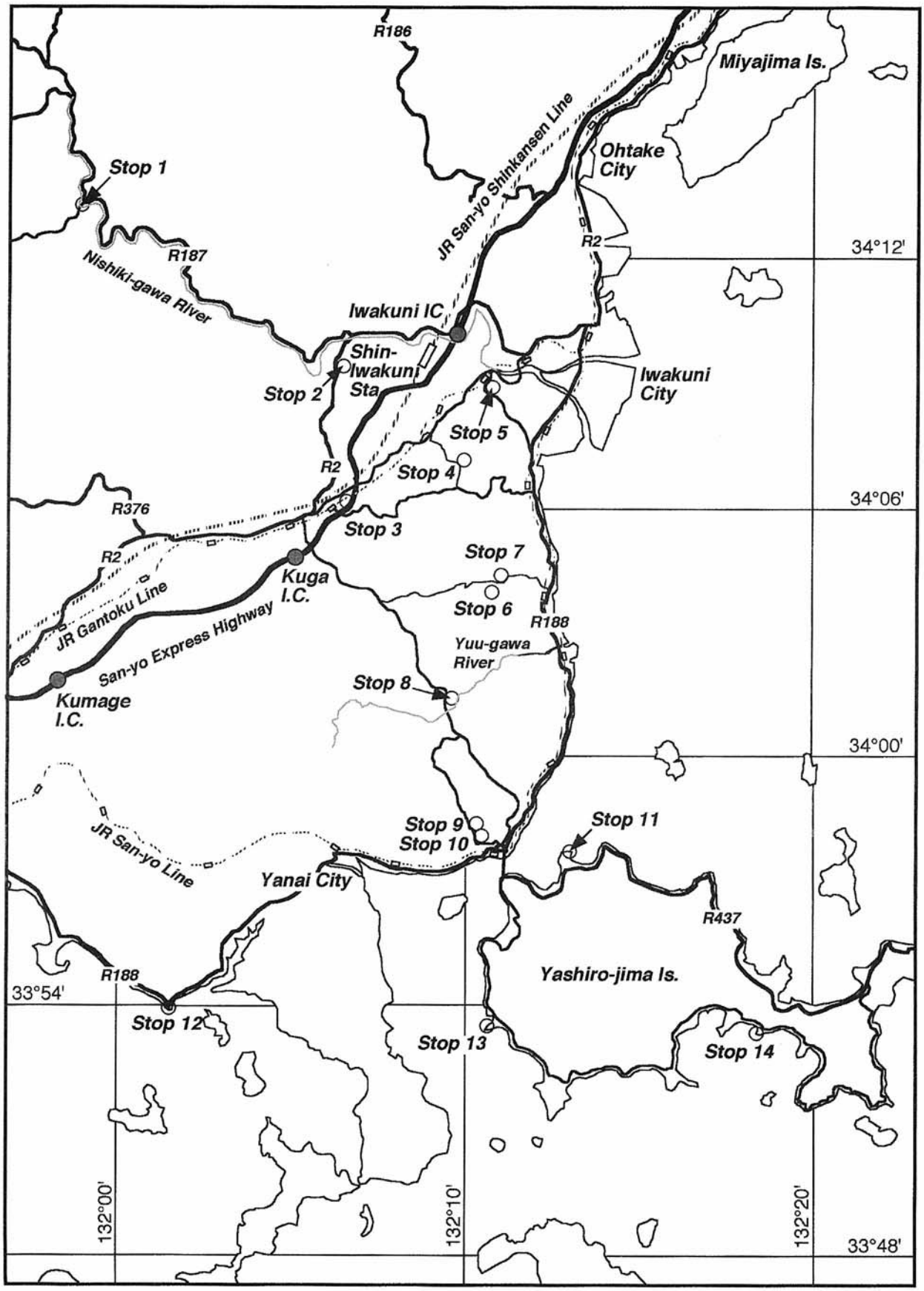

Hutton Symposium V, Field Guidebook
Geological Survey of Japan, Interim-Report no.28, p.41－60, 2003

Trip A3

Ilmenite-series pink and gray granitoids and felsic/mafic magma interaction across the late Cretaceous Inner Zone Batholith of SW Japan

Shunso ISHIHARA[1], Shin-ichi YOSHIKURA[2], Hiroaki SATO[3],
Yasushi SATAKE[4] and Shin-ichi ATSUTA[5]

Abstract: Late Cretaceous granitoids of the ilmenite-series Sanyo and Ryoke Belts are reviewed along the Okayama-Kagawa Prefecture transect (*ca.* 134°E). They are mostly monzogranite in the Sanyo Belt but granodiorite in the Ryoke Belt. One such example of pink monzogranite is shown in the Mannari quarry. The granitic activities of both the Belts were ended by fine-grained granite intrusion of stock size. Representative examples of each Belt are shown at north of Kurashiki and Aji stone quarries. The granitoids are overlain unconformably by Miocene high-Mg andesitic rocks, which are shown at Goshikidai.

In Shodoshima Island, the late Cretaceous granitoids occur closely associated with gabbroids forming the Tanoura Igneous Complex (TIC). The complex was formed by intrusion of granite and diorite and gabbro-diorite layers (Stage 1), E-W trending synplutonic mafic dike (Stage 2), N-S trending synplutonic mafic and composite dikes (Stage 3), and aplite-pegmatite and granophyre dikes (Stage 4). These complex intrusion sequence and intrermingling of felsic and mafic magmas are observed on the spectacular outcrops along the southern coast of the Tanoura Peninsula.

Keywords: Hutton symposium, field excursion, Late Cretaceous, granitoids, ilmenite series, major chemistry, trace elements, REE pattern, synplutonic dike, mafic magmatic enclave (MME), mingling and mixing, Miocene, high Mg andesite

1. Introduction

Late Cretaceous to Paleogene granitoids of the Sanyo and Ryoke Belts in the Inner Zone of Southwest Japan, forming the largest batholith in the Japanese Islands, are composed of the inner (Japan Sea side) magnetite series of the Sanin Belt and the outer (Pacific Ocean side) ilmenite series of the Sanyo and Ryoke Belts (see Fig. 1 of Okudaira *et al.* , this volume). The granitoids of both the Sanin and Sanyo Belts are mostly granodiorite and monzogranite and contrasted with their magnetic susceptibility (Fig. 1) and ferric/ferrous ratio (Ishihara, 1971). Major differences between the latter two belts are tectonic shearing prevailing in the Ryoke Belt, but massive granitoids predominant in the Sanyo Belt. The granitoids are often associated and mingled with gabbroids (including gabbro, quartz gabbro and diorite) in the Sanin and Ryoke Belts (Fig. 1); the best example of Shodoshima Island is visited in this A3 field trip.

The southern Okayama-Kagawa region of the eastern Chugoku-Shikoku District of the A3 trip, is underlain by Jurassic accretionary complex, which have been non-metamorphosed in the Sanyo Belt but regionally metamorphosed in the Ryoke Belt, and the late Cretaceous felsic volcanic rocks coeval generally to the nearby granitoids. These rocks were unconformably overlain by the late Cretaceous Izumi Sandstone to the south, and locally Miocene sediments and (high-Mg) andesite-rhyolites.

The metamorphosed accretionay complex is sporadically distributed in Kagawa Prefecture, which has been converted to cordierite and/or sillimanite-bearing rocks and thus considered as Ryoke metamorphic rocks (Kutsukake *et al.*, 1979). Nureki *et al.* (1982) found them in the Shiaku Islands composed of amphibolite-grade gneisses originated in limestones, clastic rocks and pyroclastic rocks rich in TiO_2 and K_2O.

Late Cretaceous volcanic rocks are widely distributed in the southern Okayama Prefecture but only little or none in Kagawa Prefecture. They are mostly felsic ignimbrites associated locally with caldera subsidence (Ishihara and Imaoka, 1999). Rb/Sr whole rock ages of the granitoids are determined to be 84.0±3.7 Ma with the Sr*I* ratios ranging from 0.7072 to 0.7083 in the Sanyo Belt of the southern Okayama Prefecture (Kagami *et al.*, 1988). In the Ryoke Belt of the eastern Kagawa Prefecture, coarse-grained granitoids in the south overlain by the upper Cretaceous Izumi Sandostone are oldest as 93.4 Ma (hornblende K-Ar age), and the youngest is Rb-Sr whole rock age of the fine-grained Aji granitic stock of 82.9±8.0 Ma with Sr*I* of 0.70773± 0.00007 (Yuhara *et al.*, 2003).

[1] Geological Survey of Japan, Tsukuba, 305-8567 Japan. E-mail: s-ishihara@aist.go.jp
[2] Kochi University, Kochi, 780-8520 Japan. E-mail: yoshikur@cc.kochi-u.ac.jp
[3] Kobe University, Kobe, 657-8501 Japan. E-mail: hsato@kobe-u.ac.jp
[4] Hiroshima University, Higashi Hiroshima, 739-8524 Japan. E-mail: yatake@hiroshima-u.ac.jp
[5] Tohoku University, Sendai, 980-8578 Japan. E-mail: atsuta@mail.cc.tohoku.ac.jp

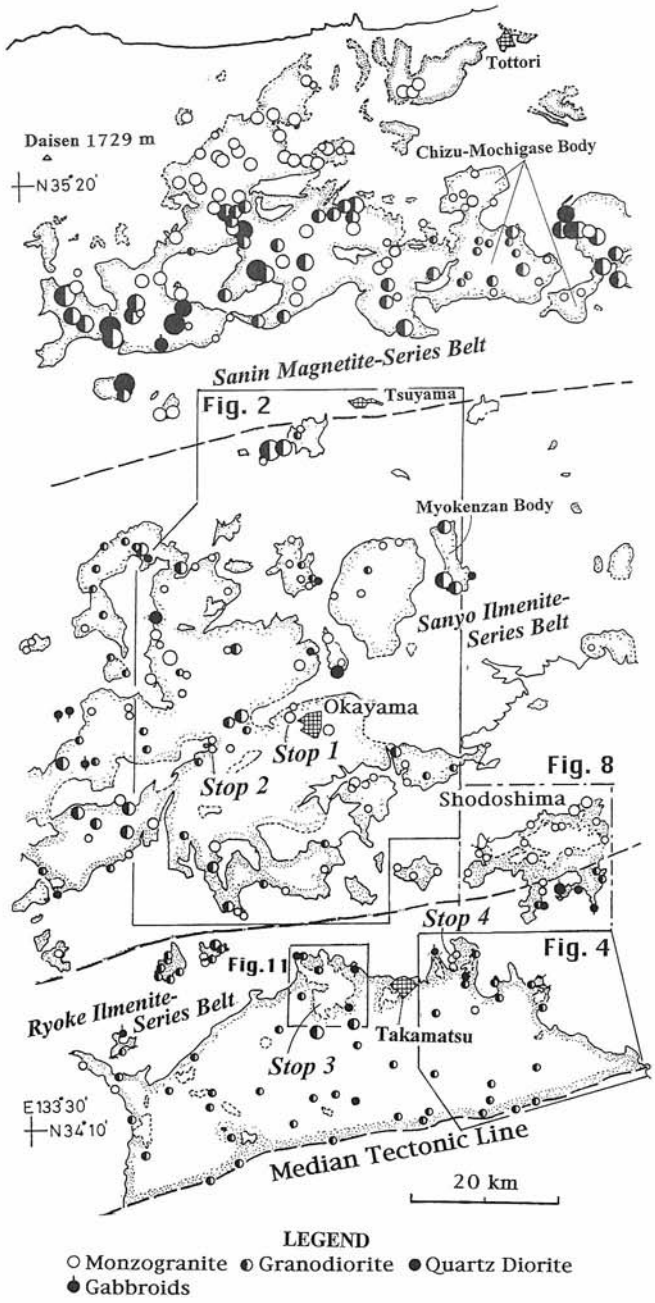

Fig. 1. Rock composition and magnetic susceptibility of the granitoids and gabbroids of the eastern Chugoku and Shikoku District. Size of the circles in increasing diameter indicates the magnetic susceptibility, less than 50, 50-100, 100-500, 500-1,000 and more than $\times 10^{-6}$ emu/g, whereby 100×10^{-6} is boundary between the magnetite-series and ilmenite-series granitoids. Chizu-Mochigase granitoids are exceptional ilmenite-series body in the Sanin Belt, while the Myokenzan granitods are exceptional magnetite-series body in the Sanyo Belt. Locations of Figures 2, 4, 8 and 11, and stop points 1 through 4 are shown.

2. Granitoids of Okayama Prefecture

Granitoids of the southern Okayama Prefecture consist essentially of coarse- to medium-grained phases having biotite and/or hornblende-biotite mineral assemblages and fine-grained granitic stocks with varying composition and muscovite-biotite leucogranites occurring at the margin of the coarse-grained biotite granite batholith and related to tungsten ore deposits (Ishihara, 1971). Amphibole gabbroids occur very sporadically as blocky inclusion bodies or dikes in these fine to coarse-grained granitoids.

Nureki *et al.* (1979) classified the coarse- to medium-grained granitoids into types I to IV, and unclassified fine-grained phases (Fig. 2), as follows:

Type I: coarse- to medium-grained biotite syenogranite. K-feldspar is pinkish and has highest triclinicity (Fig. 3), thus close to microcline.

Type II: coarse- to medium-grained hornblende-biotite monzogranite. K-feldspar is pink and porphyritic or glomeroporphyritic. This type has an intermediate triclinicity between microcline and orthoclase, and shows no microcline lattice texture under the microscope. The famous dimension stone of Mannari Stone we visit (see Table 1 for the modal composition), is mined from this type.

Type III: coarse- to medium-grained hornblende-biotite monzogranite similar to the type II, but quartz is rounded and glomeroporphyritic. K-feldspar is pink with low degree of triclinicity.

Type IV: coarse- to medium-grained hornblende-biotite monzogranite. Plagioclase is porphyritic to glomeroporphyritic. K-feldspar is white and glomeroporphyritic.

Fine-grained granitoids includes fine-grained felsic phase containing abundant mafic microgranular enclaves (MME, *e.g.*, Fukuwatari body) and muscovite-biotite leucogranite related to tungsten ore deposits at north of Kurashiki and Ibara cities. The latter leucogranite occurs at margin of the coarse-grained granites and is very fractionated (Rb/Sr～34) and high in F (Table 2).

The ore deposits are composed of wolframite-quartz veins with greisenization and were mined at Kibi (WO_3 51.7 tons), Ibara (WO_3 34.5 tons) mines, and small mines of Miyoshi, Okayama, Sankei and Keigamaru. Uranium minerals, mainly coffinite as primary mineral, and many secondary minerals are often associated with them (*e.g.*, Miyoshi mine; Hida *et al.*, 1961). The largest metal mines in the southern Okayama Prefecture is Obie copper mine (Cu 16,500 tons) of chalcopyrite-quartz vein type occurring in the Jurassic slates just above concealed fine-grained granite at east of Kurashiki (JMIA, 1968).

3. Granitoids in Kagawa Prefecture

The late Cretaceous granitoids of Kagawa Prefecture are divided into coarse- to medium-grained granodiorite and granite batholith and fine-grained biotite granitic stocks. The former rocks are massive or deformed, as shown by alignment of mafic silicates, microscopic kink and bend of

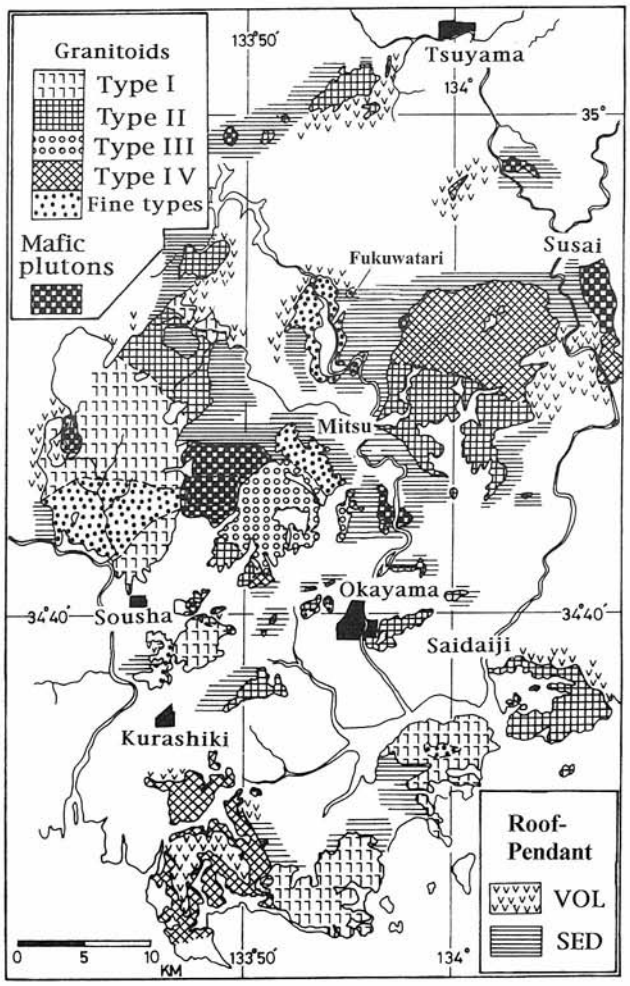

Fig. 2. Geologic map of the southern Okayama Prefecture (Nureki *et al.*, 1979). Mafic plutons include gabbro, quartz diorite, quartz monzodiorite, and granodiorite. Roof-pendant: SED, Pre-Cretaceous sedimentary rocks including the Yakuno Group. VOL, Late Cretaceous felsic lavas and pyroclastic rocks.

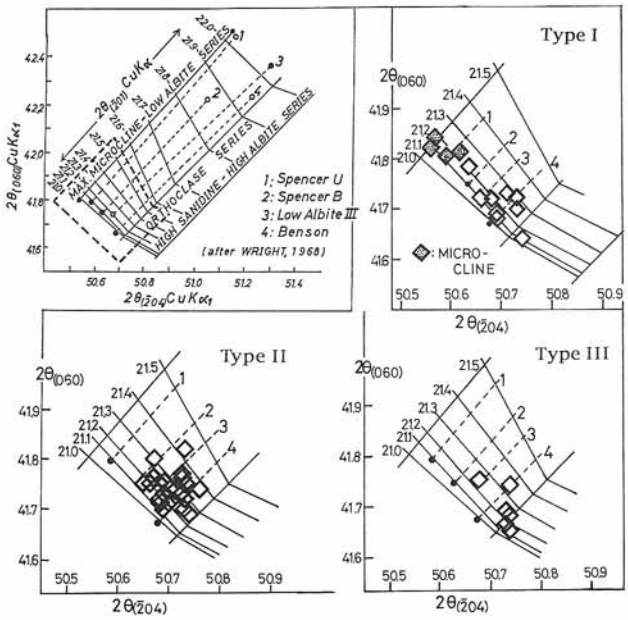

Fig. 3. Structural status of alkali feldspar of the Sanyo granitoids in the southern Okayama Prefecture (Nureki *et al.*, 1979).

Table 1. Modal compositions (vol. %) of the granitoids of Stops 1, 2 and 4.

Field No. & Locality	Pl	Kfs	Qtz	Hbl	Bt	Ms	Others	C.I.	Kfs+Qtz
Mannari Granite (Nureki *et al.*, 1979)									
Quarry A 1-7 (avg., n=7)	23.7	35.6	31.2	9.6*		none	n.d.	9.6	66.8
Quarry B 8-11 (avg, n=4)	27.6	31.6	29.4	11.5*		none	n.d.	11.5	61.0
Quarry C 12-14 (avg., n=3)	31.3	29.1	28.2	11.5*		none	n.d.	11.5	57.3
Leucogranite (Ishihara, 1971)									
6910156 Mitsuhata Quarry	24.7	34.0	38.3	none	2.6	none	0.4	3.0	72.3
6910157 Miyoshi mine	28.6	27.5	41.0	none	1.9	1.0	tr	2.9	68.5
Aji Granite (Kutsukake *et al.*, 1979)									
75110119 Aji Pen. Takei	31.5	30.3	31.4	none	6.6	none	0.2	6.8	61.7
75110119' ditto, Sasao	32.1	33.5	27.7	none	6.2	none	0.4	6.6	61.2
75110121 ditto, Nyotaisan	43.4	26.4	23.1	none	6.7	none	0.2	6.9	49.5
75110284 Yashima	36.1	29.1	29.8	0.1	4.9	none	0.1	5.1	58.9
75110307 ditto	41.6	19.7	35.2	none	3.5	none	tr	3.5	54.9
75110329 Aji, Tomisan	40.6	19.1	29.1	0.1	10.8	none	0.3	11.2	48.2

The modal analyses of Nureki *et al.* (1979) were done on cut surface larger than 60 cm^2 with 2.5 mm interval after staining K-feldspar by cobalti-nitrite. The other modal analyses were done on regular thin section after staining K-feldspar. Pl, plagioclase; Kfs, K-feldsapr; Qtz, quartz; Hbl, hornblende; Bt, biotite; Ms, muscovite; C. I., color index. * Mafic silicates (biotite much more than hornblende).

Table 2. Selected chemical compositions of the Stops 1, 2 and 3.

Elements	Mannari Gr.	Leucogranites		Aji Granite
	MAN01	W Prov.(157)	Mo Prov.(605)	72TO329
SiO_2 (wt%)	74.27	76.4	76.66	72.22
TiO_2	0.19	0.04	0.15	0.27
Al_2O_3	12.93	12.22	12.21	14.63
Fe_2O_3	2.61*	0.04	0.8	0.18
FeO	n.d.	0.79	0.36	1.95
MnO	0.06	0.03	0.03	0.04
MgO	0.23	0.09	0.19	0.51
CaO	1.34	0.62	0.55	2.72
Na_2O	3.51	3.78	3.29	3.95
K_2O	4.43	4.90	4.81	2.67
P_2O_5	0.03	<0.01	<0.01	0.1
H_2O+	0.40	0.5	0.52	0.47
H_2O-	0.01	0.28	0.32	0.16
Total	100.01	99.69	99.89	99.87
Trace elements (ppm)				
Rb	157	373	189	58
Sr	102	11	35	367
Pb	17	37	13	19
Y	39	76	29	10
Th	12.8	33.3	24.6	5.9
U	3.2	6.4	7.7	<0.5
Mo	2.6	<0.2	4.2	<0.2
W	1.5	5.2	2.8	2.7
Sn	2.7	7.9	1.2	1
F	n.d.	3000	320	480
Cl	n.d.	95	193	20
Li	n.d.	30	11	32
Be	n.d.	4.2	3.1	2.0
Fe_2O_3 /FeO	n.d.	0.05	2.2	0.09
Rb/Sr	1.5	33.9	5.4	0.16

Analyzed by porarized XRF, AA and wet method.
n.d., not determined.

biotite and feldspars, and protoclastic textures in quartz. Such deformed granitoids occur from Shodoshima (Nanpudai) and Hon-jima to the mainland Kagawa Prefecture, and can be regarded as "older" granitoids related to the Ryoke metamorphism, although exact age determinations are necessary to prove the older age.

The granitoids of the eastern part of the main Kagawa Prefecture are classified and nick-named as Shido, Aji and Shirotori Granites (Fig. 4) by Kutsukake *et al.* (1979). The Shirotori Granites have hornblende K-Ar age of 93.4 Ma, Shido Granites have that of 86.8 to 82.3 Ma (Yuhara *et al.*, 2000), and the Aji Granites have that of 83.5± 1.1 Ma (Yuhara *et al.*, 2003). Granitoids of the northeastern part are termed as Shido Granites, and identified to be coarse- to medium-grained, weakly gneissic biotite-hornblende tonalite, hornblende-biotite granodiorite and porphyritic biotite monzogranite with K-feldspar megacrysts. Mafic enclaves and schlieren are commonly seen.

3.1 The Aji Granites

Aji Granites occurring mostly in previous Aji Village and surroundings intrude into the Shido Granites. The Aji Granites have Rb-Sr whole rock isochron age of 82.9±8.0 Ma with Sr*I* of 0.70773±0.00007 (Yuhara *et al.*, 2003). The hornblende K-Ar age mentioned before is the same as the whole rock age within the analytical error, both indicating an intrusion age. K-Ar age on the biotite separates vary from 80.4 to 79.4 Ma (n=6), suggesting a cooling age at *ca.* 300°C.

The Aji Granites are mostly fine-grained biotite monzogranite and partly hornblende-bearing biotite granodiorite with heterogenous spotty textures, "Fu" in Japanese, which are due to heterogeneity of the grain size and mineral assemblage; biotite and quartz providing dark spotty transparency, while the surrounding feldspars-rich part giving rise to whitish color. The heterogenous and fine-grained granitoids are considered as the best tombstone for the Japanese graveyard, and mined at many places and shipped out as Aji-ishi (stone) (Ishihara, 1991). These granitoids contain sometimes white to gray megacrysts of poikilitic K-feldspar and small amounts of mafic to intermediate igneous enclaves, and patchy biotite-rich (sedimentary) enclaves.

3.2 The Shirotori Granites

The Shirotori Granites occur widely in the southeastern part of Kagawa Prefecture. The granitoids are coarse-grained and massive, ranging in composition from hornblende-biotite granodiorite to biotite granites. Mafic enclaves are rare. The K-feldspar is weakly pink in color.

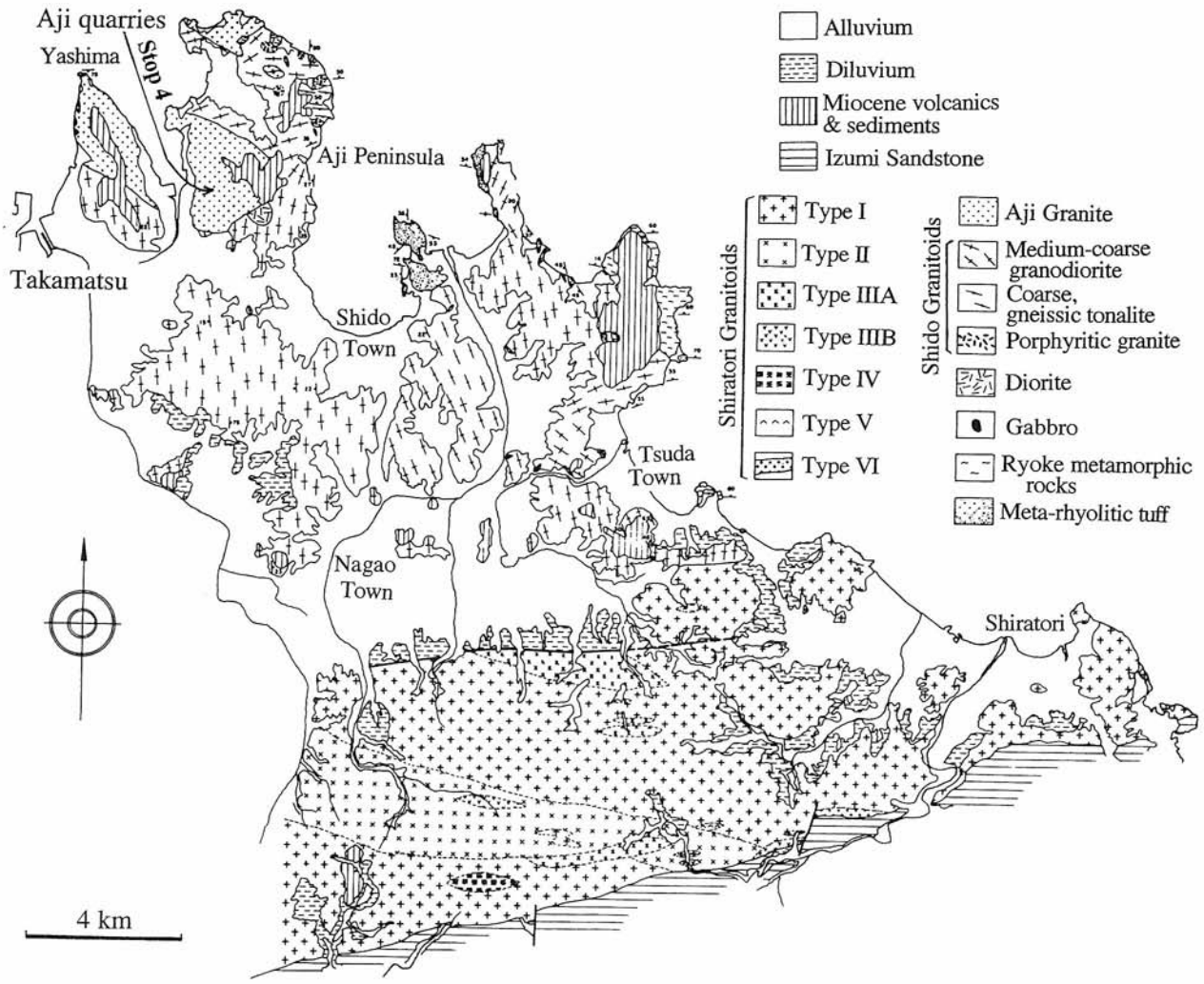

Fig. 4. Geologic map of the Ryoke granitoids in the eastern Kagawa Prefecture (Kutsukake *et al.*, 1979).

Granitoids of the western half of Kagawa Prefecture are still unclassified. They are mostly coarse- to medium-grained hornblende-biotite granodiorite to biotite monzogranite, which may be partly porphyritic. The stressed granitoids have been observed at several localities (Ishihara, 2003). Granitoids and gabbroids of the Shodoshima, Kagawa Prefecture, are very well studied, and will be mentioned later separately.

4. Chemical characteristics

Randomly sampled 39 analyses indicate that silica contents of the Sanyo granitoids vary from 63.6 to 77.4 wt% with an average of 74.1 wt% (n=25); while those of the Ryoke granitoids range from 62.6 to 75.6 wt% with an average of 71.0 wt (n=14). The total alkalis are averaged as 7.80 wt% (n=25) for the Sanyo granitoids, and 6.91 wt% (n=14) for the Ryoke granitoids. The Sanyo granitoids are more felsic than the Ryoke granitoids. In terms of the alkali-lime index of Peacock (1931), both the granitoids belong to calcic series (>61), but the Sanyo granitoids of 64.5, are more calcic than the Ryoke granitoids of 61.0.

The Ryoke granitoids are classified into general coarse-grained rocks and fine-grained Aji granitoids and plotted together with the Sanyo granitoids in the Harker diagram (Fig. 5).

4.1 Feldspars components

Both Al_2O_3 contents and the alumina saturation index (ASI, Zen, 1986) are higher in the Ryoke granitoids than in the Sanyo granitoids. The ASI varies from 0.91 to 1.08 on the Sanyo granitoids, from 0.95 to 1.06 on the Ryoke general granitoids, and from 1.02 to 1.10 on the Aji granitoids. Ga which substitutes Al shows no distinct regional variations. Enclaves contained in the Aji granitoids are higher in Ga than the other granitoids.

There are no clear regional variations on CaO. Na_2O shows decreasing tendency with increasing SiO_2 in the Ryoke granitoids, but generally increasing with SiO_2 in the Sanyo granitoids. K_2O is enriched in the Sanyo granitoids than the Ryoke granitoids. Rb substitutes generally K and increases with increasing SiO_2 (Fig. 5). The element is constantly low in the Aji granitoids as 58 to 74 ppm. These granitoids are high in Sr although Ca is not particularly high, giving rise to

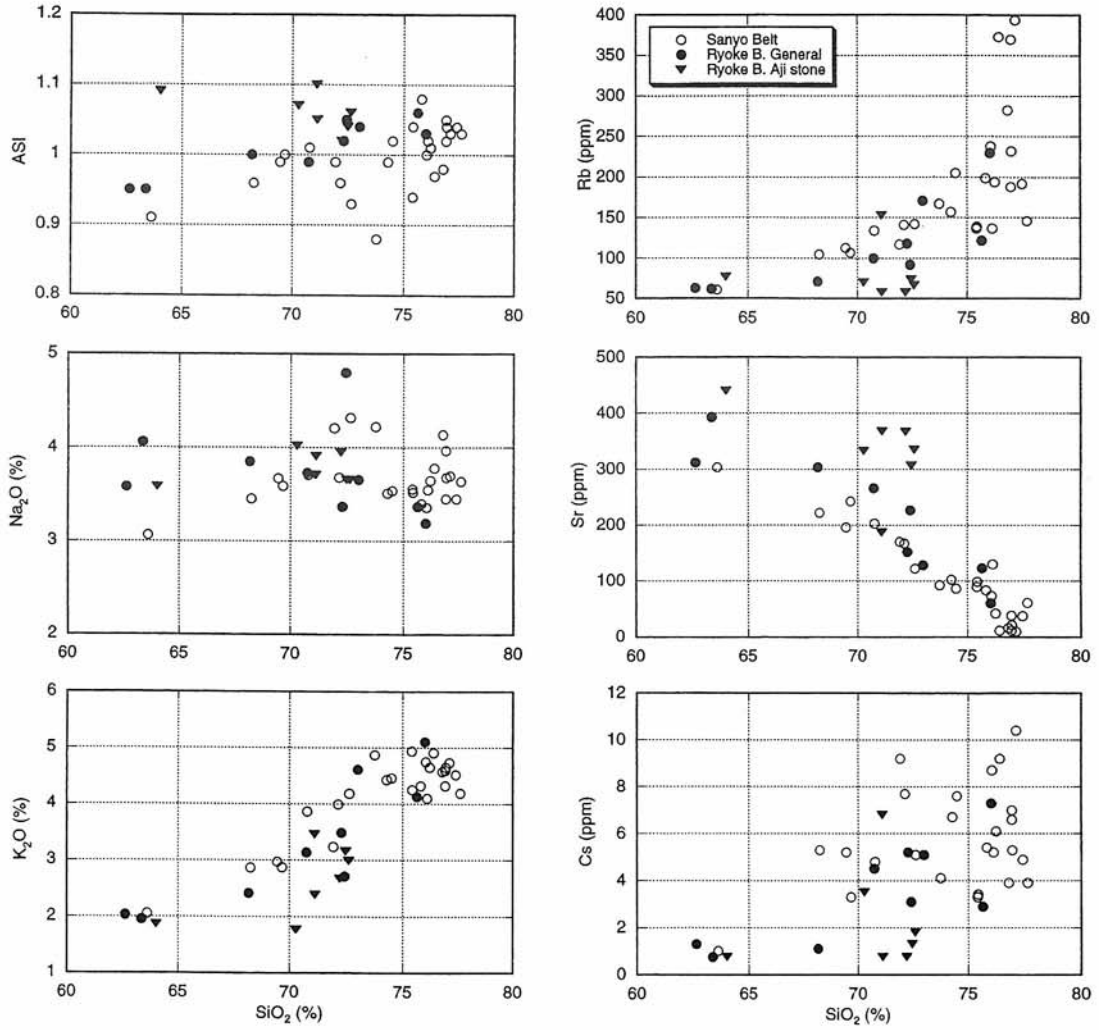

Fig. 5. Harker diagrams for selected components (1). Modified from Ishihara (2003).

low Rb/Sr ratio of 0.2. On the other hand, muscovite-biotite leucogranite of the Sanyo Belt are highest in Rb, as 370 to 394 ppm but lowest in Sr (10-11 ppm) and also CaO (0.5-0.62 %), thus yielding Rb/Sr ratios of 33.6 - 39.4. These granites are related to wolframite-quartz vein mineralizations. Similar leucogranite at the Ibara tungsten mine stock is also high in Rb (282 ppm) and Rb/Sr ratio (17.6) but low in CaO (0.51 %). Ba substitutes K in general; however, there are poor correlation between Ba and K or Rb.

Pb, Tl and Cs substitute also K; thus they increase with increasing SiO_2. There is no difference on the distribution patterns between the granitoids of the Sanyo Belt and Ryoke Belt. However, Cs is rather poor in the Ryoke granitoids, especially of the Aji granitoids.

4.2 Mafic silicate components

These components are correlated negatively with SiO_2 (Fig. 6). The total iron is higher in the Ryoke Belt of granite composition, say SiO_2 more than 70 %, while magnesium is lower in the Ryoke granitoids except for the Aji granitoids. Ti is high in the Aji granitoids and is least in the general Ryoke granitoids. V is definitely higher in the Sanyo granitoids than the Ryoke granitoids. Cr and Cu are erratically distributed, but Zn and Co are negatively correlated with SiO_2 (see Ishihara, 2003). Co is higher in the Sanyo granitoids than in the Ryoke granitoids.

4.3 Accessory mineral components

P is negatively correlated with SiO_2 in the order of abundance of the Aji granitoids, Ryoke general granitoids and Sanyo granitoids. These contents may reflect not those of monazite but apatite. There are no regional variations on Zr, La and Ce. Two granitoid localities are found rich in the LREE are granodiorite at Shido and deformed granodiorite at Nanpudai. Allanite in trace amounts are easily observed under the microscope in these granitoids; thus La and Ce are considered to be contained in this mineral.

Y is especially high, as 76 to 96 ppm, in muscovite-bearing biotite leucogranite related to W-ore deposits which contain trace amount of cassiterite. Both W and Sn are similarly high in the granite as 5.0 to 7.4 ppm and 3.5 to 7.9 ppm, respectively. Mo is, however, not as high as W and Sn in the granite. Y, Mo, W and Sn are generally higher in the Sanyo granitoids than in the Ryoke granitoids, and are most

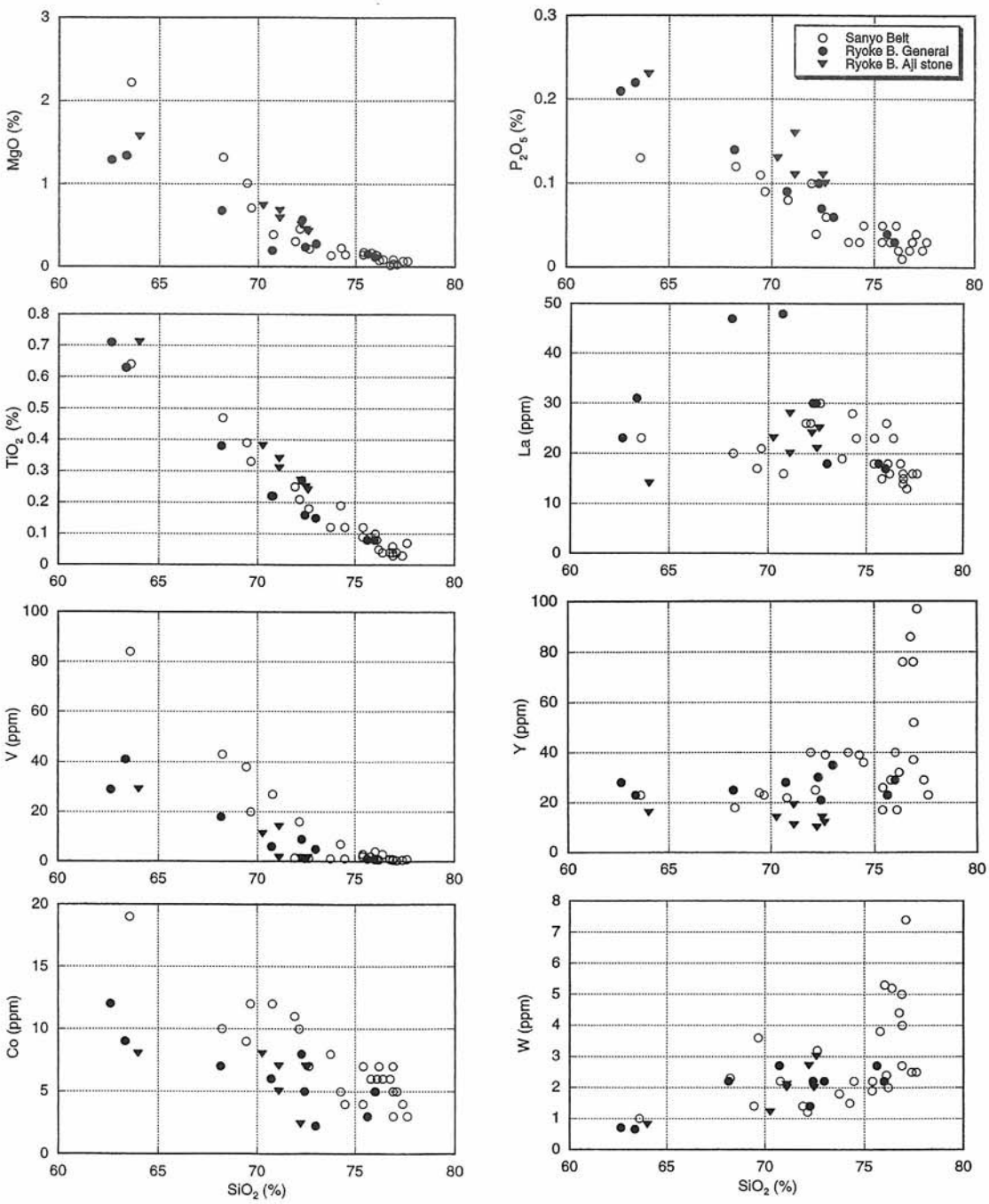

Fig. 6. Harker diagrams for selected components (2). Modified from Ishihara (2003).

depleted in the Aji granitoids.

U and Th show similar distribution patterns to those of W and Sn, reflecting possible accessory occurrence of U and Th minerals in the W ore deposits. Ta, though not shown here, is similarly distributed with W (Fig. 6). Nb, however, is only abundant in the muscovite-bearing granite as 16.4 - 19.3 ppm, and no clear differences on the other Sanyo and Ryoke granitoids.

4.4 Rare earth elements

REE patterns of the Sanyo granitoids are shown by three distinct groups. The first one is shown by pyroxene-hornblende-biotite granodiorite, which has intermediate values on the LREE, but low values from Eu to HREE. The second pattern is shown by the pink Mannari Granite and biotite granite at Ibara, which have higher LREE but intermediate HREE with weak negative Eu anomaly (Fig. 7). The third pattern is shown by muscovite-biotite leucogranites related to wolframite mineralizations. They have flat pattern with strong negative Eu anomalies, which is characteristic pattern of the Naegi Granite (Ishihara and Wu, 2001), and is considered as fractionated I-type granite.

From the Ryoke Belt, "Older" granodiorite and "Younger" Aji granitoids were selected. The older granidiorites show

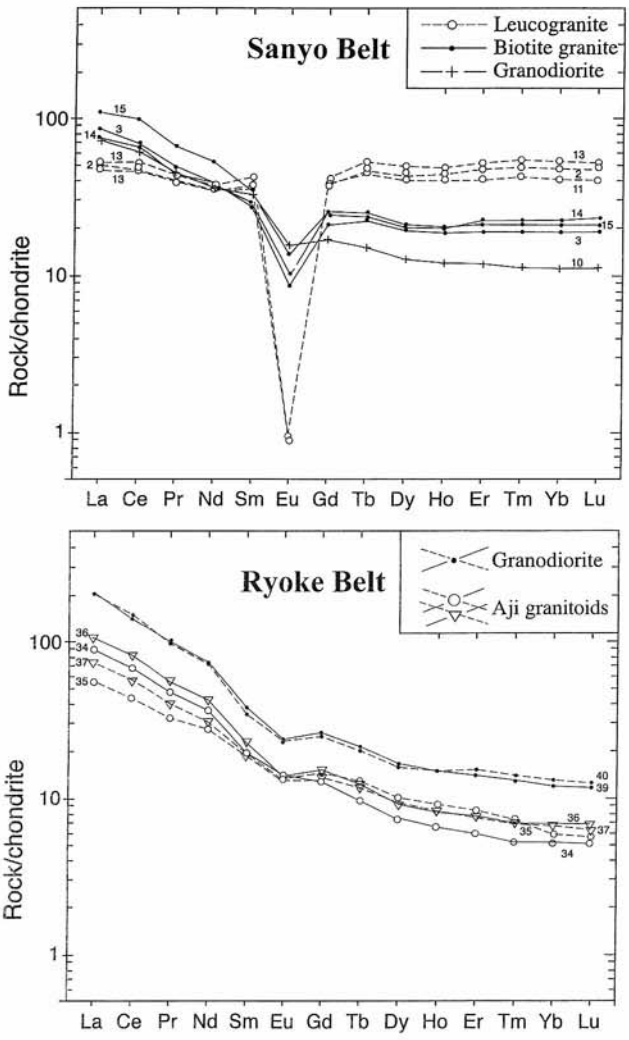

Fig. 7. REE patterns of the Sanyo and Ryoke granitoids (Ishihara, 2003). Numbers correspond to those of the appendix of Ishihara (2003).

similar REE pattern to that of the No. 10 granodiorite of the Sanyo Belt, which may be younger in age relative to the Ryoke granodiorite. The younger Aji granitoids show similar patterns to the Ryoke older granitoids, but depleted in all the REEs (Fig. 7). Two mafic and intermediate enclaves exhibit similar REE patterns to those of the host granitoids.

5. Geology and what we see in the Shodoshima Island

The Shodoshima Island is located in the eastern part of the Seto Inland Sea (see Fig. 1 for the location), 160 km southwest of Kyoto, Southwest Japan. The basement here consists mainly of the Cretaceous granitoids with small amounts of the high *dT/dP* Ryoke metamorphic rocks and the Mesozoic sedimentary strata and overlying middle Miocene volcanic rocks. The Cretaceous granitoids are divided into the older weakly to strongly foliated Yoshino Granite and Nanpudai Granite, the younger massive Shodoshima Granite and the Tanoura Igneous Complex (TIC, Fig. 8). The Yoshino Granite includes Yoshino-type and Ushigaura-type granite. The Shodoshima Granite is subdivided into Nadayama-type, Fukuda-type, Fujisaki-type, and Atehama-type granite (Atsuta, unpublished). All the granitoids belong to the ilmenite-series of Ishihara (1977) and I-type of Chappell and White (1974). These granitoids were emplaced and solidified in the following sequence: Nanpudai Granite, Yoshino Granite, and Shodoshima Granite. The TIC may be coeval with the Yoshino Granite. Yokoyama (1984) studied the dikes in the Shodoshima Island in terms of the regional stress-field analyses at time of the dike injection. The Shodoshima Granite yields Rb-Sr whole rock isochron age of 82.1± 3.0 Ma (Kagami *et al.*, 1988). The aeromagnetic and gravity anomalies center over the Shodoshima Island. This may relate to exposure of the mafic lithologies such as the gabbro-diorite layered sequence and mafic dikes and may also suggest a subsurface extension of these.

In the last decades, it has been pointed out that the styles and efficiency of interaction between resident felsic magma in a chamber and injected mafic magmas are largely controlled by host rheological properties which critically depend on the crystallinity at the time of mafic magma injection (Fernandez and Barbarin, 1991; Barbarin and Didier, 1992; Fernandez and Gasquet, 1994). Accordingly, the styles of interaction between the two magmas change successively with the degree of crystallization during cooling of a pluton. Fernandez and Barbarin (1991) proposed the following scenario for the sequential events of interaction between contrasting magmas: (1) genesis of homogeneous hybrid magmas by complete mixing at low crystallinity (<35%) of the host magma, (2) production of mafic enclaves and/or enclave swarms by mingling at higher crystallinity (35-65%), (3) appearance of synplutonic mafic dikes when crystallinity of the host magmas became high enough (>65%) to support early fractures through which mafic magmas were introduced, but hosts were still sufficiently mobile, and (3) formation of continuous late dikes after almost complete solidification of the host.

The late Cretaceous TIC in the Shodoshima Island, Southwest Japan, provides an excellent example of the plutonic record of repeated injections of mafic magma into a solidifying felsic magma chamber and the sequential changes in style of the interaction between the two contrasting magmas in a subduction zone setting. We demonstrate that in the early stage of the pluton history of the TIC, instead of complete mixing of felsic and mafic magmas, formation of layered sequence of gabbro-diorite with many characteristic features similar to those of mafic-silicic layered intrusion (MASLI) as defined by Wiebe (1993) was predominant. In the field excursion, we will examine the various styles of interaction between the felsic and mafic magmas frozen in the TIC and discuss magma chamber processes.

6. Tanoura Igneous Complex

The TIC, best exposed along the southern coast of the Tanoura Peninsula (Figs. 8, 9, 10), is largely composed of granites, tonalite, gabbro-diorite layered sequence and mafic to felsic dikes. On the basis of the field relationships,

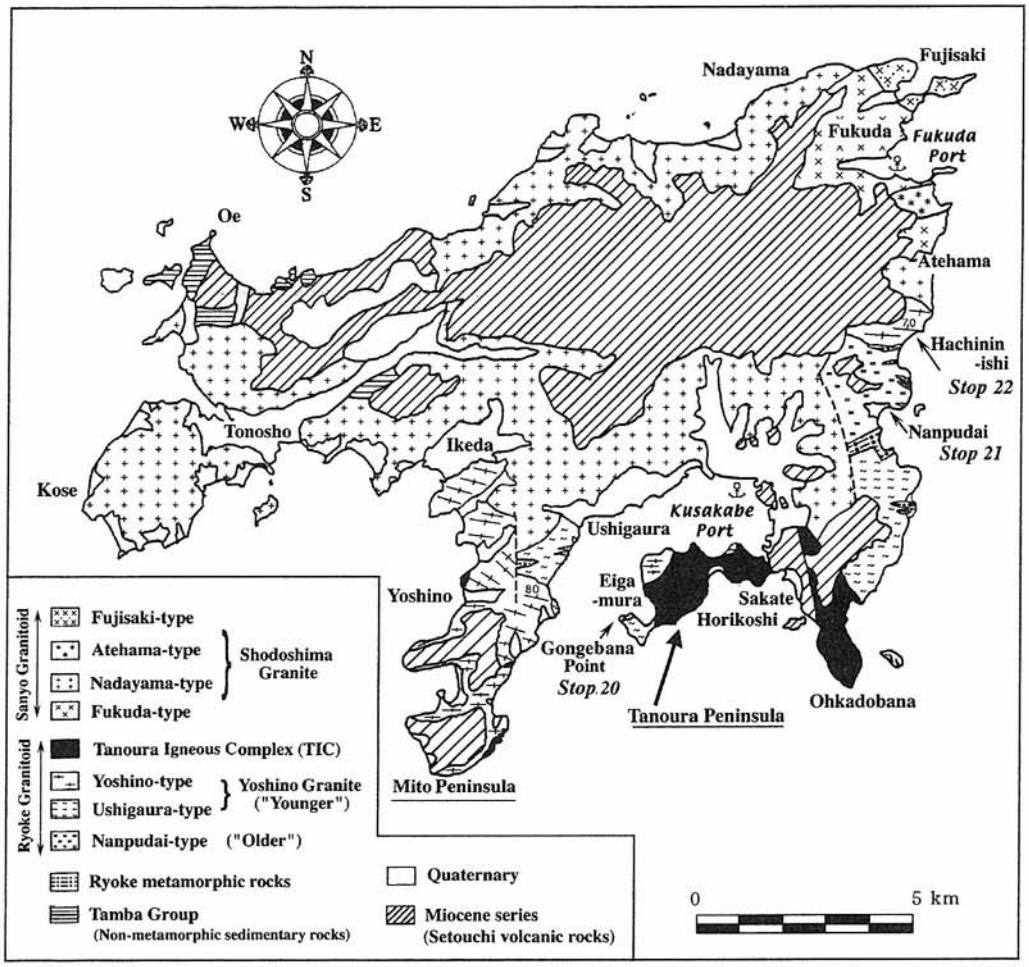

Fig. 8. Geological map of the Shodoshima Island (Atsuta and Yoshikura, in prep.) and locations of Stops 20, 21 and 22.

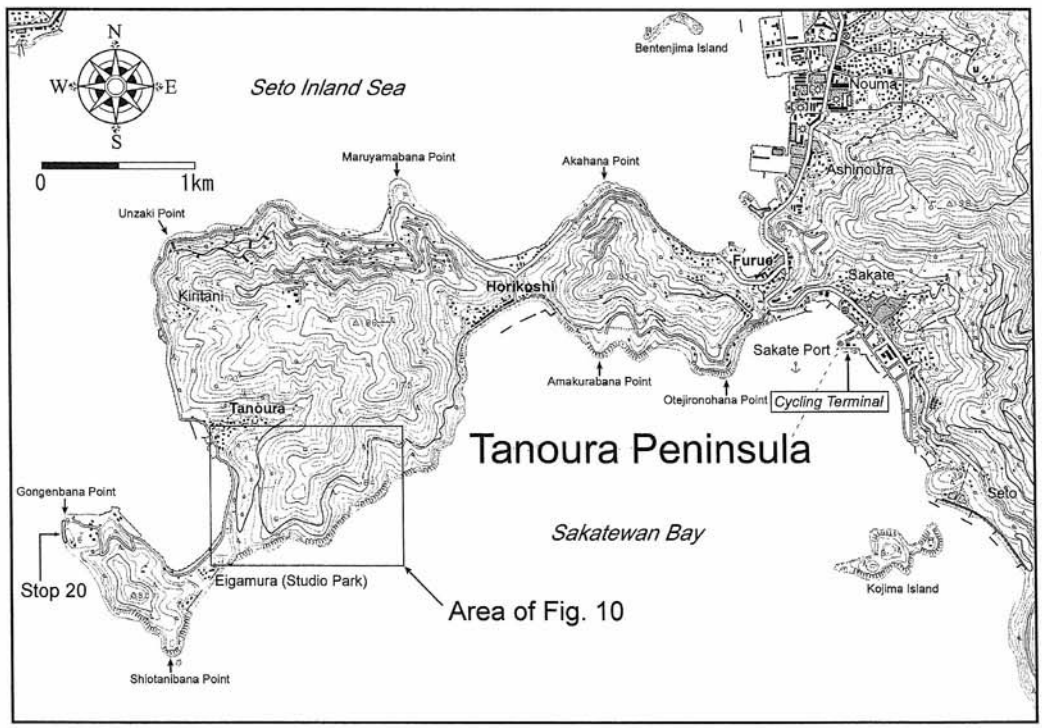

Fig. 9. Map showing the area of visit in the Tanoura Peninsula and Cycling Terminal.

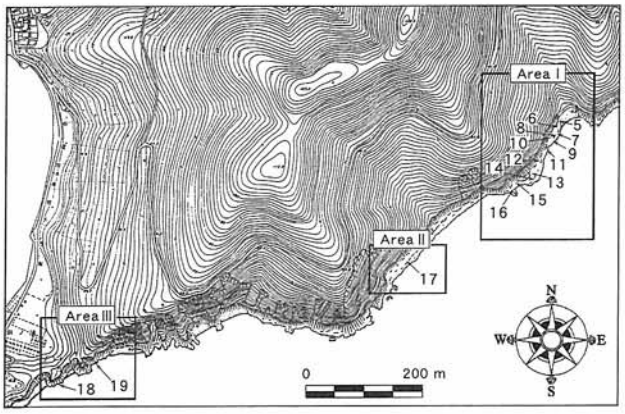

Fig. 10. Map showing the stop points 5 through 19, Tanoura Peninsula.

following four stages of the evolution of the TIC can be established.

6.1 Stage-1

6.1.1 Granite and tonalite

The granite is weakly foliated and coarse-grained containing many mafic clots. The tonalite is medium-grained and rich in lens-shaped mafic enclaves. They are aligned parallel to the foliation of the granite. Mingling contacts between the granite and the tonalite are observed in some places, indicating coeval emplacement of separate magma pulses. Prior to the emplacement, the tonalite experienced mixing and mingling between basaltic and silicic magmas in the deeper domain. This is consistent with the contrast in Rb-Sr and Sm-Nd isotopic ratios between the granites and tonalites.

6.1.2 Gabbro-diorite layered sequence

Recent field work by two of the authors (S.Y. and Y.S.) revealed that the unit previously mapped as diorite consists of the alternation of following two distinct lithologies: (1) a few centimeters to several meters thick medium- to coarse-grained heterogeneous more leucocratic diorite or quartz diorite layers enclosing mafic magmatic enclaves with different lithologies and compositions; and (2) a tens of centimeters to several meters thick fine- to medium-grained, more melanocratic gabbro layers with chilled margins against underlying diorite layers and, less commonly, against overlying layers.

Nearly 120 of gabbro-diorite units can be recognized within a distance of about 300 m section along the southern coast of the Tanoura Peninsula. The layered sequence strikes E-W and dips gently (20-40°) at the lower section but show steep dips (50-60°) at the higher section. Magmatic paleohorizontal markers such as layering and silicic pipes or diapirs suggest that the layered sequence was originally emplaced near- horizontal and was subsequently tilted northward.

This sequence shows the distinctive features that are diagnostic of mafic-silicic layered intrusion (MASLI) of Wiebe (1993) as mentioned below:

1. The base of the gabbro layers are chilled against and sunk into the underlying diorite layers forming load-cast like structures (Photo A3-1). On the contrary, the tops of the gabbro layers are generally unchilled and are broken off into many elongated mafic enclaves (Photo A3-2). Some of the pillows were highly digested.
2. The cylindrical pipes, diapirs, fingers or veins of leucocratic materials penetrate upwards from the underlying diorite layers into the overlying gabbro layers from a few to tens of centimeters.
3. Z-axial color of hornblendes in both gabbro and diorite layers change from brown through brownish-green to pale green with stratigraphic height.
4. The degree of chilling at the base of a gabbro layer increases in ascending order.
5. The diorite layers show increasing abundance of incompatible elements such as Zr and Ba and decreasing concentration of compatible elements such as Ti, Mg and Ca with stratigraphic height.
6. These chemical variations in the diorite layers are consistent with upward increase of modal quartz, biotite and zircon and decrease of hornblende and clinopyroxene.
7. Compared to the diorite layers, chemical variation of the gabbro layers throughout the succession is less significant.

Even where the underlying diorite layers are thin down to several millimeters, the base of the overlying gabbro layer is chilled against the diorite. This may be due to the loss of silicic melt by filter pressing from the underlying diorite layers after quenching the hotter gabbro magma against the cooler diorite magma. The magmatic structures and fabrics mentioned above such as load-casts and pipes formed in response to density inversion caused by gabbroic magma with the higher density resting on dioritic cumulate mush. Break-up of the top of the mafic layer and the resultant formation of the mafic enclaves may be due to the convective stirring in the dioritic magma that got reheated by the emplacement of the hotter gabbroic magma.

Recently, Chapman and Rhodes (1992), Wiebe (1993; 1996), and Wiebe and Collins (1998) developed the concept of the time-stratigraphic sequence in granitic plutons indicating periodic basalt injections into evolving felsic magma chamber. The injected mafic magmas spread laterally and form sheets or layers along the physical discontinuity between a crystal-rich chamber floor and an overlying crystal-poor magma. With repeated injections, the pluton leaves an interlayered sequence of mafic and felsic rocks which is referred to "mafic silicic layered intrusions" (MASLI) (Wiebe, 1993; 1996).

6.2 Stage-2

E-W trending synplutonic mafic dikes

The stage-2 mafic dikes intruded into granite, tonalite and gabbro-diorite layered sequence with E-W strikes. Some of them are fragmented along their length into angular blocks filled with aplitic materials. The blocks have chilled margins against the felsic host but lack them in between the blocks.

These may represent mafic magmas emplaced into the felsic host before the latter was sufficiently crystallized to sustain but still ductile. A predominant E-W trend is evident, which suggests that the dikes intruded during a period of N-S tension.

6.3 Stage-3

N-S trending synplutonic mafic dikes and composite dikes

The synplutonic mafic dikes with N-S trend of this stage crosscut the granite (Photo A3-5). The dike margins were intruded and brecciated/disrupted by veins of fine-grained tonalitic rocks (septa). The contact against the host granite was chilled but the contact with the septa lacks chilled border. This indicates that the dike margin was disrupted after chilling against the granite. The tonalitic rocks emplaced into granite as small dike with their terminals pinched out. The angular mafic blocks can be observed frozen in the processes of detachment from the dike margins. These observations strongly suggest that the rheological behavior of the host granite differ significantly within short distance at the time of the intrusion of mafic magma.

The composite dikes intruded into the granite. They are symmetrically zoned and consist of fine-grained mafic interiors and medium-grained felsic septum and margins. The felsic septum and margins are tonalitic in composition and chilled against the granitic host. They contain xenocrysts of feldspar and quartz derived from the granite host. The mafic interiors form pillow-like structures with cuspate margins against tonalitic septum. Chemical analyses suggest that it is impossible to produce the septa magma by in situ simple binary bulk mixing between the host granitic magma and mafic interior magma. It seems likely that the septa magma may have been generated by hybridization between mafic and felsic magmas deeper in the crust.

A small composite dike with thickness 15 cm pinch and swell in a sinuous fashion possibly indicating some mobility of the granite host after emplacement of the dike. The drag folding of mafic interior produced a space of tension in which coarse-grained pegmatitic quartz has grown. Along with decrease in the total thickness of the dike, the thickness of felsic margin also decreases and finally it disappears resulting in mafic interior contact directly with the host granite.

The late dikes are planar and cut all the lithologies of stage-1 and -2. Fine-grained margins are often well-developed indicating significant cooling of the host rocks before dike injection took place. Some of them form multiple dikes.

6.4 Stage-4

Aplite, pegmatite and granophyre dikes and composite dikes

These dikes are generally less than 1m and crosscut all the lithologies in TIC irregularly. At some outcrops, both mafic and segregated aplitic melts are channeled in a fracture and form a composite dike.

7. Petrologic characteristics of the TIC

The geochemistry of the mafic rocks in the TIC shows many characteristic features of subduction-related igneous rocks such as high Al_2O_3 content (high alumina basalt), enrichment of LILE relative to HFSE, negative Nb and Ta anomalies on the MORB normalized multi element spider diagrams, lower Ce/Pb ratios and higher Th/Y ratios. The lower concentration of Mg, Cr and Ni in the mafic rocks may suggest that they are not mantle-derived primitive magmas. However, these elements are also low in the least evolved rocks of active continental margin calc-alkaline series, and have been interpreted as indicating considerable fractionation of olivine and clinopyroxene from original mantle melts, probably deep in the crust or upper mantle. The abundance of hornblende and calcic plagioclase together with occurrence of gabbro pegmatite in some places all indicate that the mafic rocks in the TIC crystallized from hydrous basaltic magmas.

Based on Sr and Nd isotopic ratios, Kagami *et al.* (1992) divided the Cretaceous to Paleogene granitoids in the Southwest Japan into the North Zone, South Zone and Transitional Zone. The granitoids in Northern Zone are characterized by lower initial $^{87}Sr/^{86}Sr$ ratios (0.7048 to 0.7068) and higher initial εNd values (+3 to -2.2), whereas those in the South Zone are characterized by higher initial $^{87}Sr/^{86}Sr$ ratios (0.7070 to 0.7088) and lower initial εNd values (-3.0 to -8.0). The transitional zone is in between them. This provinciality observed in the isotopic composition of the granitoids in the Southwest Japan might be reflected the changes in crustal and/or upper mantle composition and structure.

Initial isotopic compositions of the gabbro-diorite layered sequence, tonalites and mafic dikes in the TIC are similar ranging in $^{87}Sr/^{86}Sr$ from 0.7069 to 0.7074 and εNd from - 3.8 to -5.7. The granitoids exhibit slightly more crustal signature with 0.7079 and 0.7084 $^{87}Sr/^{86}Sr$ and -6.3 and -6.9 εNd. All of these isotopic compositions are within the range for the South Zone of Kagami *et al.* (1992). Initial $^{87}Sr/^{86}Sr$ ratios of intermediate and mafic granulite xenoliths in the middle Miocene volcanics in the Shodoshima Island exhibit 0.7073 and 0.7077, respectively. The corresponding values for initial εNd are -4.4 and -4.5 (Kagami *et al.*, 1995). The similarity, in both Sr and Nd isotopic compositions, of rocks in the TIC with the lower crustal granulite xenoliths in the volcanics suggests that these rocks are related petrogenetically.

8. Source of the Granitoids - A General View

Late Cretaceous granitoids of the Sanyo and Ryoke Belts belong to ilmenite series and have relatively higher $\delta^{18}O$ (Ishihara and Matsuhisa, 2002) and lower negative $\delta^{34}S$ values (Ishihara and Sasaki, 2002) than those of the magnetite-series granitoids, implying that the granitoids were generated involving such reducing agents of sedimentary origin as organic carbon and/or biogenic sulfur.

Whole rock $\delta^{18}O$ values of the coarse-grained granodiorite-monzogranite of the Sanyo Belt vary from +8.1 to +10.7 ‰ ,

and the average is +9.7 ‰ (n=8). Similar granitoids of the Ryoke Belt range from +8.4 to +10.9 ‰ , with a mean at +9.9 ‰ , which is slightly higher than that of the Sanyo Belt. Alumina saturation index (ASI) is also high in the Ryoke granitoids. The alkali contents are, however, higher in the Sanyo granitoids than in the Ryoke granitoids. Therefore, the sources of the Sanyo granitoids could well be composed of more felsic igneous rocks than sedimentary components, while the ratio may be reversed in the Ryoke granitoids. REE contents of the batholithic granodiorites of both the Sanyo and Ryoke Belts show different abundances but the same patterns decreasing to the HREE side, without negative Eu anomaly (Fig. 7). These patterns may imply existence of garnet and/or amphibole in the source region.

Among fine-grained granitoids, the Aji granitoids are high in the $\delta^{18}O$ values (+12.5 ‰) and ASI (1.02), but low in K_2O content (Fig. 5). The granites contain more commonly igneous enclaves than sedimentary ones. Thus, they are considered to have originated from a sediment-dominant crustal material, not having much illite components. A similar fine-grained rock having garnet-muscovite-biotite assemblage is extremely high as +15.6 ‰. As mentioned previously, the Ryoke metamorphic rocks are not well preserved from erosion in the Okayama-Kagawa region. Limited studies indicate that the metamorphic rocks could contain more mafic igneous rocks than, *e.g.*, in the Chubu District, which is composed of sandstones, shales and cherts. An average $\delta^{18}O$ value of the metamorphic rocks in the Chubu District is estimated to be +15.6 ‰ (Ishihara and Matsuhisa, 2002). It can be assumed that the garnet-muscovite-biotite granite at Shido could have originated from 100 % sedimentary rocks of psammitic and pelitic origin.

In the Sanyo Belt, leucogranites are considered as highly fractionated, chilled phase of the biotite granite for the mode of occurrence and the chemical characteristics. The fluid phase concentrating metals such as W, Sn, U, etc, were deposited along fractures in the solidifying magmas. One leucogranite sample near the tungsten deposits with slightly lower $\delta^{18}O$ value of +7.7 ‰ than that of the coarse-grained biotite granite, may be due to meteoric water interaction, because the leucogranite occurs in the highest level of the granitic batholith.

As mentioned previously, the major batholithic granitoids are more mafic in the Ryoke Belt than in the Sanyo Belt. Many small gabbroic igneous bodies occur with granitoids in the Ryoke Belt, but are scarce in the Sanyo Belt. They are mostly synplutonic intrusion or dikes intruded into the Ryoke granitoids in three tectonic stages, as best seen in the TIC. Initial $^{87}Sr/^{86}Sr$ of these gabbroids and granitoids are similar (Shibata and Ishihara, 1979); i.e., 0.7081 vs. 0.7078, respectively, in the Ryoke Belt, and 0.7071 and 0.7075 vs. 0.7077, respectively, in the Sanyo Belt, implying they are isotopically homogenized during the synplutonic intrusions.

These facts may further imply that the mafic magmas from the upper mantle were closely associated with the generation of the granitic magmas within the continental crust. The mafic magmas provided both heat and material to the granitic magmas. Wherever the mafic magmas were abundantly mixed with the crust-born felsic magmas, the bulk composition became granodiorite, as seen in the Ryoke Belt. None or little mixing formed coarse-grained biotite granites of the Sanyo Belt. Some felsic parts of the biotite granite and fine-grained muscovite-biotite leucogranite of the Sanyo Belt with distinct negative Eu anomaly are considered to have formed by magmatic fractionation of the coarse-grained biotite granitic magmas.

9. Miocene andesites- Sanukitoids

Middle Miocene volcanic rocks (Tatsumi *et al.*, 2001) in northeast Shikoku constitute mesas (Spanish word for table), buttes (smaller mesa), and dissected hills on the Cretaceous Ryoke granitic basement. They form a monogenetic volcano group, among which Goshikidai plateau conforms the largest volcanic mass with sanukitoid andesites (Sato, 1982). The stratigraphy of the volcanic rocks in Goshikidai plateau is, in ascending order, garnet-biotite rhyolite tuff breccia, hornblende dacite volcanic breccia, four lava flows of sanukitoid andesite (Fig. 11). Sanukitoid was first named by Koto (1916) after the traditional alias of Kagawa Prefecture, northeastern Shikoku, Southwest Japan, and includes basalt and andesite with magnesian olivine and pyroxene phenocrysts, and almost lack plagioclase phenocrysts.

Chemical compositions of typical rock types are given in Table 3. The high-magnesian andesite has bulk rock MgO content of 7-9 wt%, and carries magnesian olivine (*Fo*=88-91, NiO=0.4wt%), and magnesian orthopyroxene phenocrysts (Mg#=88-91, Cr_2O_3=0.6-1wt%), suggesting its primary nature from mantle peridotite. However, recent geochemical studies (Ishikawa and Nakamura, 1994; Hanyu et al., 2002; Tatsumi, 2001) demonstrated that the melts from subducted sediments are incorporated in its formation. This is in contrast with boninite high-magnesian andesite, which shows strongly depleted geochemical characterisitics suggesting partial melting of fluid incorporated strongly depleted mantle peridotite.

We visit only one outcrop (a quarry) in the western part of Goshikidai plateau, where the succession from granitic basement, through rhyolitic tuff breccia, to the lava flow-III of sanukitoid andesite is observed (Stop 3 in Fig. 1).

10. Excursion Stops

Stops 1 through 4 are shown in Figure 1, stops 5 through 19 in Figure 10, and stops 20 through 22 in Figure 8.

Stop 1: Mannari Stone at Ukita quarry (Fig. 1)

This is hornblende-bearing biotite pink granite, at Ukita Quarry, Okayama city, which is the main lithology of the late Cretaceous granitoids of the Sanyo Belt. Similar pink granite extends southward to Teshima and Shodoshima within the Sanyo Belt. The granite may contain very small amount of magnetite but within the ranges of the ilmenite series. It is essentially homogeneous but aplitic and pegmatitic phases

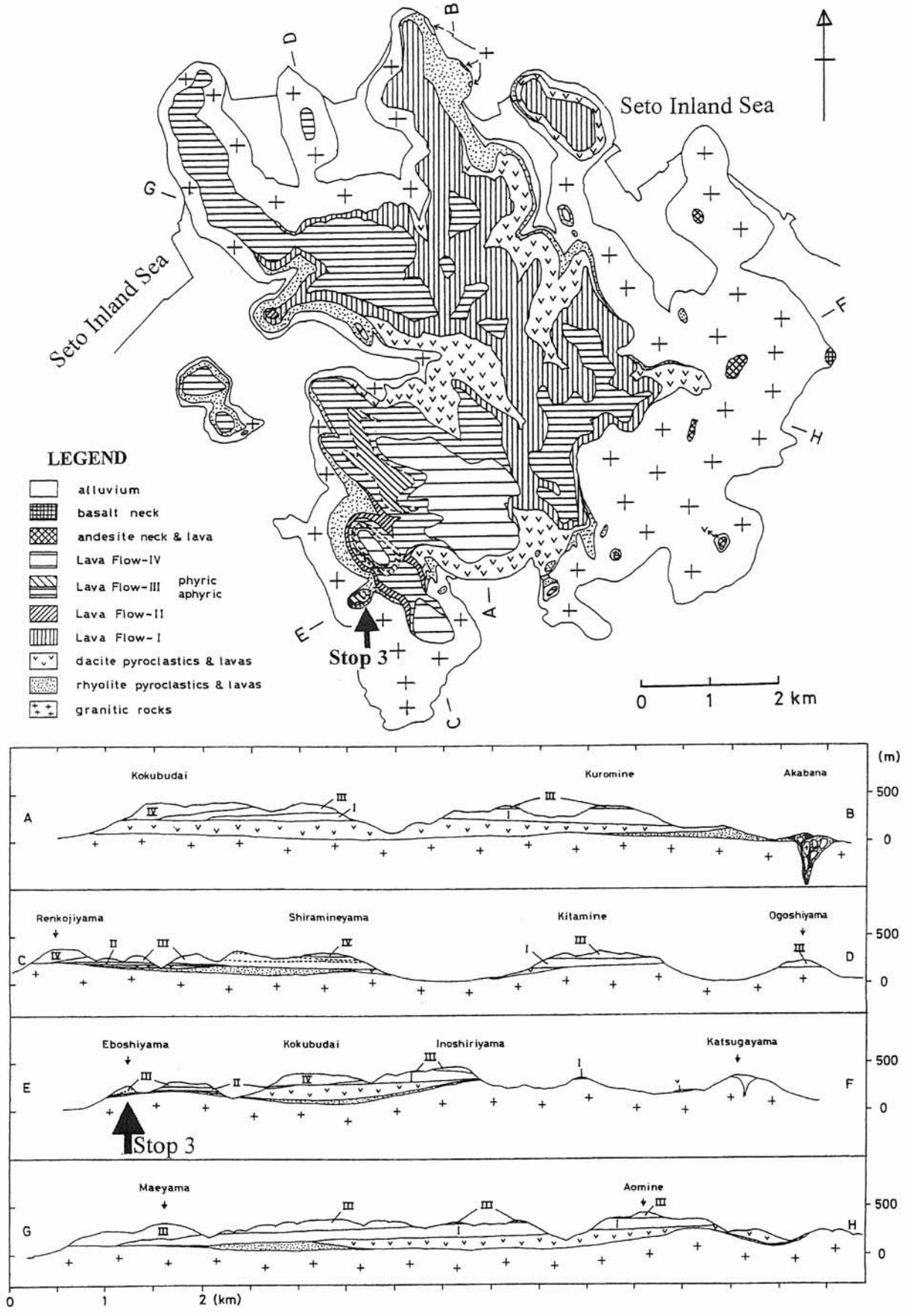

Fig. 11. Geological map and cross sections of Goshikidai (Sato and Kuchitsu, 1992).

Table 3. Bulk rock composition of some sanukitoids (Sato and Kuchitsu, 1992).

	1 Aonoyama butte basalt	2 Goshiki-dai rhyolite	3 ibid dacite	4 ibid LF-I andesite	5 ibid LF-II HMA	6 ibid LF-III phyr. andesite	7 ibid LF-III aphyric andesite	8 ibid LF-IV sanukite	9 Yashima andesite
SiO_2(%)	51.52	72.68	67.54	63.95	57.68	59.48	61.86	66.41	59.57
TiO_2	0.94	0.12	0.31	0.45	0.75	0.70	0.61	0.47	0.66
Al_2O_3	18.60	16.01	18.15	17.10	15.78	15.51	18.36	17.82	17.08
FeO*	8.20	1.61	2.86	4.32	5.79	5.28	5.18	3.50	5.43
MnO	0.16	0.03	0.04	0.08	0.12	0.13	0.14	0.09	0.11
MgO	6.22	0.25	0.30	3.16	8.33	6.93	2.87	1.61	4.85
CaO	9.31	2.16	3.85	5.14	6.67	6.38	5.50	3.83	6.31
Na_2O	2.64	4.24	4.07	3.93	3.16	3.02	4.16	4.18	3.63
K_2O	1.22	2.73	2.50	1.64	1.79	2.19	2.41	2.90	1.23
Total	98.81	99.83	99.62	99.77	100.07	99.62	101.09	100.81	98.87
Cr(ppm)	72	15	8	155	507	325	60	50	106
Ni	60	2	12	54	158	144	26	14	37
Zr	47	124	112	138	109	143	190	212	
Y	21	8	7	19	17	16	21	21	
Sr	289	186	209	235	247	255	302	281	
Rb	53	114	106	66	57	78	95	121	
$^{87}Sr/^{86}Sr$		0.70549	0.70561	0.70502	0.70620	0.70652	0.70655	0.70650	

can be observed. No sedimentary but sporadic igneous enclaves may be seen. Molybdenite and iron sulfides disseminate along fractures without significant hydrothermal alteration.

The pink color is attributed by K-feldspar having an intermediate triclinicity between orthoclase and microcline in the horblende-bearing biotite granite (Nureki *et al*., 1979).

One may argue that the pink color is iron oxide decomposed by slight weathering of trace amount of magnetite, but most of the Japanese pink granite belong to magnetite-free ilmenite series (*e.g.*, Mannari, Giin-seki, and Mikage stone). It is our opinion that the iron oxide was formed iron coming out from trace amount of Fe^{3+} substituting Al^{3+} position in the K-feldspar during the subsolidus microclinization. The modal analyses and representative chemical analyses are given in Tables 1 and 2.

Stop 2: Muscovite-biotite leucogranite (Fig. 1)

This leucogranite is related to wolframite-quartz veins accompanied with greisenization near the old Miyoshi mine site, Kurashiki city, which is the latest phase of the late Cretceous granitic activity. This granite is completely free of magnetite, and is highly fractionated as shown by the very high Rb/Sr ratio (Table 2). The outcrop here is slightly porphyritic and the quartz has a dark color, owing to radioactive damage. Weak greisenization is seen along cooling joints. Pyrite occurring in the altered wall rock at Miyoshi mine gives $\delta^{34}S$ value of -5.0 ‰. Number of NNW-striking ore veins have been mined in the leucogranite to the north of this stop point.

Wolframite and cassiterite deposits of the W province in Japan are generally associated with highly fractionated ilmenite-series leucogranite, which has low Fe_2O_3/FeO but high Rb/Sr ratios and high contents of lithophile elements such as Rb, Pb, Y, Sn, F, Li, Be etc, that are contrasting to the chemical compositions of similar leucogranite of the magnetite-series of the Mo province (see Table 2) and also the latest phase of the Aji granite in the Ryoke Belt (Stop 4). Sulfide minerals from the W province have negative $\delta^{34}S$ values, reflecting its biogenic source, while those of the Mo province have positive $\delta^{34}S$ values (Ishihara and Sasaki, 2002).

Stop 3: Miocene andesites at Goshikidai, Yamahi Quarry (Fig. 11)

The granitic basement is mostly weathered, which is overlain by 0-5 meters thick rhyolitic tuff breccia. The tuff breccia is poorly sorted consisting of subangular blocks of glassy to crystalline compact rhyolite with abundant tuffaceous matrix of the same composition. It may represent a pyroclastic flow deposit. The rhyolite has bulk rock composition of low Y and HREE contents, suggesting its possible derivation from partial melting of subducted slab. The rhyolitic tuff breccia is overlain by the lava flow-III of *ca.* 60 meters thick. The lowest 5 meters of the lava flow consists of welded clinker. The lava flow-III shows a composite structure consisiting of lower nearly aphyric sanukitoid andesite (MgO=2-3wt%) and upper high-magnesian augite-olivine- orthopyroxene andesite (MgO=6-8 wt%). Near the boundary of the two sanukiotid andesites, lensoidal occurrence of one lava in another is observed. The boundary between the two sanukitoid lavas is generally sharp, as can be seen in the left hand (southwest) side of the quarry, but in part they show a diffuse zone of *ca.* 1 cm thick. Rough columnar joint is developed throughout the composite lava. The phyric high-magnesian sanukitoid andesite is generally porous. Metamorphosed argillaceous xenoliths are locally abundant in the phyric high-magnesian sanukitoid

andesite. On the other hand, aphyric sanukitoid andesite is compact without xenoliths.

Stop 4: Aji gray granitoids at Okubo Enterprise Quarries (Fig. 4)

Typical Aji granite and its product are seen in this stop. Silica contents of the granite here are typically 72 % and whole rock $\delta^{18}O$ is high as 12.5 ‰. ASI is peraluminous but below 1.1. The fine grain size and heterogeneous looking are considered significant as high-quality tombstone. Enclaves and pegmatite are rare, but molybdenite, chalcopyrite and iron sulfides occur along cracks. The molybdenite has -3.7 ‰, and chalcopyrite and pyrite have -7.2 ‰ $\delta^{34}S$ (Ishihara and Sasaki, 2002). Modal analyses and representative chemical analyses of the Aji stones are given in Tables 1 and 2.

The opposite side of the quarried Aji Peninsula is the mesa of Yashima, which was formed by covering of sanukite lava more resistant to the underlying Miocene sediments and weathered late Cretaceous granitoids of the basement. The eastern cliff is the famous ancient battle field between the Families Genji and Heike in February of 1185.

Stop 5: Granite and tonalite, Tanoura Igneous Complex

Stop points 5 to 19 are of the Tanoura Igneous Complex (TIC, Fig. 8). Colored sketch maps of the visiting coast are given in field. At this stop (Fig. 12), granite and tonalite are exposed. The tonalite is medium-grained and rich in mafic enclaves and clots. It encloses some blocks of the granite. The granite is medium- to coarse-grained and weakly foliated. It contains significant amounts of mafic clots.

Stop 6: Composite dike

A small composite dike with 15 cm wide intruded into the granite (Fig. 12). It consists of medium-grained tonalitic margin with xenocrysts derived from the granite host and melanocratic fine-grained interior. In contrast to the dike margin, the interior shows brittle deformation. This may be due to the difference in rheological behavior between the felsic margin and mafic interior. The mafic interior magma quenched and rapidly became rigid and the dike was disrupted during subsequent movement of the still mobile host granite. But the rounded terminals of the interior indicate primary mingling contact with tonalitic margin magma. The drag folding of mafic interior produced a space of tension in which coarse-grained pegmatitic quartz has grown.

Stop 7: Synplutonic mafic dike

At this outcrop (Fig. 12), one of the Stage-3 synplutonic mafic dikes ranging in thickness from 2 to 3 m was emplaced in the granite (Photo. A3-5). At the dike margin, the mafic dike disrupted into numbers of elongated enclaves with the long axis oblique to the contact. Some angular mafic blocks can be observed frozen in the process of detaching from the dike. The shape of the contact varies considerably over short distances. This may be due to the presence of local variations in rheological state in the host granite at the time of intrusion of the mafic dike magma. Transfer of heat and volatiles from the cooling mafic dike magma to the host granite might promote its remobilization , leading to disruption of the mafic dike and the formation of mafic enclaves and blocks.

Stop 8: Late mafic dike

A stage-3 late mafic dike striking NW-SE and dipping almost vertical intruded into the granite and the tonalite and chilled much stronger against the tonalite than the granite (Fig. 12).

Stop 9: Composite dike

A composite dike with tonalitic margin and pillowed basaltic interior intruded the granite at this locality (Fig. 12). The pillows have cuspate and lobate margins against the tonalitic margin. The tonalitic margin may be the product of hybridization between mafic and felsic magmas but the hybridization process can not be modeled by simple binary in situ mixing between the mafic enclave and host granitic magmas. This suggests that the magma of the felsic margin might be generated in the deeper domain.

To the southwest of this stop, the older (Stage-2) E-W trending dikes cut the granitoids and in turn is cut by younger (Stage-3) 1 m wide NW-SE trending dikes.

Stop 10: Load cast-like structure

Here (Fig. 12), we will examine the structures at the contact between the gabbro and diorite layers. The convex-downward lobate structure similar to sedimentary load cast is well developed at base of the gabbro layers resting on the diorite layers (Photo. A3-1). Coarser-grained leucocratic granitic material has concentrated at the top of the diorite layer and intruded between convex-downward lobes of the overlying gabbro. This granitic material may represent filter-pressed interstitial liquid from the underlying crystal mush. These gravity-controlled structures provide good way-up indicators.

The dikelets or veins injected into the gabbro layer from the diorite layer could be conduits through which felsic melt moved upward buoyantly, thereby forming some leuco-granitic and pegmatitic pockets, pools or dikes in the gabbro-diorite layered sequence. The grain size increases upward drastically in the gabbro layer.

Stop 11: Pipe

Pipe of silicic material extends approximately 20 cm from the underlying diorite layer upward into the overlying basally chilled gabbro layer (Fig. 12). The pipe becomes more felsic progressively to the top. At top end, there are some open vugs. The formation of the pipe could be due to the gravitational instability of the basaltic magma resting on silicic cumulate mush (Wiebe, 1993). The pipe can be used as a paleohorizontal marker to reveal primary attitude of the pluton. As pointed out by Chapman and Rhodes (1992), the fact that primary magmatic structures such as pipe and load cast are preserved implies there was no vigorous convection in the gabbro layers large enough to destroy them.

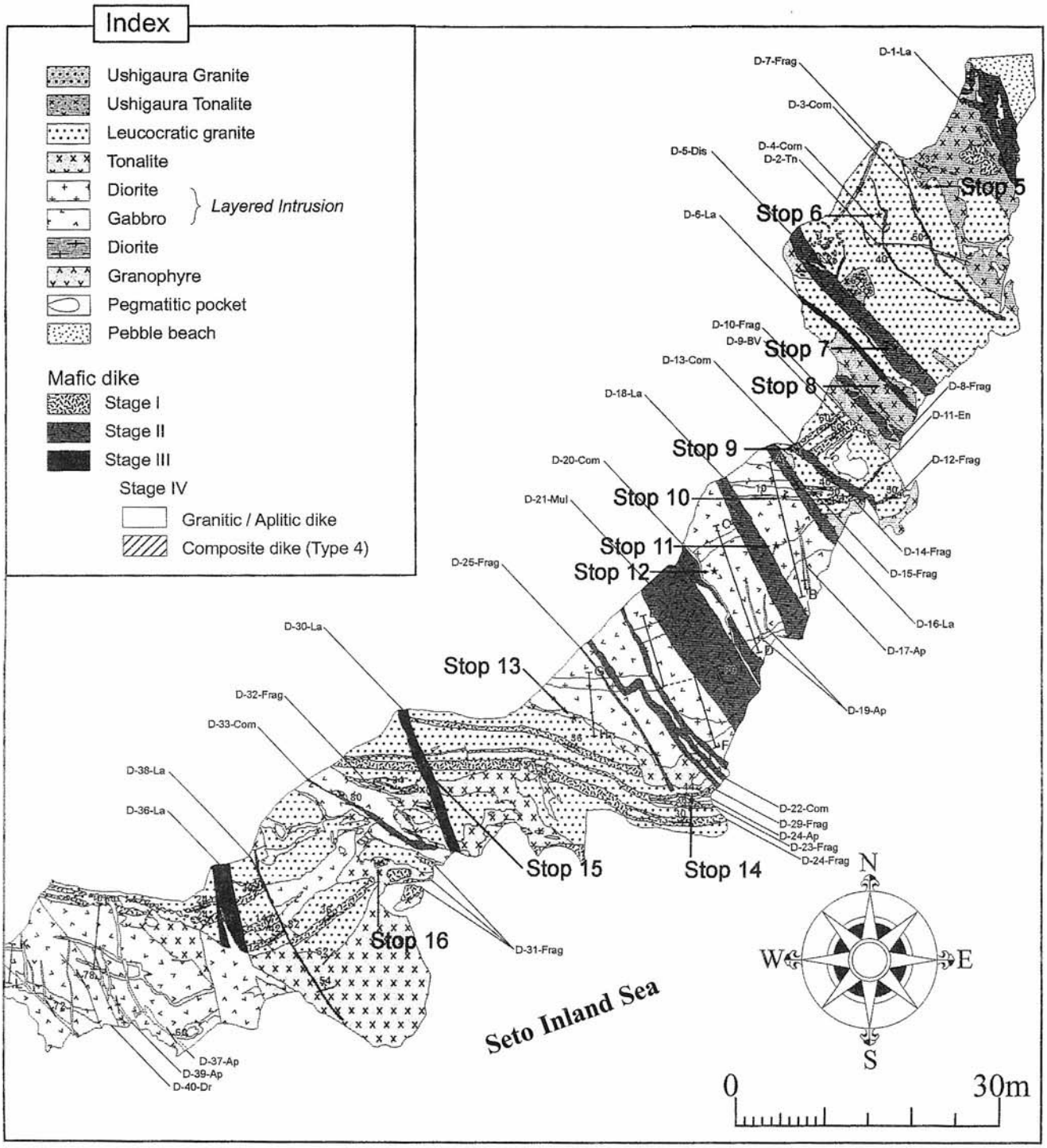

Fig. 12. Geological map of the area I coast and stop locations (Satake and Yoshikura, unpublished).

Stop 12: Thinly layered gabbro-diorite sequence

Layering of gabbro and diorite developed on a centimeter to decimeter scale at some localities (Fig. 12).

Stop 13: Granite and gabbro-diorite unit

The Stage-1 granite is in contact with the diorite of the gabbro-diorite unit (Fig. 12). There is no clear crosscutting relationship between them. Elongated and aligned mafic enclaves in the diorite are deflected around the granite at the contact. This indicates magma-magma contact and their coevality. An E-W striking thin mafic dike with chilled margins intruded into the granite and was fragmented into several pieces.

Stop 14: Fragmented dike of Stage 3

The mafic dike of the Stage-3, 60-80 cm wide, intruded into the granite (Fig. 12). The dike is fragmented into polygonal blocks with interspaces filled by aplitic materials (Photo A3-4). The dike, however, still maintained original morphology without dispersion of the blocks. The

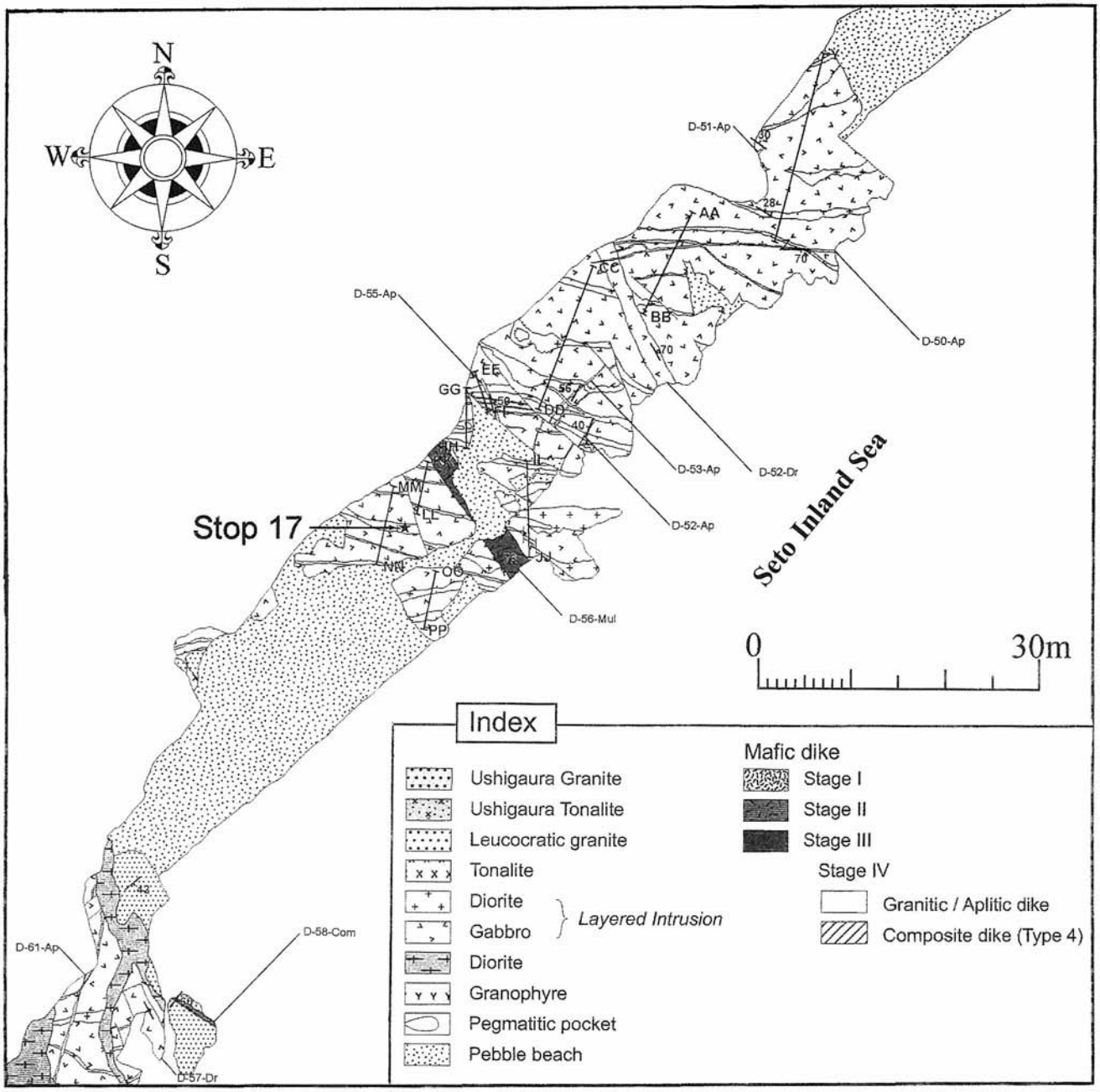

Fig. 13. Geological map of the area II coast and stop location (Satake and Yoshikura, unpublished).

fragmented blocks have fine-grained borders at the contact with the host granite but lack these at the contact with the injection of aplitic veins between the blocks. This occurrence provides evidence of basaltic injection into granite that was sufficiently ductile to break off but not enough mobile to scatter the blocks.

Sop 15: Mafic dikes of Stages 2 and 3

N-S trending late mafic dikes of the Stage-3 crosscut the disrupted mafic dikes of the Stage-2 with E-W strike at this stop (Fig. 12)..

Stop 16: Back-veined dike of Stage 3

The mafic dike of Stage-3, back-veined and brecciated by granite-derived aplitic veins cut the granite (Fig. 12). The breccias chilled against the granite host but not against the aplitic veins.

Stop 17: Gabbro-diorite unit

The major feature of this outcrop (Fig. 13) is the gabbro-diorite unit. Note the contrasting character of the tops and bases of the gabbro layers (Photo A3-2). The base of the gabbro layer strongly chilled against the underlying diorite layer. Immediately above this chilled rim, the grain sizes increase abruptly to interior. On the contrary, the top of the gabbro layer is unchilled and shows evidence for detachment of the mafic enclaves from the upper surface of the top of the gabbro layer and mechanical mixing with the overlying

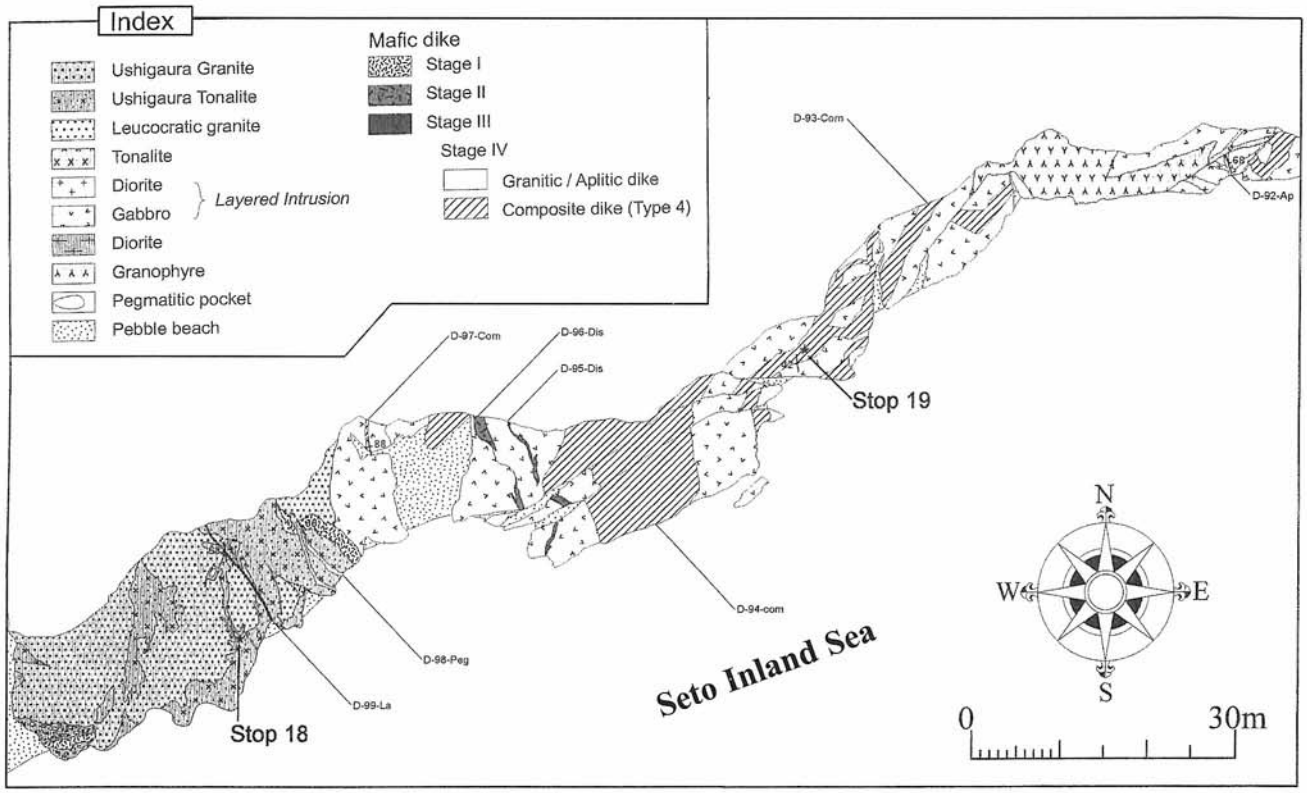

Fig. 14. Geological map of the area III coast and stop locations (Satake and Yoshikura, unpublished).

diorite layer. The diorite layer is texturally and compositionally heterogeneous with variably digested mafic enclaves. The mafic enclaves are flattened and aligned parallel to the contact between the gabbro and diorite layers. Felsic pipes or fingers penetrate upward into the overlying gabbro layer.

Stop 18: Ushigaura Granite and Ushigaura Tonalite

At this stop (Fig. 14), the Ushigaura Granite intermingled with the Ushigaura Tonalite indicating the coeval emplacement of two distinct magmas. The Ushigaura Granite can be distinguished from the Stage-1 granite at Stop 5 by lower color index, higher content of K-feldspar, massive appearance and smaller grain size. Compared to the Stage-1 tonalite at the Stop 5, the Ushigaura Tonalite is poor in mafic enclaves.

Stop 19: Composite dike

At this location (Fig. 14), two NE-SW trending composite dikes 1-1.5 m wide, consisting of felsic margins and mafic interior intruded into the gabbro-diorite layered sequence (Photo A3-3). The pillows are elongated along strike forming sausage-like structure with aspect ratio of 5 to 15. They are arranged in 7 to 8 parallel rows in one dike and 4 to 5 in another. Snyder and Tait (1995) and Snyder *et al.* (1997) revealed by the fluid-mechanic experiments that this type of composite dikes form from a flow-front instability that develop when a mafic magma invades felsic magma with higher viscosity between two parallel rigid walls. To the north of this stop, aplitic and basaltic dikes came in contact within a fracture and formed a small composite dike.

11. Optional stops

Stop 20: Middle Miocene volcanic rocks at the Gongenbana Point

The middle Miocene volcanic sequence on the Shodoshima Island is named Shodoshima Group and is divided into two formations, Uchinomi and Kankakei. Among them, the Uchinomi Formation is subdivided into the Sakate lava and Seto pyroclastic rocks. The brecciated rhyolite lava of the Sakate lava from Furue area yields a zircon fission track age of 14.0± 1.2 Ma (Tatsumi, 1983).

Along the shoreline of the Gongenbana Point (Fig. 9), the lava and volcanic breccia (volcaniclastic rocks) of the Sakate lava are exposed. They are dacitic to rhyolitic in composition. The lava developed prominent columnar and platy joints. The weathered surface shows honeycomb structure. There are many pits along the joint fractures indicating an incipient stage of the honeycomb structure.

The volcanic breccias consist of ill sorted angular to subangular blocks of rhyolitic lava with flow banding and lesser amounts of accidental granitic and mafic igneous blocks set in the matrix rich in clasts derived from granitic rocks. The breccias range in diameter of 1 to 50 cm. In the rhyolitic blocks, flaky biotite crystals can be observed with naked eyes.

Stop 21: Ryoke metamorphic rocks and Nanpudai Granite

In Nanpudai area, amphibolite-facies gneiss of the Ryoke metamorphic rock and granites are distributed (Fig. 8). The protoliths of the gneiss are psammitic and pelitic rocks with some intercalations of mafic rock, chert and limestone. In the psammitic and pelitic gneiss, the banded structure of 1-2mm is remarkable. Typical mineral assemblage is cordierite + garnet + biotite + muscovite + K-feldspar + plagioclase + quartz. Ryoke metamorphic belt has been divided into biotite zone, cordierite zone, sillimanite zone-1, and sillimanite zone-2 with increasing metamorphic grade (Hayama, 1964). The metamorphic rocks of this area belong to the cordierite zone (Kutsukake *et al.*, 1979).

The Nanpudai Granite occurs closely associated with the metamorphic rocks and is characterized by foliation that is concordant with that in the metamorphic rocks. The foliation strikes N 70-90° E and dips steeply. The granite is a medium-grained granodiorite consisting mainly of plagioclase, quartz, K-feldspar and biotite with accessories of apatite, zircon, and ilmenite. It shows several lines of evidence for cataclastic deformation and recrystallization such as distinct undulatory extinction and deformation lamellae in quartz, sutured grain boundaries of quartz, recrystallized fine-grained aggregates of felsic minerals, preferred orientation of elongated biotite clots, and kink band in biotite. In some places, the granite encloses xenoliths of pelitic to psammitic gneiss. The magnetic susceptibility of the Nanpudai granite ranges from 0.13 to 0.15×10^{-3} S.I. unit and suggests that the granite is classified into ilmenite-series granitoids by Ishihara (1977). Two mafic dikes with N-S strike and garnet-bearing pegmatite dike intruded into the Nanpudai granite.

Stop 22: Hachinin-ishi Chouba (ancient quarry)

More than three hundreds years ago, many granites were quarried and shipped to Osaka from the Shodoshima Island for the reconstruction of the stone wall of the Osaka Castle. The Hachinin-ishi chouba ("chouba" means quarry in Japanese) is one such ancient quarry in this area (Fig. 8). At this stop, there are two blocks of granite with dimension of 6.5 m long side, 2.2 m short side and 2.8 m height, and 6.5 m, 4.4 m and 1.1 m. They once formed a huge block. According to a local legend, during the quarrying, the block was split right down the middle suddenly and eight stonemasons were crushed to death under the block. Since then, these huge blocks of granite have been called "hachinin-ishi" which means rocks of eight stonemasons in Japanese. Along a path in the bush, there are many abandoned blocks of granite with various types of carved trademark and aligned pits to split the stones by wedge, chisel and hammer.

Acknowledgements: We thank Professors T. Nureki and K. Kase, Okayama University, and the owners of Ukita, Yamahi and Ookubo quarries for their guidance and help during the preparation of this field excursion.

References

Barbarin, B. and Didier, J. (1992) Genesis and evolution of mafic microgranular enclaves through various types of interaction between coexisting felsic and mafic magmas. *Trans. Roy. Soc. Edinburgh, Earth Sci.*, **83**, 145-153.

Chapman, M. and Rhodes, J. M.(1992) Composite layering in the Isle au Haut Igneous Complex Maine: evidence for periodic invasion of a mafic magma into an evolving magma reservoir. *Jour. Volcanol. Geothermal Res.*, **51**, 41-60.

Chappell, B. W. and White, A. J. R. (1974) Two contrasting granite types. *Pacific Geol.*, no. 8, 173-174.

Fernandez, A. N. and Barbarin, B. (1991) Relative rheology of coeval mafic and felsic magmas: Nature of resulting interaction processes and shape and mineral fabrics of mafic microgranular enclaves. *In* Didier, J. and Barbarin, B. eds., *Enclaves and granite petrology.* Elsevier, Amsterdam, 263-275.

Fernandez, A. N. and Gasquet, D. (1994) Relative rheological evolution of chemically contrasted coeval magmas: example of the Tichka plutonic complex (Morocco). *Contrib. Mineral. Petrol.*, **116**, 316-326.

Hanyu, T., Tatsumi, T. and Nakai, S. (2002) A contribution of slab-melts to the formation of high-Mg andesite magmas: Hf isotopic evidence from SW Japan. *Geophys. Res. Lett.*, **29**, no.22, 2051.

Hayama (1964) Progressive metamorphism of pelitic and psammitic rocks in the Komagane district, Nagano Prefecture, central Japan. *Jour. Fac. Sci., Univ. Tokyo, Sec.2*, **15**, 321-365.

Hida, N., Shimazu, M. and Igarashi, T. (1961) Granitic rocks and related uranium metallic ore deposits in Sanyo District. *In* Natural Occurrence of Uranium in Japan. *Rept. Geol. Surv. Japan*, **190**, 68-79*.

Ishihara, S. (1971) Modal and chemical compositions of the granitic rocks related to the major molybdenum and tungsten deposits in the Inner Zone of Southwest Japan. *Jour. Geol. Soc. Japan*, **77**, 441-452.

Ishihara, S. (1977) The magnetite-series and ilmenite-series granitic rocks. *Mining Geol.*, **27**, 293-305.

Ishihara, S. (1991) The Aji stone: The historical and modern use and its geologic background. *Chishitsu News*, **441**, 60-67.**

Ishihara, S. (2002) Chemical characteristics of the mineralized granitoids (I). Mo and W provinces of the Inner Zone of Southwest Japan. *Bull. Geol. Surv. Japan*, **53**, 657-672.*

Ishihara, S. (2003) Chemical contrast of the Late Cretaceous granitoids of the Sanyo and Ryoke Belts, Southwest Japan: Okayama-Kagawa transect. *Bull. Geol. Surv. Japan*, **54**, 95-116.

Ishihara, S. and Imaoka, T. (1999) A proposal of caldera-related genesis for the Roseki deposits in the Mitsuishi mining area, Southwest Japan. *Resource Geol.*, **49**, 157-162.

Ishihara, S. and Wu, C. Y. (2001) Genesis of late Cretaceous-

Paleogene granitoids with contrasting chemical trends in the Chubu District, central Japan. *Bull. Geol. Surv. Japan*, **52**, 471-491.

Ishihara, S. and Matsuhisa, Y. (2002) Oxygen isotopic constraints on the geneses of the Cretaceous-Paleogene granitoids in the Inner Zone of southwest Japan. *Bull. Geol. Surv. Japan*, **53**, 409-426.

Ishihara, S. and Sasaki, A. (2002) Paired sulfur isotopic belts: Late Cretaceous-Paleogene ore deposits of Southwest Japan. *Bull. Geol. Surv. Japan*, **53**, 461-477.

Ishikawa, T. and Nakamura, E. (1994) Origin of the slab component in arc lavas from across-arc variation of B and Pb isotopes. *Nature*, **370**, 205-208.

JMIA (Japanese Mining Industry Association) (1968) *Ore deposits of Japan, Vol. 2*. 941p.**

Kagami, H., Honma, H., Shirahase, T. and Nureki, T. (1988) Rb-Sr whole rock isochron ages of granites from northern Shikoku and Okayama, Southwest Japan: Implications for the migration of the late Cretaceous to Paleogene igneous activity in space and time. *Geochem. Jour.*, **22**, 69-79.

Kagami, H., Iizumi, S., Tainosho, Y. and Owada, M. (1992) Spatial variations of Sr and Nd isotope ratios of Cretaceous-Paleogene granitoid rocks, Southwest Japan Arc. *Contrib. Mineral. Petrol.*, **112**, 165-177.

Kagami, H., Yuhara, M., Iizumi, S., Tainosho, Y., Owada, M., Hayama, Y. and Nureki, T. (1995) Temporal variation in Sr and Nd isotopic composition of Jurassic to Miocene igneous rocks in the Seto Inlanda Sea and Kinki Districts of the Ryoke Belt, Southwest Japan Arc. *Mem. Geol. Soc. Japan*, no. 44, 309-320.*

Koto, B. (1916) On the volcanoes of Japan: The ancient volcanoes of the Inland Sea and its western extension in Kyushu. *Jour. Geol. Soc. Tokyo*, **23**, 95-127.

Kutsukake, T., Hayama, Y., Honma, H., Masaoka, K., Miyakawa, K., Nakai, Y., Yamada, T. and Yoshida, M. (1979) Geology and petrology of the Ryoke belt and Shodo-shima Island and eastern Sanuki region. *Mem. Geol. Soc. Japan*, no. 17, 47-68.*

Nureki T., Asami, M. and Mitsuno, C. (1979) Granitic rocks in central to southern Okayama Prefecture. *Mem. Geol. Soc. Japan*, no. 17, 35-46.

Nureki T., Asami, M., Shibata,T. and Ohira, K. (1982) The Ryoke Belt of the southwestern part of the Siaku Island-shoto area in the Seto Inland Sea. *Jour. Geol. Soc. Japan*, **88**, 499-510.

Peacock, M. A. (1931) Classification of igneous rock series. *Jour. Geol.*, **39**, 54-67.

Sato, H.(1982) Geology of Goshikidai and adjacent areas: field occurrence and petrography of sanukitoid and associated volcanic rocks. *Sci. Rept. Kanazawa Univ.*, **27**, 13-70.

Sato, H. and Kuchitsu, N. (1992) Sanukite and high-magnesian andesite in Northeast of Shikoku. *IGC Fieldtrip Guidebook*, **4**, 201-212.

Shibata, K. and Ishihara, S. (1979) Initial $^{87}Sr/^{86}Sr$ ratios of plutonic rocks in Japan. *Contrib. Mineral. Petrol.*, **70**, 381-390.

Snyder, D. and Tait, S. (1995) Replenishment of magma chambers: comparison of fluid mechanic experiments with field relations. *Contrib. Mineral. Petrol.*, **122**, 230-240.

Snyder, D., Crambes, C., Tait, A. and Wiebe, R.A. (1997) Magma mingling in dikes and sills. *Jour. Geol.*, **105**, 75-86.

Tatsumi, Y. (1983) Volcanic geology of Shodo-Shima Island, Kagawa Prefecture, Southwest Japan and its bearing on paleoenvironment of the Seto Inland Sea area. *Jour. Geol. Soc. Japan*, **89**, 693-706.*

Tatsumi, Y. (2001) Geochemical modeling of partial melting of subducting sediments and subsequent melt-mantle interaction: Generation of high-Mg andesites in the Setouchi volcanic belt, southwest Japan. *Geology*, **29**, 323-326.

Tatsumi, Y., Ishikawa, N., Anno, K., Ishizaki, K. and Itaya, T. (2001) Tectonic setting of high-Mg andesite magmatism in SW Japan: K-Ar chronology of the Setouchi volcanic belt. *Geophys. Jour. Intern.*, **144**, 625-635.

Wiebe, R. A. (1993) Basaltic injections into floored silicic magma chamber. *EOS, Trans. Amer. Geophys. Union*, **74**, 1, 3.

Wiebe, R. A. (1996) Mafic-silicic layered intrusions; the role of basaltic injections on magmatic processes and the evolution of silicic magma chambers. *Trans. Roy. Soc. Edinburgh, Earth Sci.*, **87**, 233-242.

Wiebe, R. A. and Collins, W.J. (1998) Depositional features and stratigraphic sections in granitic plutons: implications for the emplacement and crystallization of granitic magma. *Jour. Struct. Geol.*, **20**, 1273-1289.

Yokoyama, S. (1984) Geological and petrological studies of late Mesozoic dyke swarms in the Inner Zone of Southwest Japan. *Geol. Rept. Hiroshima Univ.*, **24**, 1-63.*

Yuhara, M., Kagami, H. and Nagai, K. (2000) Geochronological characterization and petrogenesis of granitic rocks in the Ryoke belt, Southwest Japan Arc: constraints from K-Ar, Rb-Sr and Sm-Nd systematics. *The Island Arc*, **9**, 64-80.

Yuhara, M., Miyazaki, T., Kagami, H. and Yuhara, M. (2003) Rb-Sr and K-Ar geochronology and petrogenesis of the Aji Granite in the eastern Sanuki district, Ryoke Belt, southwest Japan. *Jour. Mineral. Petrol. Sci.*, **98**, 19-30.

Zen, E-an (1986) Aluminum enrichment in silicate melts by fractional crystallization: some mineralogic and petrographic constraints. *Jour. Petrol.*, **27**, 1097-1117.

* in Japanese with English abstract.
** in Japanese.

Received June 3, 2003
Accepted July 10, 2003

Hutton Symposium V, Field Guidebook
Geological Survey of Japan, Interim-Report no.28, p.61－80, 2003

Trip A4

Miocene granites and the Hishikari gold deposits in Kyushu

Masahiko YAMAMOTO[1], Yoshinobu KAWANO[2], Akira IMAI[3] and Koshi NISHIMURA[4]

Abstract: Geological and petrological features were reviewed for the Shibi-san granodiorite and Takakuma-yama granite stocks and the Osumi granodiorite batholith in the Outer Zone of Kyushu. These intrusive bodies are composed of ilmenite-series granitoids, but are different in lithology from each other. The Shibi-san granodiorite stock was derived from a heterogeneous dacitic liquid through differentiation of andesitic magma, and the lithological variation within the stock was formed through much assimilation by the surrounding country rocks *in situ*. The Takakuma-yama granite stock was derived from a fairly homogeneous granitic liquid through differentiation of dacitic magma, and the lithological variation within the stock was formed through concentration of fluid-rich residual liquid *in situ*. The concordant Osumi granodiorite batholith is poor in lithological variation, and was formed by intrusions of several heterogeneous dacitic magmas different slightly in degree of assimilation by the uppermost crustal materials.

Southern Kyushu has been known as a gold mining district. The Hishikari gold deposits discovered in 1981 are known as one of the major gold deposits in the western Pacific region. An underground visit at the Hishikari mine will be conducted during the field excursion A4. In this paper, geological features of the Hishikari gold deposits are briefly reviewed. The Hishikari deposits, consisting of the Honko (Main), Sanjin and Yamada deposits, are epithermal low sulfidation vein-type deposits. The age of mineralization at the Hishikari deposits has been dated to be 1.25-0.66 Ma.

Keywords: Hutton Symposium, field excursion, Shibi-san, Takakuma-yama, Osumi, Miocene, granitoids, Hishikari, gold deposit.

1. Introduction

Southern Kyushu is tectonically located in the westernmost of the Outer Zone of Southwest Japan and in the northern part of Nansei (Ryukyu) island arc. The geological map of southern Kyushu is shown in Figure 1.

The basement rocks in southern Kyushu are mainly composed of accretional sedimentary complexes. The accretional sedimentary complexes are divided into two major supergroups, the Chichibu Supergroup in the northern belt called the Chichibu terrane and the Shimanto Supergroup in the southern belt called the Shimanto terrane. The Chichibu Supergroup is composed of pre-Cretaceous rocks. The Shimanto Supergroup is subdivided into two groups, the Lower Shimanto Group in the northern Shimanto terrane and the Upper Shimanto Group in the southern Shimanto terrane. The former is composed of late Cretaceous rocks and the latter is of mainly Paleogene rocks.

Igneous activities in southern Kyushu began at early Miocene. Miocene granitic bodies are sparsely exposed in both the northern Shimanto terrane and the Paleogene southern Shimanto terrane (Fig. 1). They are composed of ilmenite-series granitoids (Takahashi *et al.*, 1980), but are different in mode of occurrence from each other. The granitic body occurring in the northern Shimanto terrane is of a discordant stock with abundant porphyry dikes, such as the Shibi-san, Hioki, Kinpo-zan, Kaseda and Kasasa stocks. On the other hand, the granitic body occurring in the southern Shimanto terrane is only the concordant Osumi batholith with less porphyry dikes. The Takakuma-yama stock is lithologically similar to the Osumi batholith, but intrudes discordantly the late Cretaceous rocks. Lithological variation is also found within each body. It is therefore important for petrogenesis to clear difference in mode of occurrence and variation in lithology.

Volcanic rocks are widely distributed in three districts, the Hisatsu, Hokusatsu and the Nansatsu (Fig. 1). Quaternary volcanoes comprising the present-day volcanic front of the Ryukyu arc include the Kirishima, Sakurajima and Kaimon-dake volcanoes. The present-day volcanic front is situated in a volcano-tectonic depression zone named the "Kagoshima graben". The depression is associated with the Quaternary Kakuto, Aira, and Ata calderas. The Ito pyroclastic flow deposit effused from the Aira caldera widely covers the southern Kyushu.

Southern Kyushu has been known as a premier gold mining district in Japan. The Hishikari gold deposits were discovered in 1981, and are known as the highest-grade ones in the world. An underground tour will be conducted at the Hishikari mine during the field excursion A4, to observe the

[1] Kagoshima University, Korimoto 1-21-35, Kagoshima, 890-0065 Japan. E-mail: myama@sci.kagoshima-u.ac.jp
[2] Saga University, Honjo 1, Saga, 840-8502 Japan. E-mail: kawanoy@cc.saga-u.ac.jp
[3] Kyushu University, Hakozaki 6-10-1, Fukuoka, 812-8581 Japan. E-mail: imai@mine.kyushu-u.ac.jp
[4] Kyoto University, Noguchibaru, Beppu, 874-0903 Japan. E-mail: nishimura@bep.vgs.kyoto-u.ac.jp

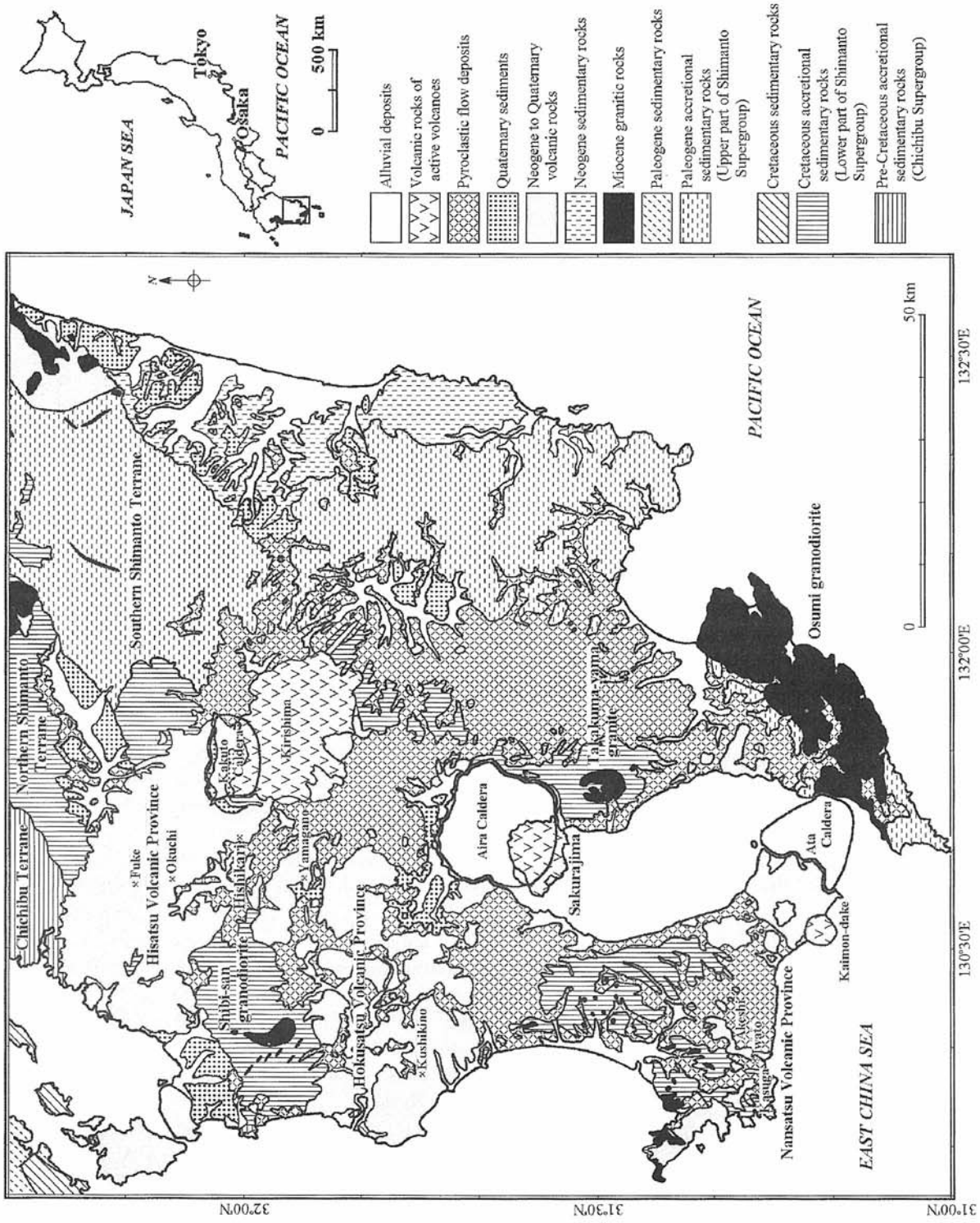

Fig. 1. Index and geological maps of South Kyushu (compiled from Imai *et al.*, 1980).

mode of occurrence of productive quartz veins associated with high grade gold mineralization at underground mining faces.

Over 16 Plio-Pleistocene gold deposits including the Hishikari, Kushikino, Yamagano and Okuchi deposits are known in the Hokusatsu-Hisatsu district, with a reserve in excess of 350 metric tons of gold (Feebrey *et al.*, 1998). The reserve and produced gold at the Hishikari, Kushikino, Yamagano and Okuchi mines are approximately 260 t, 56 t, 28 t and 22 t, respectively (Izawa and Watanabe, 2001). Most of the gold deposits in the Hokusatsu-Hisatsu district are classified into low-sulfidation, adularia-sericite type epithermal vein-type deposits, based on the ore, gangue and alteration mineral assemblage.

On the other hand, the Kasuga, Iwato and Akeshi deposits are located in the Nansatsu district. These deposits consist of silicified volcanic rocks associated with gold mineralization and have been known as the Nansatsu-type deposits. The reserve and produced gold at the Kasuga, Iwato and Akeshi mines are approximately 9 t, 8 t and 9 t, respectively (Izawa and Watanabe, 2001), and thus they are smaller than the principal deposits in the Hokusatsu-Hisatsu district in terms of the quantity of contained gold. Characteristic alteration including vuggy silica and the presence of alunite, and the occurrence of characteristic ore minerals such as enargite suggest that the Nansatsu-type deposits are high-sulfidation, acid-sulfate type epithermal deposits (Hedenquist *et al.*, 1994).

A general eastward younging of the volcanic rocks and epithermal gold deposits toward the present-day volcanic front has been pointed out (Izawa and Urashima, 1989; Izawa *et al.*, 1992; Izawa and Watanabe, 2001). The age of the Kushikino deposit in the west was dated to be 4.0 Ma, whereas the Hishikari deposits near the present-day volcanic front were dated to be 1.25-0.66 Ma (Izawa and Urashima, 1989; Sekine *et al.*, 1998, 2002). The ages of the Kasuga, Iwato and Akeshi, in the eastward order, in the Nansatsu district, were reported to be 5.0 Ma, 4.4 Ma and 3.7 Ma, respectively (Izawa and Urashima, 1989), showing eastward younging as well.

A number of hot springs are distributed throughout the southern Kyushu, especially where volcanic rocks are distributed, *i.e.*, in the Hisatsu, Hokusatsu and Nansatsu districts. Geothermal systems at Ogiri in the Kirishima volcano and at Yamagawa in the Kaimon-dake volcano both at the present-day volcanic front are developed and utilized for the geothermal power stations.

Many studies have been reported for the Miocene granites and the Hishikari gold deposits. This paper gives reviews of modes of occurrence, petrography, bulk composition, mineral composition and petrogenesis for the Shibi-san, Takakuma-yama and the Osumi bodies, and geological background and outline of the Hishikari gold deposits.

2. The Shibi-san Granodiorite Stock

The Shibi-san granodiorite body is located in the northwestern part of Kagoshima Prefecture (Fig. 1). It is exposed in the central part of Shibi Mountains having summits higher than 600 meters above sea level, and is well-dissected along the Tomarino river running in the southerly direction. Geological and petrological studies of the Shibi-san granodiorite have been reported by Oba (1957, 1962), Yamamoto *et al.* (1988) and Yamamoto and Ushijima (1994) and Ishihara *et al.* (1999).

2.1 Geology

Figure 2-(a) shows the distribution of intrusive bodies in the Shibi Mountains, and Figure 2-(b) shows the geological map of Shibi-san granodiorite stock and its surrounding areas. The main geological constituents in the mapped areas include the lower part of Shimanto Supergroup (Lower Shimanto Group), the Shibi-san granodiorite and the related dike rocks, the Hokusatsu volcanic rocks and alluvial deposits, in ascending order.

The Lower Shimanto Group of late Cretaceous age is bent by an anticlinal axis plunging northwest. The stratum in the northeast of axis strikes in the direction of northeast, and dips steeply northwestward, and that in the southwest strikes in the direction of north, and dips steeply westward. The Group is composed of accretional sedimentary complex of shales, sandstones, alternation beds of sandstone and shale, slump beds and green rocks.

The Shibi-san granodiorite and the related dike rocks intrude discordantly the Lower Shimanto Group. The Shibi-san granodiorite body is a stock exposed in the lenticular areas of 11 km in north and south×4 km in east and west, indicating that it is elongated in the north-northwesterly direction. The boundary between the stock and the country rocks shows a sharp outward contact, and dips steeply in the southern part of stock and gently in the northern one. A satellite body crops out at the top of Hokotate-yama in the north of stock.

The related dike rocks around the stock are linearly distributed in three zones having the direction of northwest, as shown in Figure 2-(a). One of them is sharply cut and thermally metamorphosed by the intrusion of stock, and its fragment is found within the stock as an enclave, indicating that the dike rocks were formed before the intrusion of stock.

The country rocks are thermally metamorphosed by the intrusion of stock. The cordierite isograd of pelitic hornfelses expands to the areas up to 600 meters wide in the southern aureoles and up to 1,000 meters in the northern ones (Oba, 1957). The innermost aureole inside the garnet isograd is characterized by the appearance of garnet, sillimanite and/or K-feldspar in the pelitic hornfelses (Adachi *et al.*, 1969).

The Hokusatsu volcanic rocks of Pliocene age composed of pyroxene andesite lavas are distributed in the southeast of stock.

2.2 Modes of Occurrence

The Shibi-san granodiorite stock is lithologically divided into two types, the Kusubae and the Hirabae (Oba, 1957). The Kusubae-type rock is composed of coarse- to medium-

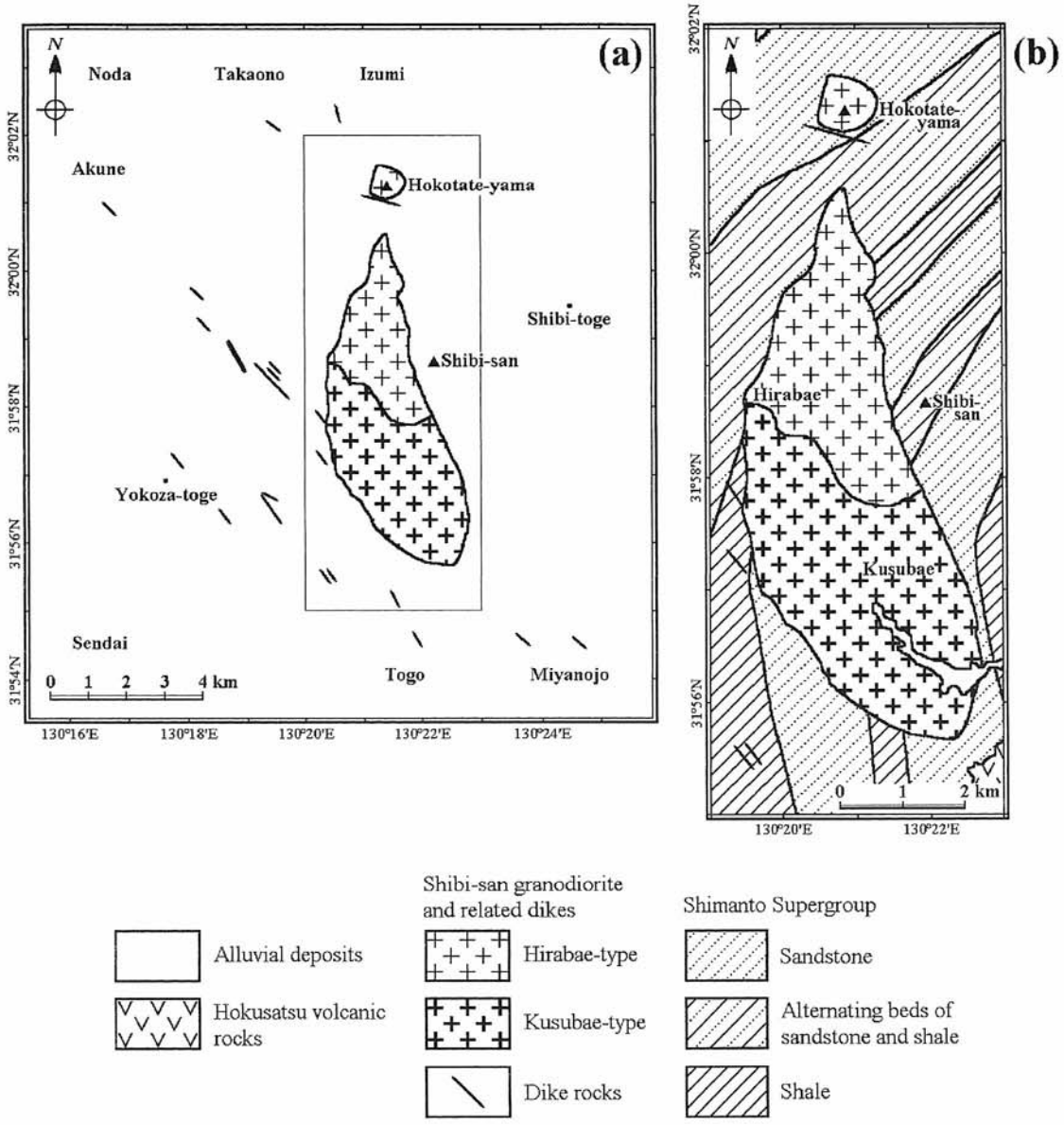

Fig. 2. (a) Map showing the distribution of intrusive bodies in the Shibi Mountains. (b) Geological map of the Shibi-san granodiorite and the surrounding areas. Compiled from Yamamoto *et al.* (1988), Kagoshima Prefecture (1990) and Yamamoto and Ushijima (1994).

grained and light gray-colored hornblende-biotite granodiorite rich in K-feldspar megacryst, and the Hirabae-type rock is of medium- to fine-grained and light gray-colored biotite granodiorite poor in K-feldspar megacryst. The former constitutes the core of stock and the latter the roof. The boundary between them shows a gradational relation with about 500 meters wide. Medium-grained and light-colored biotite granite intrudes the Kusubae-type and lies at the top of Hirabae-type, and fine-grained and light-colored biotite aplitic granite intrudes the Hirabae-type. Joints are well-developed throughout the stock, and their widths in the Hirabae-type are slightly finer than those in the Kusubae-type. A flow structure is rarely found in the Hirabae-type.

The stock contains a large amount of migmatitic and hornfelsic enclaves and a small amount of gabbroic and dioritic ones, and these enclaves are rimmed by a biotite aggregate. The gabbroic and dioritic enclaves occur mainly in the Kusubae-type and the hornfelsic ones in the Hirabae-type.

The K-Ar age of biotite from the stock indicates 15 ± 4 Ma (Miller *et al.*, 1962) and 13.6 Ma (Kawano and Ueda, 1966), the middle Miocene age.

The related dike rocks are composed of dark-colored quartz diorite porphyry and dark gray-colored granodiorite porphyry, and contain gabbroic and dioritic enclaves with a porphyritic texture.

The mineralization is essentially barren.

2.3 Petrography

Major constituent minerals in both the Kusubae-type and Hirabae-type rocks include plagioclase, quartz, K-feldspar,

Table 1. Representative bulk compositions of the Shibi-san granodiorite

Major Elements (wt.%)							
Type	Kusubae-type		Hirabae-type		Granite	Aplitic Granite	Granodiorite Porphyry
No.	1	2	3	4	5	6	7
SiO_2	66.42	67.34	66.04	66.46	72.75	75.86	62.95
TiO_2	0.72	0.64	0.72	0.71	0.14	0.13	0.79
Al_2O_3	15.02	15.38	15.35	15.54	14.17	13.66	15.53
Fe_2O_3	0.54	0.46	0.46	0.28	2.58*	0.29	5.18*
FeO	4.09	3.81	4.44	4.19	nd.	0.95	nd.
MnO	0.09	0.08	0.09	0.08	nd.	0.04	0.10
MgO	1.31	1.18	1.41	1.31	0.30	0.11	2.58
CaO	2.71	2.79	2.69	2.71	1.61	0.59	3.83
Na_2O	3.43	3.47	3.37	3.53	3.27	3.09	2.76
K_2O	4.40	4.08	3.83	3.70	4.55	4.25	3.37
H_2O^+	1.02	0.85	1.27	1.04	nd.	0.81	nd.
H_2O^-	0.16	0.10	0.22	0.06	nd.	0.10	nd.
P_2O_5	0.07	0.07	0.06	0.11	nd.	0.03	0.16
Total	99.98	100.25	99.95	99.72	99.37	99.91	96.73
Trace Elements (ppm)							
Li	39	35	43	24	34	129	37
Rb	130	110	110	100	217	410	118
Sr	200	227	181	196	122	26	268
Ni	19	14	25	38	33	17	nd.
Cr	27	26	34	31	53	15	nd.
Cu	13	12	18	24	nd.	6	nd.
Zn	50	54	56	56	nd.	27	nd.
Pb	5	5	9	9	nd.	7	nd.

*Total Fe as Fe_2O_3.
After Yamamoto *et al.* (1988) and Yamamoto and Ushijima (1994).

hornblende and biotite. K-feldspar megacryst has several centimeters in diameter. It is most abundant in the granodiorite of gradational zone, rich in the Kusubae-type, whereas poor in the Hirabae-type. Zoned prismatic plagioclase and prismatic perthite intergrowth are common. Prismatic hornblende rimmed by actinolite is common in the Kusubae-type but rare in the Hirabae-type. Anhedral clinopyroxene occurs rarely within the core of hornblende crystal. Biotite occurs sometimes as an aggregate of euhedral flakes. Accessory minerals in both the types include garnet, cummingtonite, zircon, apatite, sphene, ilmenite and pyrrhotite. Garnet is most abundant in the granodiorite of gradational zone, rich in the Hirabae-type, whereas poor in the Kusubae-type. The color index in the Kusubae-type is about 16 and that in the Hirabae-type ranges from 23 to 13.

The biotite granite is composed of plagioclase, quartz, K-feldspar and biotite, and the average color index is 10. The aplitic granite is composed of plagioclase, quartz, K-feldspar and biotite, and the color index is 4.

The quartz diorite porphyry and the granodiorite porphyry of related dikes are composed of phenocrysts of plagioclase, quartz, clinopyroxene, hornblende and biotite with an altered groundmass. K-feldspar, garnet or muscovite is rarely found as accessories.

2.4 Bulk Compositions

Bulk compositions of the Shibi-san granodiorite are listed in Table 1. The average SiO_2 content is 67 wt.% in the Kusubae-type, 65 wt.% in the Hirabae-type, 73 wt.% in the granite and 76 wt.% in the aplitic granite. Normative diopside less than 0.4 wt.% or normative corundum less than 0.4 wt.% is calculated in the Kusubae-type, and normative corundum more than 0.9 wt.% in the Hirabae-type, indicating that the former is subaluminous and the latter is peraluminous. As compared to the average chemical composition of Japanese granitoids (Aramaki *et. al.*, 1972), the bulk compositions show that FeO and K_2O contents are higher, whereas CaO and Na_2O contents are lower.

Incompatible trace elements are fairly uniform throughout the stock, but are concentrated toward the aplitic granite. Li and Rb contents exceed 100 ppm and 400 ppm, respectively, in the aplitic granite. The average S and C contents are 38 ppm and 285 ppm, respectively, in the Kusubae-type and 423 ppm and 213 ppm, respectively, in the Hirabae-type (Ishihara *et al.*, 1999). $\delta^{34}S$ value in the Hirabae-type ranges from -6.2 ‰ to -5.7 ‰ (Ishihara *et al.*, 1999). $\delta^{18}O$ value ranges from +10.0 ‰ to +10.3 ‰ and is averaged as +10.2 ‰ (n=3) (Ishihara and Matsuhisa, 1999). Initial $^{87}Sr/^{86}Sr$ ratio is 0.7062 (Shibata and Ishihara, 1979).

SiO_2 content of granodiorite porphyry dike is 63 wt.%, indicating that the dikes are more basic than the stock. The dikes are rich in MgO, whereas the stock is rich in total Fe_2O_3, indicating that the compositional trends are different from each other.

2.5 Mineral Compositions

Chemical compositions of major constituent minerals from the Shibi-san granodiorite are listed in Table 2.

Zoned plagioclase ranges in composition from An_{58} to An_9 in the Kusubae-type and from An_{48} to An_{17} in the Hirabae-type.

Clinopyroxene from the Kusubae-type is $Wo_{43}En_{29}Fs_{29}$ in composition. Hornblende is ferro-hornblende ($Mg/Mg+Fe^{+2}$ =0.42) in the Kusubae-type and actinolitic hornblende ($Mg/Mg+Fe^{+2}$=0.52) in the Hirabae-type. Biotite shows also an increase slightly in phlogopite molecule from the former toward the latter, and that from the aplitic granite is rich in annite and siderophyllite-eastonite molecules. Garnet from the Hirabae-type is almandine with a slight progressive zoning, suggesting that it is metamorphic (Nakamura *et al.*, 1986).

2.6 Petrogenesis

The Shibi-san granodiorite is composed of ilmenite-series granitoid of Ishihara (1977) and I-type granitoid of Chappell and White (1974). The Kusubae-type magma would be derived from a fractionated liquid of andesitic magma, such as compositionally the associated quartz diorite dike, assimilated strongly by accretional sedimentary complex. It was a high temperature magma, and intruded at a shallow depth. The Hirabae-type magma would be formed through more sedimentary assimilation and contamination at the upper part of Kusubae-type magma (Oba, 1962). The biotite granite and the biotite aplitic granite would be formed from the residual liquid concentrated through filter-pressing at the top of the Shibi-san magma chamber.

Table 2. Chemical compositions (wt.%) of constituent mafic minerals from the Shibi-san granodiorite

Type	Kusubae-type		Hirabae-type				Aplitic Granite
Mineral	Hornblende	Biotite	Hornblende	Biotite	Garnet Core	Garnet Rim	Biotite
SiO_2	46.08	34.91	49.87	35.02	37.10	38.43	37.18
TiO_2	1.08	4.89	1.01	4.70	0.07	0.04	4.63
Al_2O_3	5.70	13.50	3.46	14.62	21.84	21.52	14.85
FeO*	22.31	25.22	19.21	24.16	30.23	29.89	19.79
MnO	0.51	0.38	0.47	0.33	4.86	1.47	0.34
MgO	9.28	7.82	11.50	7.85	4.58	7.17	11.01
CaO	10.53	0.06	10.93	0.04	1.31	1.30	0.09
Na_2O	1.24	0.22	0.55	0.14	nd.	nd.	0.16
K_2O	0.62	8.80	0.26	8.91	nd.	nd.	8.88
Total	97.35	95.80	97.26	95.77	99.99	100.02	96.93
$Mg/Mg+Fe^{+2}$	0.426	0.356	0.516	0.367	0.213	0.300	0.498

*Total Fe as FeO.
After Nakamura *et al.* (1986) and Yamamoto *et al.* (1988).

3. The Osumi Granodiorite Batholith

The Osumi granodiorite body is located in the southeastern part of Osumi Peninsula, Kagoshima Prefecture (Fig. 1). It is exposed in the Kimotsuki Mountains having summits higher than 800 meters above sea level. Geological and petrological studies of the Osumi granodiorite have been reported by Oba (1965), Kawano *et al.* (1966), Nozawa and Ota (1967), Yamamoto and Oba (1983) and Yamamoto *et al.* (1983), Tateishi *et al.* (1986), Nishimura and Yamamoto (1994) and Ishihara *et al.* (1999).

3.1 Geology

Figure 3 shows the geological map of Osumi granodiorite body and its surrounding areas. The main geological constituents in the mapped areas include the upper part of Shimanto Supergroup (Upper Shimanto Group), the Osumi granodiorite, the Ata and the Ito pyroclastic flow deposits and alluvial deposits, in ascending order.

The Upper Shimanto Group of Paleogene to Early Miocene age strikes in the direction of northeast, and dips steeply westward, however, it is usually disturbed. It is composed of accretional sedimentary complex of shales, sandstones, alternation beds of sandstone and shale and slump beds.

The Osumi granodiorite intrudes concordantly the Upper Shimanto Group. It is a batholith exposed in the wide areas of 48 km in east-northeast and west-southwest and 15 km in north-northeast and south-southwest, indicating that it is elongated in the east-northeasterly direction. The boundary between the batholith and the country rocks shows a sharp outward contact, and dips steeply in the northern margins of batholith and gently in the southern ones. There are three mylonitized zones at Yunotani, Uchinoura and Oura, and each zone strikes in the direction of northeast, as shown in Figure 3.

The country rocks are thermally metamorphosed by the intrusion of batholith. The cordierite isograd of pelitic hornfelses expands to the areas up to 750 meters wide in the western aureoles and up to 1,000 meters in the southern ones. The innermost aureole inside the garnet isograd is characterized by the appearance of garnet and/or K-feldspar in the pelitic hornfelses.

The Ata and the Ito pyroclastic flow deposits of Pleistocene age, composed of welded tuff and pumice tuff, respectively, cover the batholith.

3.2 Modes of Occurrence

The Osumi granodiorite batholith is lithologically divided into major four types, the Heda-Okawa, Oura, Koyama and the Hanaze, and into minor three types, the Kawaguchi, Hoyoshi-dake and the Kunimi (Yamamoto and Oba, 1983). The Heda-Okawa-type rock is distributed in the southwestern margin of batholith, and composed of medium- to fine-grained and light gray-colored hornblende-bearing biotite granodiorite. The Oura-type rock is distributed in the eastern and southern parts, and composed of medium- to fine-grained and light gray-colored orthopyroxene-cummingtonite-bearing biotite granodiorite. The Koyama-type rock is distributed in the northern part, and composed of medium-grained and light gray-colored garnet-orthopyroxene-cummingtonite-bearing biotite granodiorite. The Hanaze-type constitutes the core of batholith, and is composed of medium- to fine-grained cummingtonite-bearing biotite granite. The boundary between the Oura- and Hanaze-type rocks shows a gradational relation, but other boundaries are probably intrusive relations.

The Kawaguchi-type rock intrudes probably the Oura-type and shows a gradational relation with the Koyama-type. It is composed of coarse- to medium-grained and dark-gray colored orthopyroxene-cummingtonite-bearing biotite granodiorite. The Hoyoshi-dake-type rock intrudes both the Oura- and the Hanaze-types, and constitutes the top of Kimotsuki Mountains. It is composed of light gray-colored biotite granite porphyry. The Kunimi-type rock shows a gradational relation with the Koyama-type, and constitutes the top of Kunimi-yama. It is composed of fine-grained and light-colored muscovite-biotite aplitic granite. Outward and inward low-angle dipping joints are well-developed in the northeasterly direction throughout the batholith.

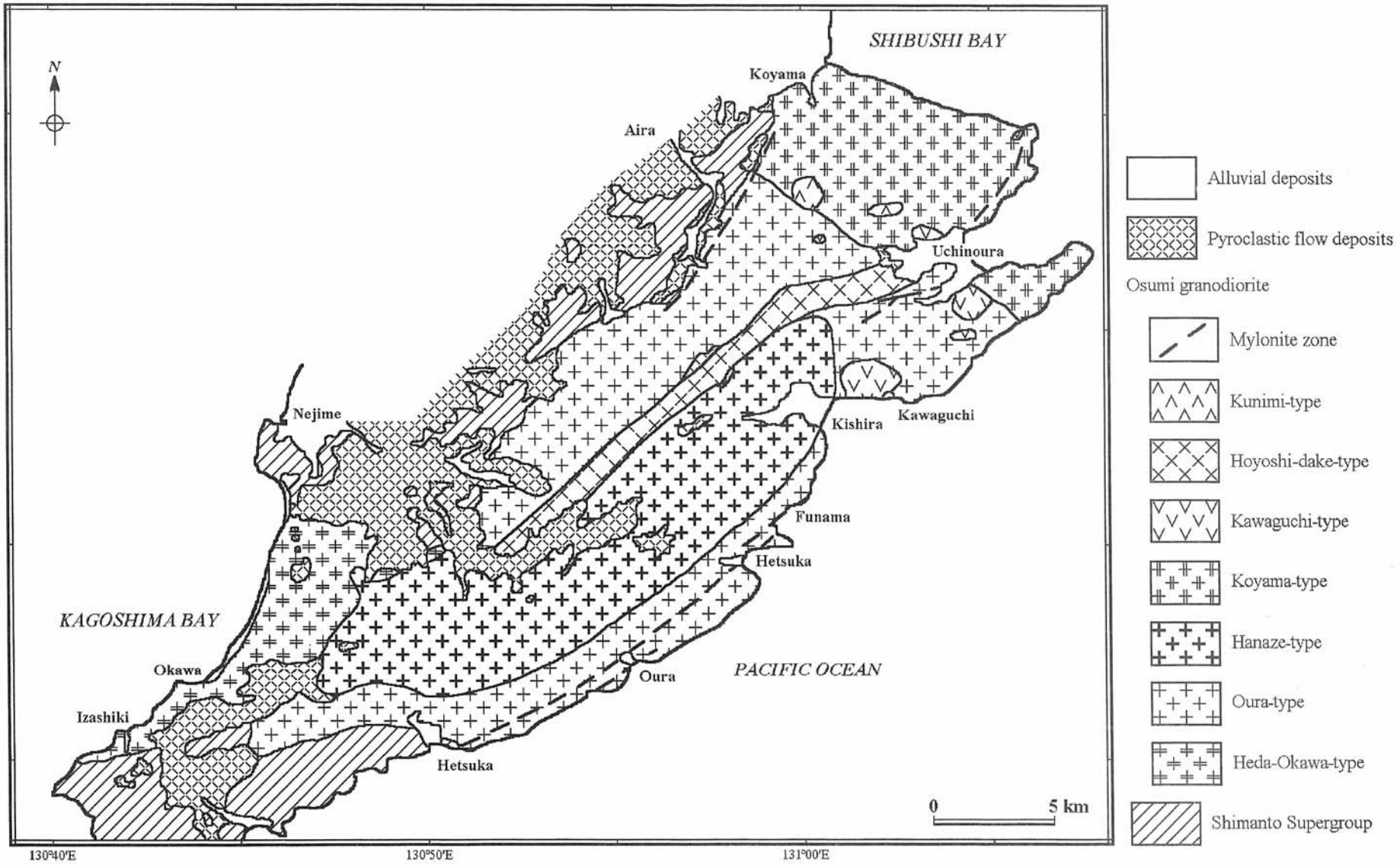

Fig. 3. Geological map of the Osumi granodiorite and the surrounding areas (modified from Yamamoto *et al.*, 1983).

Three types of xenoliths are classified as hornfels xenolith, xenolith of metamorphic rock appearance and that of igneous rock appearance (Tateishi *et al.*, 1986). Migmatitic and hornfelsic enclaves and dark inclusions are included throughout the batholith, but are dominant especially in the margins. The enclaves are rimmed by a biotite aggregate, and the dark inclusions occur as a globular-shaped and dark green-colored clot having several centimeters in diameter without a clear outline.

The K-Ar age of biotite from the stock indicates 14±1 Ma, the middle Miocene age (Miller *et al.*, 1962).

The mineralization is essentially barren.

3.3 Petrography

Major constituent minerals are composed of plagioclase, quartz, K-feldspar and biotite, and minor ones are of hornblende, orthopyroxene, cummingtonite, garnet and spinel. Zoned plagioclase and perthite intergrowth are common. Biotite occurs sometimes as an aggregate of euhedral flakes. Hornblende is contained only in the Heda-Okawa-type. Orthopyroxene occurs as a tiny euhedral crystal usually associated with cummingtonite, and is contained characteristically in the Oura-type and the Koyama-type. Cummingtonite occurs as a subhedral prism or an aggregate of fibers. Garnet occurs as a subhedral to anhedral grain with parting filled with biotite or chlorite, and is contained characteristically in the Koyama-type. Spinel occurs an aggregate of tiny crystals, and is contained only in the Koyama-type. Muscovite, tourmaline, ilmenite, pyrrhotite, chalcopyrite, zircon, apatite, sphene and allanite are common as accessories. The Kawaguchi-type rock is mineralogically similar to the Koyama-type, and the Kunimi-type rock of aplitic granite contains slightly rich in muscovite.

The color index ranges from 10 to 19 (Tateishi *et al.*, 1986), and is slightly high in the Heda-Okawa-type among the four major types.

The dark clot in the Heda-Okawa-type is an aggregate of plagioclase, biotite, hornblende and cummingtonite, that in the Oura-type is of plagioclase, biotite, cummingtonite, orthopyroxene and garnet, that in the Koyama type is of plagioclase, biotite and spinel.

3.4 Bulk Compositions

Bulk compositions of the Osumi granodiorite are listed in Tables 3 and 4. SiO_2 content ranges from 66 wt.% to 70 wt.%, and is fairly uniform in composition throughout the major four types. Normative corundum is usually calculated. As compared to the average chemical composition of Japanese granitoids (Aramaki *et. al.*, 1972), the bulk compositions show that FeO and K_2O contents are higher, whereas CaO and Na_2O contents are lower.

Abundances for trace elements show that the batholith is rich in base metal elements such as Cu and Zn, whereas incompatible elements are not strongly concentrated throughout the batholith. Li and Rb contents in the Kunimi-yama aplitic granite are lower than the aplitic granite dike in the Shibi-san stock and the Sarugajo-type aplitic granite in the Takakuma-yama. U content ranges from 1.9 ppm to 5.3 ppm, and Th content from 7 ppm to 12 ppm (Kawachi, 1961, Katsura *et al.*, 1969). The average S and C contents are 493 ppm and 191 ppm, respectively (Ishihara *et al.*, 1999). $\delta^{34}S$ value ranges from -8.3 ‰ to -7.0 ‰ (Ishihara *et al.*, 1999). $\delta^{18}O$ value ranges from +10.3 ‰ to +12.7 ‰ and is averaged as +11.5 ‰ (n=6) (Ishihara and Matsuhisa, 1999), higher than that of the Shibi-san granodiorite. Initial $^{87}Sr/^{86}Sr$ ratio is 0.7071±0.0002 (Yanagi *et al.* 1971).

Table 3. Representative bulk compositions (wt.%) of the Osumi granodiorite

Type	Heda-Okawa	Oura	Hanaze	Koyama
SiO_2	66.42	66.76	69.63	67.23
TiO_2	0.54	0.70	0.53	0.64
Al_2O_3	15.77	15.73	14.07	15.52
Fe_2O_3	0.86	0.79	0.56	0.60
FeO	4.06	3.66	3.26	4.40
MnO	0.04	0.07	0.02	nd.
MgO	1.63	1.58	1.36	1.31
CaO	3.24	3.30	2.98	2.37
Na_2O	3.30	3.05	3.30	3.70
K_2O	3.10	2.92	3.30	3.23
H_2O^+	0.51	0.66	0.60	0.62
H_2O^-	0.05	0.23	0.11	0.22
P_2O_5	0.13	0.14	0.03	0.30
Total	99.65	99.61	99.74	100.14

After Oba (1963), Kawano *et al.* (1966), and Yamamoto (1976).

3.5 Mineral Compositions

Chemical compositions of major constituent minerals from the Osumi granodiorite are listed in Table 5.

Zoned plagioclase ranges in composition from An_{51} to An_{19} in the Heda-Okawa-type (Oba, 1962).

Hornblende from the Heda-Okawa-type is ferro-hornblende ($Mg/Mg+Fe^{+2}=0.34$) in the core and actinolitic hornblende ($Mg/Mg+Fe^{+2}=0.54$) in the rim. Biotite ranges from $Phl_{0.46}$ in the Koyama-type to $Phl_{0.37}$ in the Hanaze-type. Garnet from the Koyama-type is almandine with a progressive zoning, which the core is rich in MnO and CaO, whereas the rim is rich in MgO, suggesting that it is metamorphic. Orthopyroxene from the Koyama-type has also a slight progressive zoning, which the core is rich in FeO, whereas the rim is rich in MgO. Cummingtonite is compositionally similar to the rim of orthopyroxene.

3.6 Petrogenesis

The Osumi granodiorite is composed of ilmenite-series granitoid of Ishihara (1977). It is also like S-type granitoid of Chappell and White (1974), but the mode of occurrence of Heda-Okawa-type suggests that it was essentially of I-type. It was formed probably by intrusions of several heterogeneous dacitic magmas different slightly in degree of assimilation by the uppermost crustal materials. Only the Kunimi-type magma would be formed from the residual liquid concentrated at the top of the Koyama-type magma.

Table 4. Trace element abundances (ppm) of the Osumi granodiorite

Type	Heda-Okawa	Oura	Hanaze	Koyama	Kawaguchi	Kunimi
Li	42	56	52	59	55	86
Rb	130	116	91	127	107	182
Sr	146	135	143	150	154	71
Cu	64	31	45	40	26	22
Zn	54	84	74	92	74	46
Pb	20	21	13	20	18	16

After Yamamoto and Oba. (1983).

Table 5. Chemical compositions (wt.%) of constituent minerals from the Osumi granodiorite

Mineral	Honblende		Biotite		Garnet		Orthopyroxene		Cummingtonite
	Core	Rim	Hanaze	Koyama	Core	Rim	Core	Rim	
SiO_2	49.37	47.34	35.61	34.56	36.82	37.16	50.08	50.53	51.94
TiO_2	0.03	0.48	3.73	4.78	0.11	0.02	nd.	nd.	0.09
Al_2O_3	2.57	3.97	14.14	16.38	21.95	22.78	0.32	0.76	0.44
Cr_2O_3	nd.	nd.	nd.	nd.	0.26	0.26	nd.	nd.	nd.
FeO*	25.04	19.07	21.88	23.61	28.27	30.18	36.24	33.55	30.24
MnO	0.84	0.61	0.16	0.65	4.13	0.34	2.60	1.03	1.28
MgO	7.34	12.38	10.46	7.78	2.77	8.02	10.90	13.82	12.92
CaO	11.92	10.36	0.10	0.06	6.35	1.72	0.22	0.46	0.72
Na_2O	0.50	0.79	0.23	0.21	nd.	nd.	nd.	nd.	0.17
K_2O	0.19	0.41	9.02	9.05	nd.	nd.	nd.	nd.	0.01
Total	97.80	95.41	95.33	97.08	100.66	100.48	100.36	100.15	97.81
$Mg/Mg+Fe^{+2}$	0.343	0.536	0.461	0.367	0.149	0.321	0.349	0.423	0.432

*Total Fe as FeO.
After Yamamoto *et al.* (1983).

4. The Takakuma-yama Granite Stock

The Takakuma-yama granite body is located in the central part of Osumi Peninsula, Kagoshima Prefecture (Fig. 1). It is exposed in the western side of Takakuma Mountains having summits higher than 800 meters above sea level, and is well-dissected along the Honjo river running in the westerly direction. Geological and petrological studies of the Takakuma-yama granite have been reported by Hamachi and Ishihara (1958), Oba (1958), Ishihara and Kawachi (1961), Kawachi (1961), Ota (1964), Ota and Kawachi (1965), Yamamoto (1975) and Yamamoto and Oba (1983).

4.1 Geology

Figure 4 shows the geological map of Takakuma-yama granite body and its surrounding areas. The main geological constituents in the mapped areas include the lower part of Shimanto Supergroup (Lower Shimanto Group), the Takakuma-yama granite, the Ata and the Ito pyroclastic flow deposits and alluvial deposits, in ascending order.

The basement rock in the mapped areas is the Lower Shimanto Group of late Cretaceous age. It strikes in the direction of north-northeast, and dips steeply westward. It is composed of accretional sedimentary complex of pelitic rocks such as phyllite, clayslate and shale, sandstones, alternating beds of sandstone and shale, slump beds and a small amount of green rocks.

The Takakuma-yama granite intrudes discordantly the Lower Shimanto Group. It is a stock exposed in the circular-shaped areas of 7 km in north and south and 6 km in east and west. The boundary between the stock and the country rocks shows a sharp outward contact, and dips steeply in the northern and western margins of stock and gently in the southern and eastern ones. A satellite body crops out in the southeast of stock, indicating that the stock is elongated in the northwesterly direction. A roof pendant of the country rocks lies at the top of Nanatsu-dake.

The country rocks are thermally metamorphosed by the intrusion of stock. The cordierite isograd of pelitic hornfelses expands to the areas up to 1,000 meters wide in the northwestern aureoles and up to 2,300 meters in the southeastern ones (Ota and Kawachi, 1965, Ogura *et al.*, 1970). The innermost aureole inside the garnet isograd is characterized by the appearance of garnet, andalusite and/or K-feldspar in the pelitic hornfelses.

The Ata and the Ito pyroclastic flow deposits of Pleistocene age, composed of welded tuff and pumice tuff, respectively, cover the stock.

4.2 Modes of Occurrence

The Takakuma-yama granite stock is lithologically divided into two types, the Shinkoji and the Sarugajo (Kawachi, 1961). The Shinkoji-type rock is composed of coarse- to medium-grained and light gray-colored biotite granite, and the Sarugajo-type rock is of fine-grained and light-colored aplitic granite. The former constitutes the core of stock and the latter the margin and the roof. The boundary between them shows a gradational relation with about 500 meters wide. The rock in the gradational zone is composed of medium-grained and light-colored biotite aplitic granite

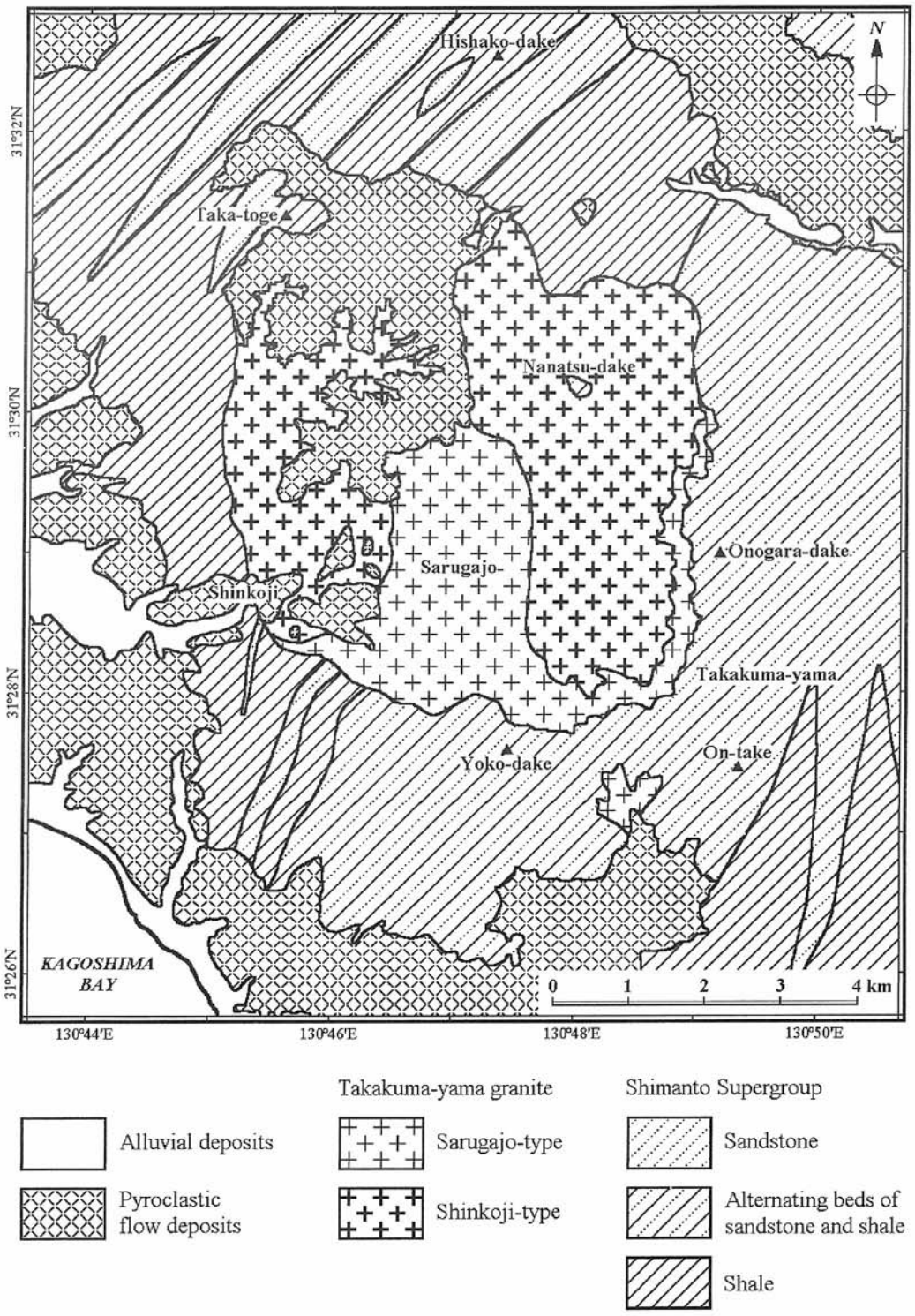

Fig. 4. Geological map of the Takakuma-yama granite and the surrounding areas (compiled from Ota, 1964, Ota and Kawachi, 1965, Yamamoto, 1975 and Kagoshima Prefecture, 1990).

having both characters of the two types. Joints are well-developed throughout the stock, and their widths in the Sarugajo-type are finer than those in the Shinkoji-type.

The Shinkoji-type rock contains a small amount of migmatitic enclave rimmed by a biotite aggregate. The Sarugajo-type rock contains a small amount of hornfelsic enclave and a large amount of dark clot. The dark clot occurs as a globular-shaped and dark green-colored rock having several centimeters in diameter without a clear outline.

The K-Ar age of biotite from the stock indicates 16 ± 2 Ma, the middle Miocene age (Miller *et al.*, 1962).

The major associated mineralization includes tin, tungsten and boron (Oba and Miyahisa, 1977).

Table 6. Representative bulk compositions of the Takakuma-yama granite

Major Elements (wt.%)						
Type	Shinkoji-type		Gradational Zone		Sarugajo-type	
No.	1	2	3	4	5	6
SiO_2	70.66	71.20	74.80	74.44	76.62	75.82
TiO_2	0.42	0.30	0.18	0.08	0.01	0.09
Al_2O_3	14.84	14.22	14.08	14.25	13.33	13.94
Fe_2O_3	0.24	1.01	0.16	0.66	0.19	0.19
FeO	1.78	1.47	0.65	0.69	0.60	0.48
MnO	tr.	0.07	0.03	0.03	tr.	tr.
MgO	1.00	0.97	0.39	0.31	0.13	0.25
CaO	2.77	2.40	1.34	1.27	0.70	0.74
Na_2O	2.23	2.88	3.54	3.06	3.41	3.30
K_2O	3.20	3.70	4.10	3.72	3.78	4.10
H_2O^+	2.16	1.14	0.62	0.66	0.62	0.32
H_2O^-	0.86	0.26	0.22	0.34	0.40	0.24
P_2O_5	0.09	0.08	0.02	0.03	0.02	0.03
Total	100.25	99.70	100.13	99.54	99.81	99.50
Trace Elements (ppm)						
Li	59	99	109	106	119	177
Rb	170	190	420	360	440	460
Sr	146	105	27	38	17	14
Ni	20	24	18	17	10	22
Cr	36	39	6	14	10	10
Cu	5	7	3	12	5	7
Zn	27	29	13	20	7	16
Pb	6	17	33	24	32	21

After Yamamoto (1975) and Yamamoto and Oba (1983).

4.3 Petrography

Major constituent minerals in the Shinkoji-type granite include plagioclase, quartz, K-feldspar and biotite. Zoned or porphyritic prismatic plagioclase, porphyritic subhedral quartz, fine-grained myrmekite intergrowth and prismatic perthite intergrowth are common. Biotite occurs sometimes as an aggregate of euhedral flakes. Accessory minerals include garnet, muscovite, tourmaline, zircon, apatite, sphene, ilmenite and pyrrhotite. The average color index is 7.

Major constituent minerals in the Sarugajo-type aplitic granite include plagioclase, quartz, K-feldspar, biotite, muscovite, garnet and tourmaline. Porphyritic subhedral quartz, fine-grained myrmekite intergrowth and prismatic perthite intergrowth are common. Biotite occurs sometimes as an interstitial flake. Muscovite is usually associated to K-feldspar. Accessory minerals include zircon, apatite, sphene, monazite, ilmenite and pyrrhotite. The average color index is 2.

Modal compositions show that the Shinkoji-type granite is plotted on the granodiorite field in the Q-A-P diagram, in spite of its low color index, that plagioclase and biotite decrease, whereas quartz, K-feldspar, muscovite and tourmaline increase, from the Shinkoji-type through the gradational zone toward the Sarugajo-type, and that garnet is most abundant in the aplitic granite of gradational zone.

The dark clot in the Sarugajo-type is composed of biotite, cordierite, K-feldspar and quartz, with minor garnet, tourmaline and green spinel (Ishihara and Kawachi, 1961), indicating that it is rich in aluminous minerals.

4.4 Bulk Compositions

Bulk compositions of the Takakuma-yama granite are listed in Table 6. The average SiO_2 content is 71 wt.% in the Shinkoji-type, 74 wt.% in the gradational zone and 76 wt.% in the Sarugajo-type. Normative corundum is calculated more than 1.3 wt.% throughout the stock, indicating that the stock is compositionally peraluminous. As compared to the average chemical composition of Japanese granitoids (Aramaki *et. al.*, 1972), the bulk compositions show that FeO and K_2O contents are higher, whereas CaO and Na_2O contents are lower.

Incompatible trace elements are remarkably concentrated from the Shinkoji-type toward the Sarugajo-type. Li, Rb and Pb contents exceed 100 ppm, 350 ppm and 20 ppm, respectively, in the Sarugajo-type. U content ranges from 2.7 ppm to 6.5 ppm in the Shinkoji-type and from 1.6 ppm to 8.0 ppm in the Sarugajo-type, and Th content ranges from 15 ppm to 17 ppm in the Shinkoji-type and from 9 ppm to 16 ppm in the Sarugajo-type (Kawachi, 1961, Ishihara *et al.*, 1969). The average Sn and F contents are 8.8 ppm and 390 ppm, respectively (Ishihara and Terashima, 1978). $\delta^{18}O$ values of both types vary from +11.4 ‰ to +11.9 ‰ and are averaged as +11.6 ‰ (n=3) (Ishihara and Matsuhisa, 1999).

Table 7. Chemical compositions (wt.%) of constituent minerals from the Takakuma-yama granite

Type	Shinkoji-type		Gradational Zone			Sarugajo-type			
Mineral	Biotite	K-feldspar	Biotite	K-feldspar	Garnet	Biotite	K-feldspar	Muscovite	Garnet
SiO_2	34.52	64.16	33.40	64.20	37.16	33.96	64.44	49.26	35.96
TiO_2	2.84	nd.	1.82	nd.	0.06	1.64	nd.	0.22	0.10
Al_2O_3	16.94	19.34	19.38	18.94	19.40	20.22	18.94	30.72	19.99
Fe_2O_3	4.19	0.24	4.84	0.16	3.66	6.79	0.28	0.56	4.13
FeO	18.52	nd.	20.72	nd.	23.30	18.76	nd.	2.07	22.45
MnO	0.41	nd.	0.82	nd.	9.82	0.84	nd.	0.23	13.37
MgO	9.12	0.08	5.20	0.08	3.81	3.28	0.08	0.96	1.12
CaO	0.60	0.71	0.74	0.33	1.60	0.67	0.31	0.96	1.73
Na_2O	0.40	2.20	0.48	2.25	0.64	0.28	1.98	1.84	0.18
K_2O	7.60	12.73	7.00	12.94	0.12	7.00	12.79	8.18	0.06
H_2O^+	3.76	0.80	5.12	0.96	nd.	4.78	0.84	4.56	nd.
H_2O^-	0.72	nd.	0.24	nd.	0.48	1.52	nd.	0.36	0.60
P_2O_5	0.10	nd.	0.08	nd.	nd.	0.02	nd.	0.02	0.03
Total	99.72	100.26	99.84	99.86	100.05	99.76	99.66	99.81	99.72
$Mg/Mg+Fe^{+2}$	0.467		0.309		0.226	0.238			0.082

After Yamamoto (1975, 1978).

4.5 Mineral Compositions

Chemical compositions of major constituent minerals from the Takakuma-yama granite are listed in Table 7.

Plagioclase ranges in composition from An_{44} to An_{22} in the Shinkoji-type (Ishihara and Kawachi, 1961) and from An_{18} to An_{14} in the Sarugajo-type (Yamamoto, 1975). K-feldspar is orthoclase microperthite having $Or_{74\text{-}77}$ in the former and $Or_{79\text{-}80}$ in the latter.

Biotite is Fe-biotite, and shows the increase in annite and siderophyllite-eastonite molecules, from the Shinkoji-type toward the Sarugajo-type. Muscovite from the Sarugajo-type contains about 26% paragonite molecule. Garnet is manganiferous almandine without a progressive zoning, and shows the decrease in pyrope molecule and the increase in spessartine one, from the gradational zone toward the Sarugajo-type, suggesting that it is magmatic (Nakamura *et al.*, 1986).

4.6 Petrogenesis

The Takakuma-yama granite is composed of ilmenite-series granitoid of Ishihara (1977) and I-type granitoid of Chappell and White (1974). The Shinkoji-type magma would be derived from a fractionated liquid of dacitic magma assimilated strongly by accretional sedimentary complex. It was a high temperature magma rich in vapor, and intruded at a shallow depth. The Sarugajo-type magma would be composed of a vapor-rich residual liquid concentrated through filter-pressing at the top of Shinkoji-type magma chamber. The dark clot within the Sarugajo-type would be composed of restite through melting of pelitic rocks broken off the roof and the wall of Sarugajo-type magma chamber.

5. The Hishikari Epithermal Gold Deposits

5.1 Introduction

The Hishikari gold mine is located in the northern part of Kagoshima Prefecture, about 60 km north of Kagoshima City, southern Kyushu, Japan. The Hishikari deposits were discovered in 1981 underneath old adits by Metal Mining Agency of Japan (MMAJ) in 1981, and subsequent development by the property owner, Sumitomo Metal Mining Co. Ltd. (SMM) has shown the Hishikari deposits to be one of the major gold deposits in the western Pacific (Izawa *et al.*, 1990; Ibaraki and Suzuki, 1993).

Since the discovery of the Hishikari deposits, a number of researchers studied the ore genesis (*e.g.*, Izawa *et al.*, 1990). Some recent papers reported fracture formation (Uto *et al.*, 2001; Sekine *et al.*, 2002), fluid inclusion microthermometry (Izawa *et al.*, 1990; Nagayama, 1993; Imai and Uto, 2002; Etoh *et al.*, 2002a) and gas composition (Etoh *et al.*, 2002b), and the origin of ore fluid based on $\delta^{18}O$ (Shikazono and Nagayama, 1993; Morishita, 1993; Matsuhisa and Aoki, 1994; Hayashi *et al.*, 2000, 2001; Shikazono *et al.*, 2002), $\delta^{13}C$ (Morishita, 1993; Imai and Uto, 2002), δD (Imai *et al.*, 1998; Faure *et al.*, 2002), $\delta^{34}S$ (Ishihara *et al.*, 1986; Shikazono, 1999) and rare earth elements' composition (Takahashi *et al.*, 2002), in addition to description of the constituent minerals (Nagayama, 1993; Imai and Uto, 2002; Etoh *et al.*, 2002c).

5.2 Geologic Background

The basement rocks in the Hokusatsu district consist of Late Cretaceous sedimentary piles, which belong to the Shimanto Supergroup. The basement rocks are exposed only in the northwestern part of the Hokusatsu district (Fig. 5). The Neogene to Quaternary terrestrial volcanic activity and the formation of lacustrine sedimentary basins characterize the district (Hase, 1987; Izawa and Urashima, 1989).

The Hishikari area is underlain by sedimentary basement rocks of the Late Cretaceous Shimanto Supergroup, volcanic rocks of Quaternary age and alluvial deposits (Fig. 6). The Shimanto Supergroup is recognized at +120 m elevation relative to sea level (100 m below surface) in the central part of the Honko-Sanjin zone, but it occurs 400 m deeper in the surrounding area of the Hishikari deposit (Fig. 6). The Shimanto Supergroup around the Hishikari deposits consists of shale, sandstone with a minor amount of intercalated tuffaceous shale and chert. Quaternary volcanic rocks around the Hishikari deposits consist mainly of the Hishikari Lower Andesites, Kurozonsan Dacites, Hishikari Middle Andesites, Shishimano Dacites, Hannyaji Welded Tuff, Hishikari Upper Andesites and Ito Pyroclastic Flow Deposits, in ascending order (Abe *et al.*, 1986; Izawa *et al.*, 1990; Ibaraki and Suzuki, 1993). The Hishikari Lower Andesites unconformably overlie the Shimanto Supergroup. These Quaternary volcanic rocks are calc-alkaline and were subaerially deposited. (Izawa *et al.*, 1990). Their magnetic susceptibility shows typical magnetite-series values (Ishihara *et al.*, 1986; Izawa *et al.*, 1990). K-Ar age data on the volcanic rocks around the Hishikari deposits revealed that the volcanic activities occurred 1.8-0.5 Ma (Izawa *et al.*, 1990). Among the volcanic rocks around the Hishikari deposits, the volcanic activity of the Shishimano Dacites having Sr*I* ratios of 0.70474-0.70486 (Ishihara *et al.*, 1990) has been assumed to be related to the hydrothermal activity responsible for the mineralization at the Hishikari deposits (Ishihara *et al.*, 1990; Ishihara, 1992).

The Hishikari deposits are classified as epithermal adularia-sericite (Heald *et al.*, 1987) or low-sulfidation (Hedenquist, 1987) vein-type. Mineralization occurred in 1.25-0.66 Ma on the basis of K-Ar dating on adularia from veins (*e.g.*, Izawa *et al.*, 1993a; Sekine *et al.*, 1998; 2002). Extensional movement in southern Kyushu seems to have provided sufficient strain for the formation of veins at the Hishikari deposits (Uto *et al.*, 2001).

5.3 Outline of the Hishikari Deposits

The Hishikari deposits comprise the Honko (Main), Yamada and Sanjin deposits (Fig. 7). Each deposit consists of groups of subparallel, steeply dipping veins. Gold-silver bearing veins occur in the Shimanto Supergroup and the Hishikari Lower Andesites within in an area of 2.5 km×0.8 km. The veins in the Honko-Sanjin deposits generally strike N50° E and dip 70°-90° N. The veins in the Yamada deposit

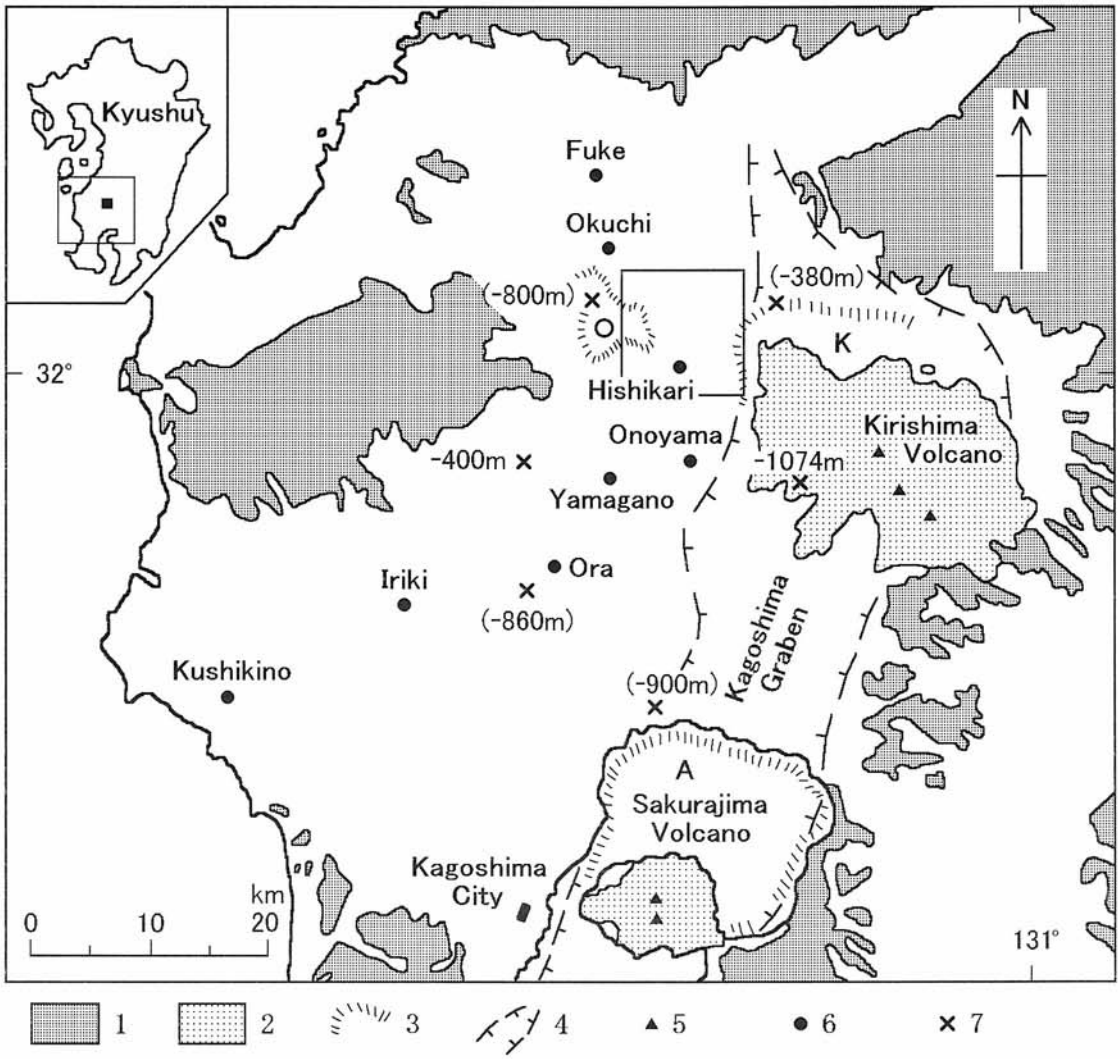

Fig. 5. Location and structural map of the Hokusatsu district (quoted and modified from Fig. 1 of Izawa et al., 1990). 1=outcrops of the Shimanto Supergroup; 2=Holocene volcanic rocks; 3=caldera and basin, O=Okuchi basin, K=Kakuto caldera, and A=Aira caldera; 4=Kagoshima graben; 5=volcanic center; 6=gold deposit; 7=deep drill hole with elevation of the top of the Shimanto Supergroup (parenthesis indicates that the drill hole did not reach the basement), data from Aramaki (1968), Kubota (1986), MITI (1988). The area in square is shown in Figure 6.

are located 1.2 km southwest of the Honko-Sanjin deposits and strike N50° E, N30° E and N70° E (Sekine *et al*., 1998).

The Honko deposit is composed of the Daisen, Zuisen, Ryosen, Hosen and Kinsen vein groups, having known bonanza zones at elevations from +115 m to -35 m relative to the sea level. The Sanjin deposit, located to the southeast of the Honko deposit, is composed of the Keisen and Shosen vein groups with known bonanza zones at elevations from +55 m to -35 m. About 60% of the minable ore in the Honko deposit and more than 90% in the Sanjin deposit occur in the Shimanto Supergroup (Ibaraki and Suzuki, 1993). The Yamada deposit, located to the southwest of the Honko and Sanjin deposits, is composed of the Seisen and Yusen vein groups. In the Yamada deposit, veins occur in the Hishikari Lower Andesites. The known bonanza zone of the Yusen vein group is located between +150 m and -50 m (Ibaraki and Suzuki, 1993). Sinter-like siliceous lacustrine beds are preserved above the Yamada deposit at a present elevation of +170 m relative to sea level (Izawa *et al*., 1993b), suggesting a shallow formation depth.

Major gangue minerals in the Hishikari deposits are quartz, adularia and clay minerals associated with a certain amount of calcite. The clay minerals are predominantly smectite and minor kaolinite. The principal metallic minerals are electrum, naumannite-aguilarite, pyrargyrite, chalcopyrite, pyrite and marcasite, with minor amounts of sphalerite, galena, tetrahedrite, miargyrite, hessite, Ag-Au selenide, acanthite and hematite (Izawa *et al*., 1990). Stibnite occurs as a late stage mineral. Bladed textures displayed by quartz that replaced initial bladed calcite are often observed (Imai and Uto, 2002; Etoh *et al*., 2002c). Typical precipitation sequence from initial columnar adularia to later quartz was described in detail by Nagayama (1993). Symmetrical structure displayed by a sequence of mineral precipitation is an evidence of episode of vein opening. Most major veins contain multiple parallel, sub-parallel or sometimes oblique smaller veinlets,

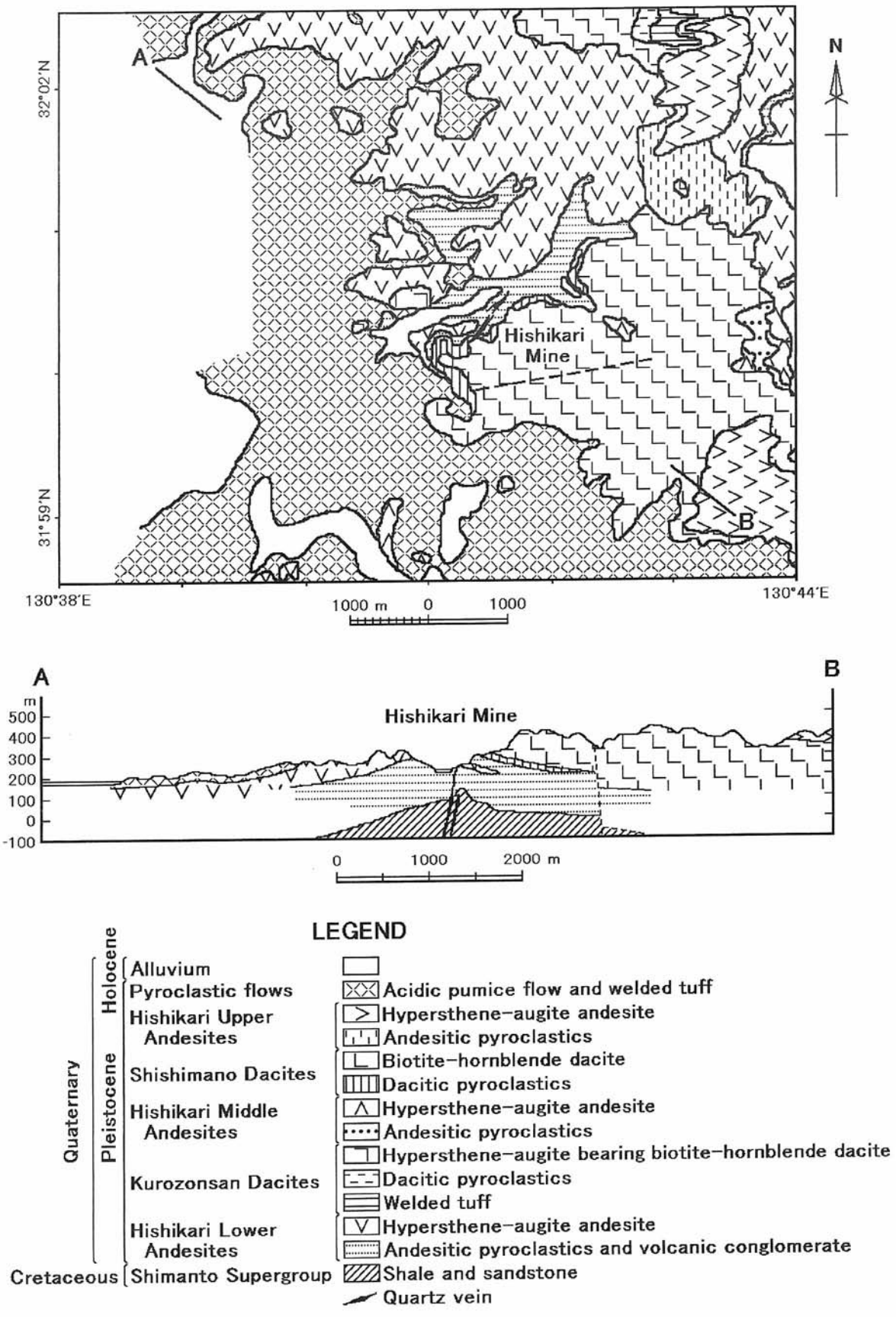

Fig. 6. Geological map of the Hishikari area and cross section along A-B (quoted and modified from Fig. 3 of Izawa *et al.*, 1990).

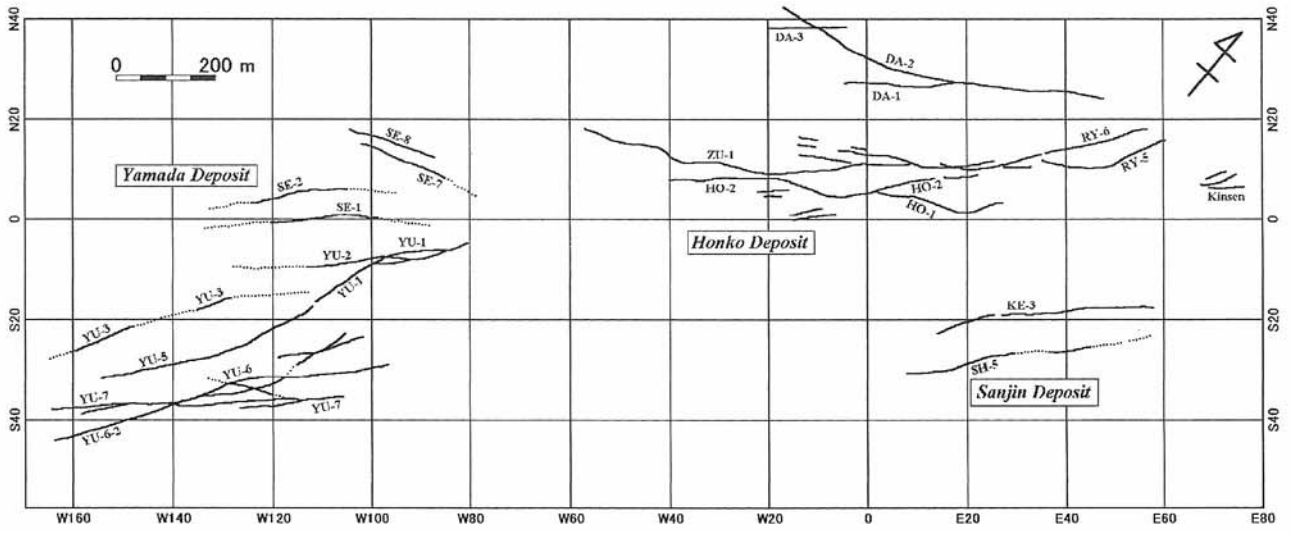

Fig. 7. Simplified vein plan map of the Hishikari deposits (quoted and modified from Uto *et al.*, 2001; Imai and Uto, 2002). Vein width is not to scale. Abbreviations of the name of vein groups are as follows; HO: Hosen, RY: Ryosen, ZU: Zuisen, and DA: Daisen vein group for the Honko (Main) deposit; KE: Keisen, and SH: Shosen vein group for the Sanjin deposit; YU: Yusen, and SE: Seisen vein group for the Yamada deposit. Modified after Ibaraki and Suzuki (1993) and Sekine *et al.* (1998).

indicating multiple rupturing events. Sekine *et al.* (2002) classified the veins into early veins and late veins based on the cross-cutting relations. In addition, blocks of the country rocks contained in the veins, as well as brecciated vein materials are often observed.

Fluid inclusions in quartz, adularia and calcite in veins associated with gold mineralization consist of aqueous liquid and vapor phases, thus, liquid-rich dilute aqueous fluid inclusions. Microthermometry on vein quartz associated with gold mineralization suggests the temperature of ore solution responsible for gold mineralization was around 200° C (Izawa *et al.*, 1990; Nagayama, 1993). Likewise, homogenization temperatures of fluid inclusions in adularia and calcite were determined to be 175-215° C (Etoh *et al.*, 2002a) and 180-217° C (Imai and Uto, 2002), respectively. Temperatures of the last melting point of ice of fluid inclusions in adularia and calcite were determined to be -1.2 to -0.1° C (Etoh *et al.*, 2002a) and -0.4 to ±0.0° C (Imai and Uto, 2002), respectively, suggesting low salinity corresponding to 2.1-0.2 wt.% NaCl equivalent and 0.8-0.0 wt.% NaCl equivalent, respectively.

6. Observation Sites in the Excursion

Figure 8 shows fourteen stops on the driving course ready for the excursion, including the Hishikari mine. Explanations of outcrop in each stop are described below. In addition, the 15th stop will be ready for sightseeing at the Sakurajima volcano.

Stop 1.

The Hishikari mine is located in Hishikari Town, Kagoshima Prefecture. Though the place in the Hishikari mine to be visited during the field excursion is not decided at the time of preparation of the field excursion guidebook, an underground tour will be conducted to visit some (at least one, depending on conditions) underground mine working face(s). Principal productive vein(s) either in the Honko, Sanjin or Yamada deposits will be observed. At the present underground working levels, the major host rocks to the most productive veins in the Honko and Sanjin deposits are sandstone, shale, and/or their alternations of the Shimanto Supergroup, while the major host rocks to the veins in the Yamada deposit are pyroclastic rocks of the Hishikari Lower Andesites.

Stop 2.

This stop is located at 31° 57.1' N in latitude and 130° 20.6' E in longitude. The Kusubae-type rock constituting the core of stock crops out on the road cutting and along the Tomarino river. It is composed of medium-grained and light gray-colored hornblende-biotite granodiorite rich in K-feldspar megacryst. Sedimentary and mafic enclaves are common. The bulk composition is presented in No. 1 of Table 1, and mineral compositions are in Table 2. Characteristic features of granitic rocks in the northern Shimanto terrane, genetical relationship between the stock and the related dikes, and formation of K-feldspar megacryst will be discussed here.

Stop 3.

This stop is located at 31° 59.0' N in latitude and 130° 20.6' E in longitude. Weathered granite sands with fresh boulders of the Kusubae-type constituting the upper part of stock crops out on the cliff. The rock is composed of medium-grained and light gray-colored biotite granodiorite. It shows a heterogeneous face, and is dominant in sedimentary enclaves. The bulk composition is presented in No. 2 of Table 1, and mineral compositions are in Table 2. Formation of the Hirabae-type rock through assimilation and contamination of the Kusubae-type one by accretional sedimentary complex will be discussed here.

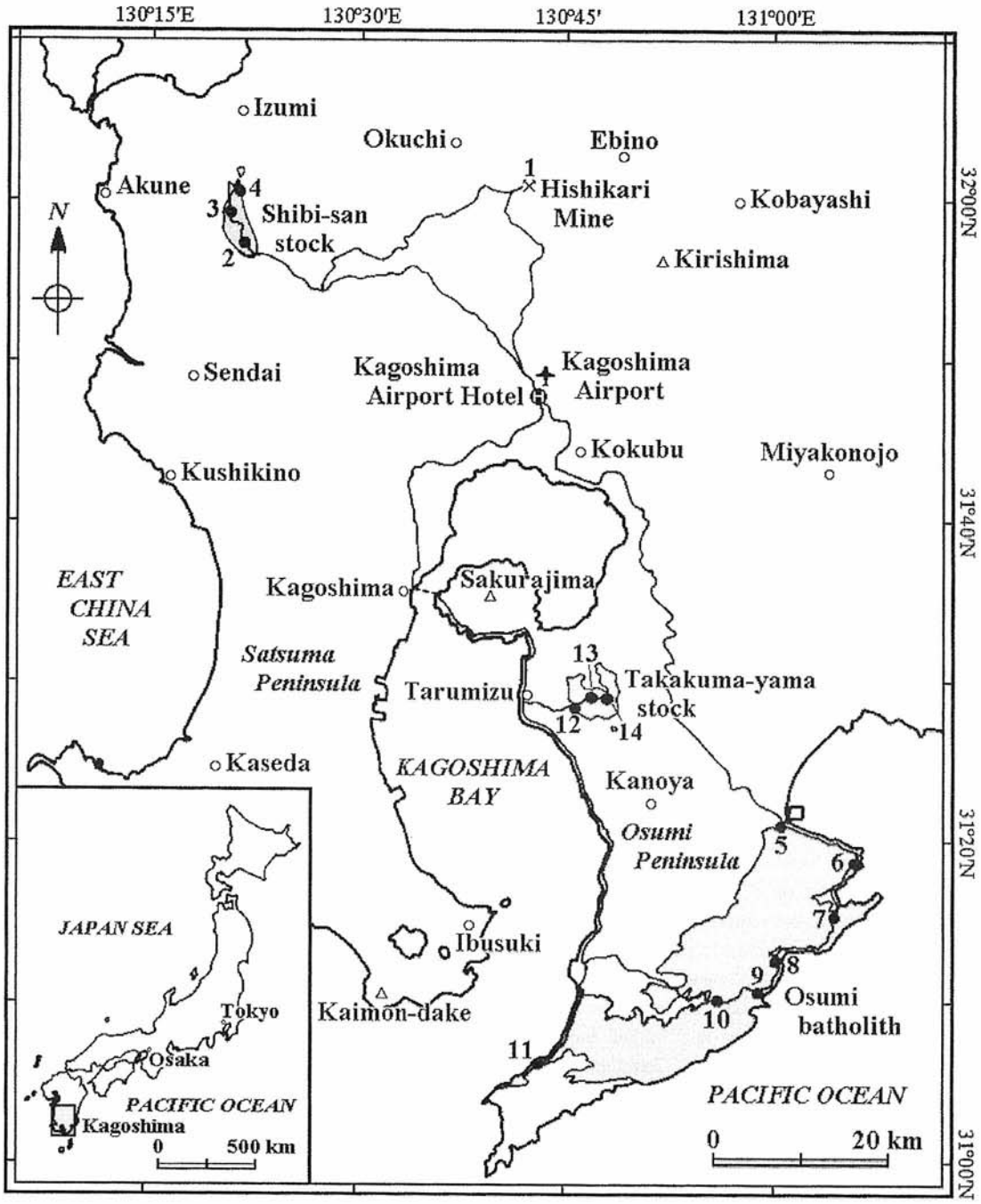

Fig. 8. Map showing the observation sites in the excursion.

Stop 4.

This stop is located at 31° 59.9' N in latitude and 130° 21.5' E in longitude. The biotite granite at the top of stock crops out on the road cutting. It is composed of medium-grained and light-colored biotite granite. It shows a fairly homogeneous face, and is poor in enclave. Bulk composition of the similar rock is presented in No. 3 of Table 1. Formation of the granite through concentration of the filter-pressed residual liquid at the top of stock will be discussed here.

Stop 5.

This stop is located at 31° 20.5' N in latitude and 131° 00.6' E in longitude. The Koyama-type rock constituting the northern margins of batholith crops out in and around the Todoroki fall. It is composed of medium-grained and light gray-colored garnet-bearing biotite granodiorite. Sedimentary enclaves are common. Characteristic features of granitoids in the southern Shimanto terrane and formation of the Koyama-type rock rich in accessory minerals such as garnet, orthopyroxene and cummingtonite through assimilation and contamination by sedimentary rocks will be discussed here.

Stop 6.

This stop is located at 31° 18.9'N in latitude and 131° 06.3' E in longitude. The Koyama-type rock crops out in the sea coast. It is composed of medium-grained and light gray-colored garnet-bearing biotite granodiorite. Sedimentary enclaves having various kinds of texture and structure occur in beach boulders. Mineralogy and origin of the enclaves will be discussed here.

Stop 7.

This stop is located at 31° 15.6'N in latitude and 131° 04.5' E in longitude. The Kawaguchi-type rock crops out along the road cutting. It is composed of coarse-grained and gray-colored garnet-bearing biotite granodiorite. Formation of the rock and difference in cooling rate among some later intrusions will be discussed here.

Stop 8.

This stop is located at 31° 12.8'N in latitude and 131° 00.5' E in longitude. The Oura-type rock constituting the eastern margins of batholith crops out in the sea coast. It is composed of medium-grained and light gray-colored biotite granodiorite rich in quartz vein. Formation of the rock through assimilation and contamination by K-rich silica dissolved from sedimentary rocks will be discussed here.

Stop 9.

This stop is located at 31° 10.9'N in latitude and 130° 59.8' E in longitude. The Oura-type rock crops out in the sea coast. It is composed of medium-grained and light gray-colored biotite granodiorite. Assimilation and contamination processes such as granulation, melting, thermal metasomatism, leaching, gas escaping, and so on can be seen between the Oura-type magma and the surrounding sedimentary rocks. Textural and compositional changes in the process of formation of sedimentary enclaves and gas escaping from the assimilated and contaminated magma at a shallow depth will be discussed here.

Stop 10.

This stop is located at 31° 10.1'N in latitude and 130° 56.2' E in longitude. The Hanaze-type rock crops out along the road cutting. Anticlinal low-angle joints are developed. The rock is composed of medium-grained and light gray-colored biotite granodiorite with a small amount of enclave. Formation of the rock, formation of cooling joints at the top of magma chamber and the sequence of intrusion of the batholith will be discussed here.

Stop 11.

This stop is located at 31° 06.6'N in latitude and 130° 42.6'E in longitude. The Heda-Okawa-type rock crops out at sea shore. We can see a felsic dike dominant in sedimentary dark enclaves. It shows about 1 m in width, strikes N75° E, and dips vertical. The Heda-Okawa-type rock is composed of medium-grained and light dark colored granodiorite, and the enclave-dominant felsic dike consists of leucocratic medium- to fine-grained granodiorite. Modal composition of the former includes 27 vol.% quartz, 24 K-feldspar, 36 plagioclase, 12 biotite, 1 amphibole, with small amount of ilmenite, apatite, and zircon, and that of the latter includes 32 quartz, 24 K-feldspar, 31 plagioclase, 10 biotite, 3 amphibole, with small amount of ilmenite, apatite and zircon. Their bulk compositions are presented in Table 8 .

Stop 12.

This stop is located at 31° 28.5'N in latitude and 130° 45.5'E in longitude. The Shinkoji-type rock constituting the core of stock crops out on the road cutting and along the Honjo river. The rock shows a homogeneous face, and sedimentary enclaves are poor. It is composed of medium-grained and light gray-colored biotite granite. Modal composition includes 25 vol.% quartz, 28 K-feldspar, 40 plagioclase and 7 biotite. The bulk composition is presented in No. 2 of Table 6, and mineral compositions are in Table 7. Intrusion of the homogeneous rock through fractionation at deeper depths will be discussed here.

Stop 13.

This stop is located at 31° 29.1'N in latitude and 130° 46.4' E in longitude. The gradational rock between the Shinkoji-type and the Sarugajo-type crops out on the road cutting. It shows a heterogeneous face, and sedimentary dark clots are common. It is composed of medium-grained and light-colored aplitic granite. Modal composition includes 33 vol.% quartz, 35 K-feldspar, 27 plagioclase and 4 biotite, with small amount of tourmaline and garnet. The bulk composition is

Table 8. Bulk compositions of rocks occurring in the Stop 11.

No.	1	2	3
Sample No.	1080904	1080906	1080913
SiO_2 (wt%)	68.59	40.54	66.66
TiO_2	0.63	1.41	0.68
Al_2O_3	13.90	29.13	15.57
Fe_2O_3*	4.70	12.17	4.50
MnO	0.10	0.27	0.08
MgO	2.24	5.38	2.04
CaO	2.53	3.14	3.53
Na_2O	2.61	2.24	3.18
K_2O	4.88	6.40	3.96
P_2O_5	0.14	0.15	0.14
Total	100.31	100.81	100.35
Ba (ppm)	568	603	536
Cr	30	154	39
Cu	19	35	26
Nb	13	23	16
Ni	9	80	9
Rb	157	166	141
Sr	172	190	217
V	45	198	56
Y	32	31	33
Zn	56	250	57
Zr	149	319	159

*Total Fe as Fe_2O_3.

1. Enclave-dominant felsic dike.
2. Sedimentary enclave.
3. Heda-Okawa-type.

presented in No. 3 of Table 6, and mineral compositions are in Table 7. Formation of the rock and fractionation *in situ* of magmatic garnet will be discussed here.

Stop 14.

This stop is located at 31° 29.2' N in latitude and 130° 47.0' E in longitude. The Sarugajo-type rock constituting the upper part of stock crops out on the road cutting. It is a heterogeneous face, and rich in sedimentary dark clot. It is composed of fine-grained and light-colored aplitic granite. Modal composition includes 34 vol.% quartz, 36 K-feldspar, 27 plagioclase, 1 biotite and 1 garnet, with small amount of muscovite and tourmaline. The bulk composition is presented in No. 5 of Table 6, and mineral compositions are in Table 7. Formation of the rock through concentration of the filter-pressed vapor-rich residual liquid at the top of stock, that of dark inclusion rich in aluminous minerals through assimilation and contamination by the surrounding sedimentary rocks and that of magmatic garnet and muscovite will be discussed here.

Acknowledgement: The authors thank Dr. S. Ishihara for his valuable comments and critical reading of the manuscript.

References

Abe, I., Suzuki, H., Isogami, A. and Goto, T. (1986) Geology and development of the Hishikari mine. *Mining Geol.*, **36**, 117-130. *

Adachi, H., Yamashita, H. and Oba, N. (1969) Paragenesis of metamorphic minerals in the Shibisan contact aureole (northern part), Kagoshima Prefecture, Japan. *Rept. Fac. Sci., Kagoshima Univ. (Earth Sci., Biol.)*, no.2, 1-13. *

Aramaki, S. (1968) Geology of the Kakuto basin, southern Kyushu and the earthquake swarm from February, 1968. *Bull. Earthq. Res. Inst.*, **46**, 1325-1343. *

Aramaki, S., Hirayama, K. and Nozawa, T. (1972) Chemical composition of Japanese granites. Part2, Variation trends and average composition of 1200 analyses. *Jour. Geol. Soc. Japan*, **78**, 39-49.

Chappell, B. W. and White, A. J. R. (1974) Two contrasting granite types. *Pacific Geol.*, no. 8, 173-174.

Etoh, J., Izawa, E. and Taguchi, S. (2002a) A fluid inclusion study on columnar adularia of the Hishikari low-sulfidation epithermal gold deposit, Japan. *Resource Geol.*, **52**, 73-78.

Etoh, J., Izawa, E. and Taguchi, S. (2002b) Gas measurement of fluid inclusions from the Hishikari epithermal gold deposit, southern Kyushu, Japan, using Laser Raman microprobe. *Resource Geol.*, **52**, 405-408.

Etoh, J., Izawa, E., Watanabe, K., Taguchi, S. and Sekine, R. (2002c) Bladed quartz and its relationship to gold mineralization in the Hishikari low-sulfidation epithermal gold deposit, Japan. *Econ. Geol.*, **97**, 1841-1852.

Faure, K., Matsuhisa, Y., Metsugi, H., Mizota, C. and Hayashi, S. (2002) The Hishikari Au-Ag epithermal deposit, Japan: Oxygen and hydrogen isotope evidence in determining the source of paleohydrothermal fluids. *Econ. Geol.*, **97**, 481-498.

Feebrey, C. A., Hishida, H., Yoshioka, K. and Nakayama, K. (1998) Geophysical expression of low sulphidation epithermal Au-Ag deposits and exploration implications -examples from the Hokusatsu Region of SW Kyushu, Japan-. *Resource Geol.*, **48**, 2, 75-86.

Hamachi, T. and Ishihara, S. (1958) Report on the ore deposits in the Takakumayama district, Kagoshima Prefecture -with special reference to the radioactive mineral deposit-. *Bull. Geol. Surv. Japan*, **9**, 765-770. *

Hase, Y. (1987) Late Cenozoic stratigraphy of southern Kyushu, Japan. *Monogr. Assoc. Geol. Collab. Japan*, **33**, 251-278. *

Hayashi, K., Maruyama, T. and Satoh, H. (2000) Submillimeter scale variation of oxygen isotope of vein quartz at the Hishikari deposit, Japan. *Resource Geol.*, **50**, 141-150.

Hayashi, K., Maruyama, T. and Satoh, H. (2001) Precipitation of gold in a low-sulfidation epithermal gold deposit: Insights from a submillimeter scale oxygen isotope analysis of vein quartz. *Econ. Geol.*, **96**, 211-216.

Heald, P., Foley, N. K. and Hayba, D. O. (1987) Comparative anatomy of volcanic-hosted epithermal deposits: Acid-sulfate and adularia-sericite types. *Econ. Geol.*, **82**, 1-26.

Hedenquist, J. W. (1987) Mineralization associated with volcanic-related hydrothermal systems in the circum-Pacific basin. *In* Horn, M. K., ed., *Circum-Pacific Energy and Mineral Resources Conference, 4th, Singapore, 1986, Trans. Amer. Assoc. Petroleum Geol.*, 513-524.

Hedenquist, J. W., Matsuhisa, Y., Izawa, E., White, N. C., Giggenbach, W. F. and Aoki, M. (1994) Geology, geochemistry, and origin of high-sulfidation Cu-Au mineralization in the Nansatsu district, Japan. *Econ. Geol.*, **89**, 1-30.

Ibaraki, K. and Suzuki, R. (1993) Gold-silver quartz-adularia veins of the Main, Yamada and Sanjin deposits, Hishikari gold mine; A comparative study of their geology and ore deposits. *Resource Geol. Spec. Issue*, **14**, 1-11.

Imai, A. and Uto, T. (2002) Association of electrum and calcite and its significance to the genesis of the Hishikari gold deposits, southern Kyushu, Japan. *Resource Geol.*, **52**, 381-394.

Imai, A., Shimazaki, H. and Nishizawa, T. (1998) Hydrogen isotope study of fluid inclusions in vein quartz, Hishikari gold deposits, Japan. *Resource Geol.*, **48**, 159-170.

Imai, I., Teraoka, Y., Ono, K., Matsui, K. and Okumura, K. (1980) *Geological Sheet Map 1:500,000 "Kagoshima"*. Geological Survey of Japan. **

Ishihara, S. (1977) The magnetite-series and ilmenite-series granitic rocks. *Mining Geol.*, **27**, 293-305.

Ishihara, S. (1992) Exploration strategy for epithermal gold

deposits in Japan. Epithermal Gold in Asia and the Pacific, Mineral Concentrations and Hydrocarbon Accumulations in the Escap Region, vol. 6, United Nations Economic and Social Commission for Asia and the Pacific, 89-102.

Ishihara, S. and Kawachi, Y. (1961) On the Takakumayama granitic stock and related uraniferous ore deposit of Nago-ko at Tarumizu mine, Kagoshima Prefecture. *Rept. Geol. Surv. Japan*, no.190, 333-349. *

Ishihara, S. and Matsuhisa, Y. (1999) Oxygen isotopic constraints on the geneses of the Miocene Outer Zone granitoids in Japan. *Lithos*, **46**, 523-534.

Ishihara, S. and Terashima, S. (1978) Tin contents of granitic rocks in Japan and its environs. *In* Stemprok, M., Burnol, L. and Tischendorf, G., eds., *Metallization associated with acid magmatism*, vol. 3, 227-234.

Ishihara, S., Sekine, S., Mochizuki, T. and Oba, K. (1969) Uranium and thorium contents in granitic rocks and their geological meaning. *Rept. Geol. Surv. Japan*, no.232, 179-219. *

Ishihara, S., Sakamaki, Y., Sasaki, A., Teraoka, Y. and Terashima, S. (1986) Role of the basement in the genesis of the Hishikari gold-quartz vein deposit, southern Kyushu, Japan. *Mining Geol.*, **36**, 495-509.

Ishihara, S., Shibata, K. and Terashima, S. (1990) Alkalinity and initial $^{87}Sr/^{86}Sr$ ratio of igneous rocks related to the late Cenozoic gold mineralization of the Ryukyu arc, Japan. *CCOP Tech. Bull.*, **21**, 1-16.

Ishihara, S., Yamamoto, M. and Sasaki, A. (1999) Sulfur and carbon contents and $\delta^{34}S$ ratio of Miocene ilmenite-series granitoids: Osumi and Shibi-san plutons, Kyushu, SW Japan. *Bull. Geol. Soc. Japan*, **50**, 671-682.

Izawa, E. and Urashima, Y. (1989) Quaternary gold mineralization and its geologic environments in Kyushu, Japan. *Econ. Geol. Monogr.*, **6**, 233-241.

Izawa, E. and Watanabe, K. (2001) Overview of epithermal gold mineralization in Kyushu, Japan. Epithermal Gold Mineralization and Modern Analogues, Kyushu, Japan: Society of Economic Geologists, Guidebook Series, vol. 34, 11-15.

Izawa, E., Urashima, Y., Ibaraki, K., Suzuki, R., Yokoyama, T., Kawasaki, K., Koga, A. and Taguchi, S. (1990) The Hishikari gold deposit: High-grade epithermal veins in Quaternary volcanics of southern Kyushu, Japan. *Jour. Geochem. Explor.*, **36**, 1-56.

Izawa, E., Taguchi, S., Kobayashi, T. and Watanabe, K. (1992) Gold mineralization in volcano-geothermal areas of Kyushu. 29th International Geological Congress Field Trip Guide Book vol. 6: Mineral Deposits of Japan and the Philippines. Soc. *Resource Geology,* 143-172.

Izawa, E., Kurihara, M. and Itaya, T. (1993a) K-Ar ages and the initial Ar isotopic ratio of adularia-quartz veins from the Hishikari gold deposit, Japan. *Resource Geol. Spec. Issue*, **14**, 63-69.

Izawa, E., Naito, K., Ibaraki, K. and Suzuki, R. (1993b) Mudstones in a hydrothermal eruption crater above the gold-bearing vein system of the Yamada deposit at Hishikari, Japan. *Resource Geol. Spec. Issue*, **14**, 85-92.

Kagoshima Prefecture (1990) *Geological Sheet 1:100,000 "Kagoshima Prefecture"*. Kagoshima Prefecture.

Katsura, K., Nishimura, S., Yagi, S., Hatuda, Z. and Asayama, T. (1969) Uranium, thorium and potassium content of rocks in Japan (3). Rocks from Kyushu district. *Jour. Japanese Assoc. Mineral. Petrol. Econ. Geol.*, **62**, 90-102.

Kawachi, Y. (1961) Granitic rocks and related uraniferous metallic ore deposits in Southern Kyushu. *Rept. Geol. Surv. Japan*, no.190, 93-104. *

Kawano, M.,, Takahashi, K. and Nozawa, T. (1966) Petrochemistry of Minami-osumi granite in Uchinoura area, Kyushu, Japan. *Bull. Geol. Surv. Japan*, **17**, 533-541.

Kawano, Y. and Ueda, Y. (1966) K-A dating on the igneous rocks in Japan (V) -Granitic rocks in southwestern Japan-. *Jour. Japanese Assoc. Mineral. Petrol. Econ. Geol.*, **56**, 191-211. *

Kubota, Y. (1986) Geological and geotectonic setting of gold-silver mineralization in the Hokusatsu district, southern Kyushu, Japan. *Mining Geol.*, **36**, 459-474. *

Matsuhisa, Y. and Aoki, M. (1994) Temperature and oxygen isotope variations during formation of the Hishikari epithermal gold-silver veins, southern Kyushu, Japan. *Econ. Geol.*, **89**, 1608-1613.

Miller, J. A., Shibata, K. and Kawachi, Y. (1962) Potassium-argon ages of granitic rocks from the Outer Zone of Kyushu, Japan. *Bull. Geol. Surv. Japan*, **13**, 712-714.

Ministry of International Trade and Industry (MITI) (1988) *Report of the Regional Geological Structure Survey: Hokusatsu-Kushikino Area, 1987 fiscal year.* 69p. **

Morishita, Y. (1993) Carbon and oxygen isotopic characteristics of epithermal veins in the Hokusatsu gold district, southern Kyushu, Japan. *Resource Geol. Spec. Issue*, **14**, 103-114.

Nagayama, T. (1993) Precipitation sequence of veins at the Hishikari deposits, Kyushu, Japan. *Resource Geol. Spec. Issue*, **14**, 13-27.

Nakamura, J., Yamamoto, M., Tomita, K. and Oba, N. (1986) Genetical consideration for garnets of the southwestern Outer Zone-type granites, South Kyushu, Japan. *Rept. Fac. Sci., Kagoshima Univ. (Earth Sci., Biol.)*, no.19, 1-29.*

Nishimura, K. and Yamamoto, M. (1994) Vertical compositional variation in the northeastern part of Osumi granodiorite batholith, Kagoshima Prefecture, Japan. *Rept. Fac. Sci., Kagoshima Univ. (Earth Sci., Biol.)*, no.27, 101-111. *

Nozawa, T. and Ota, R. (1967) *Explanatory text of the geological map of Japan, Scale 1:50,000, Uchinoura.* Geological Survey of Japan, 37p. *

Oba, N. (1957) Shibi granodiorite and xenoliths in the north-western part of Kagoshima Prefecture. *Sci. Rept. Kagoshima Univ.*, no.6, 83-98. *

Oba, N. (1958) The Takakumayama granite mass, Osumi Peninsula, Kagoshima Prefecture. *Sci. Rept. Kagoshima Univ.*, no.7, 19-30. *

Oba, N. (1962) Contamination-effects on the Shibisan and the Shimokoshikijima granodiorites, Kagoshima Prefecture. *Jour. Geol. Soc. Japan*, **68**, 190-198. *

Oba, N. (1963) Chemical composition of the Kyushu Outer Zone granitic rocks. *Sci. Rept. Kagoshima Univ.*, no.12, 35-51.

Oba, N. (1965) The heterogeneity of the Osumi granodiorite. *Sci. Rept. Kagoshima Univ.*, no.14, 59-70.

Oba, N. and Miyahisa, M. (1977) Relation between chemical composition of granitic rocks and metallization in the Outer Zone of Southwest Japan. *Bull. Geol. Soc. Malaysia*, **9**, 67-74.

Ogura, J., Hamada, K., Yamamoto, M., Oba, N. and Yamashita, H. (1970) Contact metamorphic zoning of the northern part of Takakumayama mountains, Kagoshima Prefecture, Japan. *Rept. Fac. Sci., Kagoshima Univ. (Earth Sci., Biol.)*, no. 3, 1-4. *

Ota, R. (1964) *Explanatory text of the geological map of Japan, Scale 1:50,000, Tarumizu*. Geological Survey of Japan, 25p. *

Ota, R. and Kawachi, Y. (1965) *Explanatory text of the geological map of Japan, Scale 1:50,000, Kanoya*. Geological Survey of Japan, 56p. *

Sekine, R., Morimoto, K. and Ushirone, N. (1998) Characteristics of the Yamada vein system, Hishikari mine, Kyushu, southwestern Japan. *Shigen Chishitsu*, **48**, 1-8. *

Sekine, R., Izawa, E. and Watanabe, K. (2002) Timing of fracture formation and duration of mineralization at the Hishikari deposit, southern Kyushu, Japan. *Resource Geol.*, **52**, 395-404.

Shibata, K. and Ishihara, S. (1979) Initial $^{87}Sr/^{86}Sr$ ratios of plutonic rocks from Japan. *Contrib. Mineral. Petrol.*, **70**, 381-390.

Shikazono, N. (1999) Sulfur isotopic composition and origin of sulfide sulfur in epithermal Au-Ag vein-type deposits in Japan. *Resource Geol. Spec. Issue*, **20**, 39-45.

Shikazono, N. and Nagayama, T. (1993) Origin and depositional mechanism of the Hishikari gold-quartz-adularia mineralization. *Resource Geol. Spec. Issue*, **14**, 47-56.

Shikazono, N., Yonekawa, N. and Karakizawa, T. (2002) Mass transfer, oxygen isotopic variation and gold precipitation in epithermal system: A case study of the Hishikari deposit, Southern Kyushu, Japan. *Resource Geol.*, **52**, 3, 211-222.

Takahashi, M., Aramaki, S. and Ishihara, S. (1980) Magnetite-series/ilmenite series vs. I-type/S-type granitoids. *Mining Geol. Spec. Issue*, **8**, 18-23.

Takahashi, M., Mizuta, T., Ishiyama, D., Kimura, J. and Takada, J. (2002) Characteristics of trace elements in quartz by LA-ICP-MS and the origin of ore fluid responsible for gold mineralization at the Hishikari epithermal gold deposit, Japan. *Shigen Chishitsu*, **52**, 51-67. *

Tateishi, K., Oba, N., Yamamoto, M., Tomita, K., Nakamura, J. and Kanai, T. (1986) Source and origin of xenoliths contained in Osumi granodiorite batholith, South Kyushu, Japan. *Rept. Fac. Sci., Kagoshima Univ. (Earth Sci., Biol.)*, no.19, 23-44. *

Uto, T., Imai, A. and Yamato, Y. (2001) Horizontal strain rate in relation to vein formation of the Hishikari gold deposits, southern Kyushu, Japan. *Resource Geol.*, **51**, 7-18.

Yamamoto, M. (1975) Potassium feldspars from the Takakumayama granite, Kagoshima Prefecture, Japan. *Rept. Fac. Sci., Kagoshima Univ. (Earth Sci., Biol.)*, no.8, 15-26.

Yamamoto, M. (1976) Crystallization of granitic glasses at 700°C and 1 kbar. *Rept. Fac. Sci., Kagoshima Univ. (Earth Sci., Biol.)*, no.9, 9-20.

Yamamoto, M. (1978) Biotites from the Takakumayama granite, Kagoshima Prefecture and their hydrothermal experiments at higher oxygen fugacities. *Jour. Fac. Sci., Hokkaido Univ., Ser. 4*, **18**, 105-115.

Yamamoto, M. and Oba, N. (1983) Geology and rocks in the Takakumayama granite body and the Osumi granodiorite body. Excursion Guidebook, 90th Annual Meeting (Kagoshima), Geological Society of Japan, 61-79. **

Yamamoto, M. and Ushijima, A. (1994) Granitic dikes in the Hokusatu district, Kagoshima Prefecture. *Rept. Fac. Sci., Kagoshima Univ. (Earth Sci., Biol.)*, no. 27, 91-99. *

Yamamoto, M., Nakamura, T. and Oba, N. (1983) Differentiation and intrusion of the Osumi granodiorite body. *In* Symposium: Differnetiation and Intrusion of Zoned Pluton and Ring Complex, 90th Annual Meeting (Kagoshima), Geological Society of Japan, 29-36. **

Yamamoto, M., Oba, N. and Tomita, K. (1988) Compositional variation of the Shibi-san granodiorite body, Kagoshima Prefecture, Japan. *Rept. Fac. Sci., Kagoshima Univ. (Earth Sci., Biol.)*, no. 21, 35-49. *

Yanagi, T., Yamaguchi, M. and Nozawa, T. (1971) Rb-Sr whole rock ages of the granites of Minami-osumi and Amami-oshima, Southwest Japan. *Mem. Fac. Sci., Kyushu Univ., Ser. D, Geol.*, **21**, 163-175.

* in Japanese with English abstract.
** in Japanese.

Received May 21, 2003
Accepted July 10, 2003